2019

CELL SURFACE COATINGS FOR MAMMALIAN CELL-BASED THERAPEUTIC DELIVERY

Pei-Jung Wu
University of Kentucky, peijung.wutw@gmail.com
Author ORCID Identifier:
https://orcid.org/0000-0002-9929-5704
Digital Object Identifier: https://doi.org/10.13023/etd.2019.328

STUDENT AGREEMENT:

I represent that my thesis or dissertation and abstract are my original work. Proper attribution has been given to all outside sources. I understand that I am solely responsible for obtaining any needed copyright permissions. I have obtained needed written permission statement(s) from the owner(s) of each third-party copyrighted matter to be included in my work, allowing electronic distribution (if such use is not permitted by the fair use doctrine) which will be submitted to UKnowledge as Additional File.

I hereby grant to The University of Kentucky and its agents the irrevocable, non-exclusive, and royalty-free license to archive and make accessible my work in whole or in part in all forms of media, now or hereafter known. I agree that the document mentioned above may be made available immediately for worldwide access unless an embargo applies.

I retain all other ownership rights to the copyright of my work. I also retain the right to use in future works (such as articles or books) all or part of my work. I understand that I am free to register the copyright to my work.

REVIEW, APPROVAL AND ACCEPTANCE

The document mentioned above has been reviewed and accepted by the student's advisor, on behalf of the advisory committee, and by the Director of Graduate Studies (DGS), on behalf of the program; we verify that this is the final, approved version of the student's thesis including all changes required by the advisory committee. The undersigned agree to abide by the statements above.

Pei-Jung Wu, Student

Dr. Brad J. Berron, Major Professor

Dr. Steve Rankin, Director of Graduate Studies

CELL SURFACE COATINGS FOR MAMMALIAN CELL-BASED THERAPEUTIC DELIVERY

DISSERTATION

A dissertation submitted in partial fulfillment of the
requirements for the degree of Doctor of Philosophy in the
College of Engineering
at the University of Kentucky

By

Pei-Jung Wu

Lexington, Kentucky

Director: Dr. Brad J. Berron, Professor of Chemical Engineering

Lexington, Kentucky

2019

ABSTRACT OF DISSERTATION

CELL SURFACE COATINGS FOR MAMMALIAN CELL-BASED THERAPEUTIC DELIVERY

The cell plasma membrane is an interactive interface playing an important role in regulating cell-to-cell, cell-to-tissue contact, and cell-to-environment responses. This environment-responsive phospholipid layer consisting of multiple dynamically balanced macromolecules, such as membrane proteins, carbohydrate and lipids, is regarded as a promising platform for various surface engineering strategies. Through different chemical modification routes, we are able to incorporate various artificial materials into the cell surface for biomedical applications in small molecule and cellular therapeutics.

In this dissertation, we establish two different cell coating techniques for applications of cell-mediated drug delivery and the localization of cell-based therapies to specific tissues. The first part of this dissertation establishes a membrane-associated hydrogel patch for drug delivery. The crosslinking of a grafted polymeric patch from a mammalian cell membrane is achieved through surface-mediated photolithographic polymerization. With the use of photomask, the formation of nanoparticle-loaded PEGDA hydrogel is controlled to deposit various geometric features on photoinitiator-immobilized surfaces. Through microarray patch patterning, we analyzed the influence of processing parameters on the accuracy of polymer patterning on a microarray. We then optimized the patterning approach for the formation of PEGDA patches on live A549 cells.

In the second part of this dissertation, we study the use of tissue-adhesive coatings to improve the retention of therapeutic mesenchymal stem cells (MSCs) in the heart following intramyocardial or intravenous injection. MSCs were coated with antibodies against ICAM1 to adhere to CAM-overexpressed endothelium present in the heart following MI. Through intramyocardial or intravenous delivery, we observe higher number of coated cells retained in the heart over uncoated ones, supporting enhanced affinity for the inflamed endothelium near the infarct. We correlate the detachment force of antigen-interacted MSCs by a parallel laminar flow assay with the density of ICAM on the substrate and the density of anti-ICAM on the MSC surface. MSC retention on CAM-modified surfaces or activated HUVECs was significantly increased on antibody-coated groups (~90%) under physiologically hemodynamic forces (< 30dyne/cm^2), compared to uncoated MSCs (~20%). Moreover, a dramatic reduction of immune cell quantity was observed after intravenous injection, indicating the enhanced immunoregulatory efficacy by systemically delivering ICAM-adhesive MSCs to the site of inflammation.

KEYWORDS: cell surface coating, hydrogel patch, surface-mediated polymerization, antibody incorporation, endothelium targeting, biotin streptavidin affinity

Pei-Jung Wu

(Name of Student)

[07/23/2019]

Date

CELL SURFACE COATINGS FOR MAMMALIAN CELL-BASED THERAPEUTIC DELIVERY

By
Pei-Jung Wu

Dr. Brad Berron
Director of Dissertation

Dr. Steve Rankin
Director of Graduate Studies

[07/23/2019]
Date

DEDICATION

To my dearest parents and family

ACKNOWLEDGMENTS

During these few years, I have bravely reached this stage with countless support and assistance from many people. First of all, I would like to give my deepest thanks to my parents who give me selfless love and strength in my whole life. Although they are on the other side of the world from me, I always feel their warmness around me. I would like to express my special thanks to Hong-Ming Chen who always listens to me intently, encourages me, and keeps spreading happiness all the time. I cannot fulfill my goal on this lonely academic road without him.

I would like to extend my sincere gratitude to my academic advisor, Dr. Bradley Berron, who provides his professional guidance and instructive suggestions for this dissertation. He is always patient and kind to give me respect and freedom on my scientific thought. I would like to thank Dr. Ahmed Abdel-Latif for his instruction and knowledge in cardiovascular-based research. I wish to give sincere thanks to Dr. Ahmed Abdel-Latif, Dr. Daniel Pack, Dr. Eric Grulke and Dr. Esther Black for being my committee members and outside examiner. I'd acknowledge the support from research fund R01 HL127682 and the National Science Foundation under Award CBET-1351531.

I am grateful to my colleagues, Anuhya, Jacob, Leila, Ishan, Aman, Cong, Hsuan, Calvin, Kara and Lauren, who have enlightened me and made my lab life full of variety and interest. I wish to specially thank my classmates Shou Tang and Yue Yu for their companionship. I'd like to thank my lovely pet, Bagu, who makes my life enjoyable everyday. Last but not least, I'd like to thank for everything that my wonderful country, Taiwan, has given me.

TABLE OF CONTENTS

LIST OF FIGURES

LIST OF ABBREVIATION

ATP	Adenosine triphosphate
β2 integrin	Integrin beta chain-2
bBSA	Biotinylated bovine serum albumin
bFGF	Fibroblast growth factor
BSA	Bovine serum albumin
CAM	Cell adhesion molecule
CAR	Chimeric antigen receptors
Cd3	Cluster of differentiation 3
CD4	Cluster of differentiation 4
CD8	Cluster of differentiation 8
CD31	Cluster of differentiation 31
CD31	Cluster of differentiation 45
CD123	Interleukin-3 receptor alpha chain
CD144	Cluster of differentiation 144/ Vascular endothelial cadherin
CD326	Cluster of differentiation 326/ Epithelial cell adhesion molecule
CRIP2	Cysteine rich protein 2
CXCR4	C-X-C motif chemokine receptor 4
DNA	Deoxyribonucleic acid
DOX	Doxorubicin
ECM	Extracellular matrix
EDTA	Ethylenediaminetetraacetic acid
EPCAM	Epithelial Cell Adhesion Molecule
ERK	Extracellular signal related kinases (ERK)
Fab	Antigen-binding fragment
FBS	Fetal bovine serum
FGF	Fibroblast growth factor

FOX2	Forkhead box protein P2
GFP	Green fluorescent protein
H2O2	Hydrogen peroxide
HIF1-a	Hypoxia-inducible factor 1-alpha
HGF	Hepatocyte growth factor
HLA-G5	Human leukocyte antigen G5
ICAM1	Intercellular adhesion molecule 1
IDO	Indoleamine-pyrrole 2,3-dioxygenase
IFN-γ	Interferon gamma
IGF-1	Insulin-like growth factor 1
IgG	Immunoglobulin G
IL1α	Interleukin 1 Alpha
IL1β	Interleukin 1 beta
IL-2	Interleukin-2
IL-6	Interleukin-6
IL-10	Interleukin-10
INOS	Inducible nitric oxide synthase
LFA-1	Lymphocyte function-associated antigen 1
LPS	Lipopolysaccharides
Mac-1	Macrophage-1 antigen/ Cd11b/CD18
MLC	Myosin light chain
MMP-2	matrix metalloproteinase-2
NF-κB	Nuclear factor-κB
NHS	N-HydroxySuccinimide
NO	Nitric oxide
PBS	Phosphate-buffered saline
PE	Phycoerythrin
PGE2	Prostaglandin E2

PI3k	phosphoinositide-3-kinase–protein kinase B
Akt	Protein kinase B (PKB)/ serine/threonine-specific protein kinase
PPG	Palmitated protein-G
SDF-1	Stromal cell-derived factor-1
SLex	Sialyl LewisX
sulfo-NHS-LC-biotin	Sulfosuccinimidyl-6-(biotinamido) hexanoate
TNFα	Tumor necrosis factor-alpha
TNFR	Tumor necrosis factor receptor
TSG6	Tumor necrosis factor-inducible gene 6 protein
VBP	VCAM-binding peptide
VCAM1	Vascular cell adhesion molecule 1
VEGF	Vascular endothelial growth factor

ATRP	Atom transfer radical polymerization
AL	Alginate
DBCO	Dibenzocyclooctyne
DMPE	1,2-Dimyristoyl-sn-glycero-3-phosphoethanolamine
DOPE	1,2-Dioleoyl-sn-glycero-3-phosphoethanolamine
DSPE	1,2-Distearoyl-sn-glycero-3-phosphoethanolamine
FHP	Feraheme, heparin and protamine
FITC	Fluorescein isothiocyanate
HA	Hyalyuronic acid
LbL	Layer-by-layer
NP	Nanoparticle
PAH	Polyallylamine hydrochloride
PEG	Polyethylene glycol
PEGDA	Polyethylene (glycol) diacrylate
PEI	Polyethylenimine

PEM	Polyelectrolyte multilayer
PDADMAC	Polydiallyldimethylammonium chloride
PLL	poly-l-lysine
SAEITC	Streptavidin-eosin-isothiocyanate
SDS	Sodium dodecyl sulfate
sulpho SMCC	Sulfosuccinimidyl 4-(N-maleimidomethyl) cyclohexane-1-carboxylate
SPION	Superparamagnetic iron oxide nanoparticles
TEA	Triethanolamine
VP	Vinyl pyrollidinone

ASL	Antigen-specific lysis
FDA	Food and Drug Administration
IBD	Inflammatory bowel disease
LV	Left ventricular
MI	Myocardial infarction
MS	Multiple sclerosis
MRI	Magnetic resonance imaging
SSE	Sum of the squared error

Cell types

A549	Adenocarcinomic human alveolar basal epithelial cells
BMDM	Bone marrow-derived macrophage
CDC	Cardiosphere-derived stem cells
CRBC	Circulating red blood cells
EC	Endothelial cell
HEPG2	Human liver cancer cell line

hMSC	Human mesenchymal stem cell
HSC	Hematopoietic stem cells
HUVEC	Human Umbilical Vein Endothelial Cells
MELN	Luciferase-transfected human breast cancer cell line
MSC	Mesenchymal stem cell
NSC	Neural stem cells
RBC	Red blood cell

CHAPTER 1. TECHNIQUES FOR COATING MAMMALIAN CELLS

1.1 Introduction: roles of cell surface engineering

Cell membrane is a complex phospholipid bilayer covered by a variety of biological components including glycolipids, proteins and carbohydrate chains. This biointeractive interface not only acts as a safeguard against unwanted intruders but also governs the communication and essential nutrient exchanges between inner and outer region of a cell. Given diverse biological moieties displayed on the surfaces of different cell types, engineering the surface of a cell provides huge potentials to transform the intrinsic functions and activities of cell surface components to match specific therapeutic targets or biomedical needs.

Cell surfaces are composed of diverse biochemical and are characterized to achieve exclusive functions through both genetic and non-genetic techniques. Recently, the first therapy based on the genetic modification of a cell surface was approved by the FDA, and the delivery of chimeric antigen receptor-modified (CAR) T-cells is now used clinically for blood cancers such as leukemia and melanoma. T cells are collected from a patient's blood are genetically reprogrammed by gene sequence insertion using inactive viral vectors. The genetic manipulation enables reprogramming of T cell surface structure by expressing tumor antigen-recognized CAR for targeting cancer cell antigen [1].

However, challenges of genetic cell surface manipulation remain [2]. Firstly, genetic modification methods do not really induce the expression of desired substances, limiting the coating choices on cells. Secondly, genetic manipulation is subject to low transfection efficiencies, where the fraction of cells showing any significant change in

properties is significantly less than one. Beyond the efficiency, the genetically-engineered cells require time for transcription and protein synthesis, requiring hours to days for surface modification. Finally, there are still significant concerns over the safety of viral transfection approaches, and modern non-viral methods lag behind viral methods in transfection efficiency and cell toxicity. As a result, this dissertation broadly focuses on non-genetic strategies for cell surface modification of functional mammalian cells. Cell surface coating can perform unique biological functionalities that cells inherently lack. In our work, the engineered cells are capable of carrying drug payload for cell mediated drug delivery or selectively targeting tissues of interest for local cell retention in the heart, while maintaining their intrinsic cellular properties to interact with extracellular environment. Here, we describe the current strategies for non-genetic cell surface engineering. They are broadly divided into covalent and non-covalent approaches, and this chapter contrasts the strengths and weaknesses of each approach.

1.2 Current non-genetic cell surface engineering technologies: non-covalent interaction

To alter the intrinsic functionalities of cell surfaces by non-genetic methods, non-covalent and covalent bonds are two main categories of molecular binding and are widely used to attach biomaterial coatings on cell surfaces (Figure 1.1). Non-covalent binding includes electrostatic interactions, hydrogen bonds, ionic bonds and van der Waals interactions, and has relatively weak binding energy which can possibly be broken by molecule activities at physiological conditions; however, noncovalent interactions are still

considered as critical modification processes to regulate cell surface protein-protein interactions and cell membrane dynamics.

1.2.1 Cell surface coating through electrostatic interactions

The extracellular composition of glycoprotein and glycolipid residues on a cell membrane exposes negative ions provided from oligosaccharides, driving the cell plasma membrane to be a negatively charged interface that electrostatically attracts essential cations for normal cellular functions. For cell surface coating, the peripheral membrane's negative charge can be regarded as an adhesive surface for non-covalent deposition of positively charged materials, such as polycationic peptides, proteins, polymers or nanoparticles (Figure 1.2).

Notably, the fabrication of polyionic polymers through layer-by-layer (LbL) techniques offers a direct method for creating a cytoprotective coating. Through sequential deposition of oppositely charged polyelectrolyte layers, a multilayer polymer thin film is directly form on the surface of each individual cell. From Tabrizian's lab, alternative coating of anionic AL and cationic PLL polyelectrolyte on red blood cells (RBC) generated universal RBCs that are not immunologically recognized by immunotargeting [3]. This multilayer encapsulation on RBCs protected cells from antibody-A capture and showed no aggregation caused by immunorecognition after introducing antibody-A, supporting a strong reduction in immunogenicity and antigenicity of blood group antigens. Additionally, coated cells maintained their oxygen carrying capacity and also released amounts of ATP and hemoglobin consistent with the low levels of cell death of seen in uncoated cells [3]. Similarly, absorption of polycationic PEI mixed with silica nanoparticles, considered as an artificially protective cell wall, on negatively charged

mammalian cell membrane (HeLa, NIH 3T3 fibroblast and Jurkat) demonstrated coating-based cytoprotection from enzyme-induced cell apoptosis [4]. Another group has exploited LbL deposition of PLL(+)/HA(-) nanolayers to form a protective coating on mesenchymal stem cell (MSC) cell membrane without affecting cell morphology, showing the material absorption potential on MSCs through electrostatic attraction. However, the long term viability of PLL-encapsulated MSCs began to decrease after several days [5].

While most studies utilize polyelectrolyte materials like PLL [3, 5], PAH [6, 7] and PEI [4], Germain M et al. have proposed PDADMAC/PSS as a more biocompatible LbL polymer coating on MELN breast cancer cells. The cell-associated PDADMAC coating showed three-fold higher on cell viability than the use of PLL, PAH and PEI. In addition, PDADMAC-coated cells demonstrated cytoprotection from macromolecular by prohibiting the internalization of 60kDa and 80kDa proteins [8].

In all, electrostatic deposition of polymeric materials provides a simple and rapid method for coating the charged surface of a cell [6, 7, 9, 10]. While the coating of polycation polymer can protect cells from unfavorable molecule invasion, the charged covering that is always destructive for cells could certainly compromise the fragile nature of mammalian cell membrane, limiting its use for long-term cell activities.

1.2.2 Cell surface coating through hydrophobic lipid interactions

Lipids are broadly used materials for protein conjugation and drug delivery due to their biocompatibility and controllable structural properties for a variety of bioconjugations. Here, they are considered as a cell surface coating material to conjugate specific bioactive molecules on the surface of living cells for specific targeting purposes. Due to poor water solubility of lipid tail, PEGylation is widely employed to create

amphiphilic PEG-derivative lipids for cell plasma membrane modification. Namagune's group [11] demonstrated the stable grafting of single lipid tailed oleyl-PEG-biotin or double lipid tailed-DOPE-PEG-FITC on surfaces of human and sheep erythrocytes. Because of the coverage of lipid tails anchored onto plasma membranes, DOPE-modified cells showed the great antigen masking efficiency to escape from the recognition of antibody against A antigen on erythrocytes.

Moreover, the uses of protein-conjugated lipids to incorporate non-naturally and non-abundantly expressed proteins on MSC surfaces were exhibited by Bull's group. Varying molecular weights of PEG groups were used to support [12, 13] the high viability of coated MSCs after phospholipid modification. MSCs were designed for targeting specific MSC homing factors using lipid-PEG conjugates with terminal targeting groups. Ligand protein SDF-1 and its cognate receptor CXCR4 are known as MSC recruiting factors, and these were conjugated on the distinct functionalized ends of two different PEGylated DMPE lipid using NHS [13] or maleimide [12] conjugation. The surface-coating of CXCR4 or SDF-1 enhanced the MSC migration toward its corresponding homing target to support the potential CXCR4/SDF1-directed MSC recruitment into ischemic myocardium by this protein-phospholipid cell surface coating. In addition, homing peptide CRPPR-grafted phospholipid (DMPE-PEG-CRPPR), conjugated through the reaction between lipid-maleimide and cysteine-containing peptide, was also hydrophobically embedded onto MSC surfaces. It indicated that by increasing the amount of intercalated homing peptide, the number of coated MSCs that migrated to the gradient of target protein CRIP2 also increased [13].

Other than synthetic lipid domains like DMPE or DOPE, multiple studies have showed the use of naturally-derived lipid products to hydrophobically decorate cell surfaces. PEGylated glycol chitosan-cholesterol-biotin was intercalated into the surface of A549 cells and labeled with a fluorescent streptavidin for cell imaging up to 8 hours [14]. The two-step biotinylation via click chemistry was processed by inserting the DBCO (dibenzocyclooctyne)-labelled cholesterol and DSPE onto RAW 247 macrophage cell membrane. The cholesterol-anchored cell surfaces gave a greater biotinylation reactivity than the DSPE phospholipid biotin; moreover, both synthetic and naturally-derived lipid anchorage exhibited negligible cytotoxic effects on lipid-modified cells [15].

Palmitate acid is another naturally formed saturated fatty acid and is known as its importance of protein lipidation and localization on cell plasma membranes. Early study from Peacock's group has first established the conjugation of antibody with NHS-derivative palmitate acid for one step cell surface antibody decoration. The pre-conjugated antibody-palmitate was hydrophobically intercalated into the membrane of P388D1 cells. Interestingly, it was found that P388D1 macrophages bearing artificial receptor (anti-CRBC) was able to interact with CRBC cells to enhance cell-cell interaction [16]. The advantage of hydrophobic lipid-anchorage on cell membrane modification is that non-permanent lipid insertion preserves intrinsic protein properties on plasma membrane and has less harmful effects on cellular functions. However, the retention of cell surface-intercalated lipids might decrease over time due to their weak binding. The irreversible and transient kinetics of lipid-membrane interaction could be simply interfered by the dynamically fluctuated phospholipid interface. Additionally, lipid breakdown could cause instability of cell surface structure. The presence of multiple lipid enzymes, in an

extracellular microenvironment, could naturally digest lipid chains into smaller pieces, leading to functionality loss of lipidated bioconjugate.

1.2.3 Cell surface coating through antibody-antigen specificity

Every cell population has its unique profile of cell surface markers, allowing antibody-antigen affinity to drive adhesion to the surface of targeted cells. This targeted adhesion creates opportunities for specific or nonspecific coupling of ligands to the cell surface. Most commonly, NHS-ester groups are used to tether biotin [17], horseradish peroxidase (HRP) [18, 19], magnetic beads [20], nanoparticles [21, 22] and a variety of fluorophores to antibodies, and this diversity expands the portfolio of potential biological applications in cell surface coating.

Our lab uses antibody-antigen specificity to purify cells based on marker-expression through antigen-specific lysis [23-25]. An ultrathin hydrogel coating was grafted from the membrane of antigen positive cells by surface-initiated photopolymerization. A biotinylated antibody was specifically adhered to antigen-positive cells in order to support immobilization of a streptavidin-photoinitiator, and crosslinked coatings were generated through the surfaces of antibody/photoinitiator-conjugated Jurkat or A549 cells under visible light irradiation. These hydrogel coatings form and protect only antigen-positive cells from lysis conditions by surfactants or hypotonic solutions. A similar antigen specific cell coating was reported by Sakai et al to encapsulate antigen positive cells by enzyme-mediated polymerization [26]. Horseradish peroxidase is a protein enzyme commonly used to catalytically label antigens in immunohistochemical staining and ELISAs. HRP is a potent activator for radical polymerization of vinyl

monomers or aromatic derivatives [27, 28], and HRP was used in this study to selectively form alginate hydrogel coatings on $CD31^+$ and $CD326^+$ cells [26].

Because antibodies have unique antigen-binding domains to target specific cell surface markers, researchers have come up with a coating of bispecific antibody on cells by creating a hybrid combination of two different antibodies. This antibody-fused material with dual antigen-interacting parts was used to coat the cytotoxic killer cells for cancer cell targeting. Early work in 1990, Taizo Nitta et al. designed a heterofunctional monoclonal hybrid that has both CD3 (T cells) and LU246 (glioma cells) targeting properties by fusing two different SH-reduced antigen-binding fragment (Fab) into one asymmetric antibody structure. Effectively, the coating of glioma-recognized antibody hybrid on T effecter cells exhibited the enhanced cytotoxic targeting in glioma cells than the ones without this immunoconjugate [29]. Additionally, the coating of bispecific immunostructure on T lymphocyte [30] or cytokine-induced killer cells [31] has showed improved tumor cell targeting efficacy through different designs of antigen binding orientation [30, 31]. The dual functional antibody with both CD3 and CD123 recognized variable domains was used to coat $CD3^+$ effector T lymphocyte. The delivery of T cell-conjugated bispecific antibody that has CD123 targeting ability was successfully proved to effectively eliminate $CD123^+$ leukemia tumor cells [30].

The high selectivity of antibody anchoring presents a significant advantage over other coating grafting techniques. Critically, there are also several limitations with antibody supported coatings. Selecting an adequate cell surface marker for coating only on a target cell could be a tricky issue because 1) the same cell surface proteins might be expressed on distinct cell lineages and 2) the large variability in expression levels within

a single population of cells. In many cases, the antigen's density is too low to effectively modification the cell's surface [23]. Moreover, antibody labeling some surface receptors will trigger intracellular signaling [32-34] that could lead to unexpected cellular activities.

1.2.4 Cell surface coating through receptor-ligand interactions

Cell surface receptors are specialized transmembrane cellular proteins with unique tertiary structures that specially respond to corresponding docking ligands. To date, approaches using ligand-receptor binding affinity has been increasingly investigated in cell surface modification for specialized cell-responsive interactions. For example, the binding between hyaluronic acid (HA) ligand and its receptor CD44 is one of the key regulatory interactions for coating deposition [35]. The inflammatory CD44 upregulation drives the membranes of immune cells, such as leukocyte, macrophage or monocyte, as HA-targeted interfaces for the surface loading of polymer drug payload or backpack for cell-mediated drug delivery and uptake [35, 36].

A multilayer polymer-fabricated backpack loaded with a CD44-adhesive HA interface was specifically attached to the CD44-expressed leukocyte [37] or macrophage [38] for long-term based drug carrying. By precisely controlling the material size, geometry [39] and orientation [40], the coating through this HA-CD44 interaction allowed the sustaining loading only on living $CD44^+$ leucocytes and lymphocyte B cells with no further material engulfment. This surface-attached polymeric film was known to increase cell-cell interaction and communication. The events of cell aggregation were raised in response to the increase in surface area of CD44 contacting backpacks [39]. Similarly, the modification of Fe_3O_4 nanoparticle-loaded backpack through HA-CD44 interaction was also applied to magnetically control the migration of backpack-adhered B cells [37]. These

coating examples through ligand-receptor affinity provides a stable surface loading strategy for cytotoxic killer cells to deliver the drug payload.

While ligand-receptor interaction also offers some cell-targeting specificity, the opportunity for inadvertent activation requires caution with this approach. Surface binding on receptor could accelerate internalization of the surface coated materials and decrease the availability of the surface-loaded materials. Thus, while there are opportunities for receptor ligand anchoring, the potential for unintended biological responses often outweigh the benefits of this strategy.

1.2.5 Cell surface engineering through covalent amide bonds

Covalent attachment provides a more stable attachment then noncovalent strategies through the formation of an irreversible binding to the cell surface. The cell's peripheral membrane is composed of numerous structures for covalent binding, including proteins, phospholipids, and carbohydrate chains. In this dissertation, I commonly conjugate groups to the cell surface covalently through the formation of an amide bond on cell surface proteins.

Owing to the hydrophilic nature of amine groups, lysine residues are typically presented at the external surface of protein, and these residues are convenient for chemical modification. In this section, we focus on different types of amine-reactive chemistries used for biomaterial attachment in a physiological environment. One amine crosslinking strategy is to covalently link cyanuric chloride on cell surface glycoproteins. Blackall et al. used PEGylated cyanuric chloride to form a PEGylated layer around proteins on red blood cell to camouflage the cells from parasite invasion and immune recognition [41]. Unfortunately, potential cytotoxicity after surface modification with cyanuric chloride

limits this covalent binding for cell surface engineering beyond the relatively stable red blood cells.

NHS ester linker are frequently used to decorate living mammalian cells by forming stable covalent amide-bonds in mild and slightly alkaline biological conditions (pH 7-8) [12, 23, 42-47]. In contrast to long metabolic engineering processes for covalent binding, NHS covalently binds structures to cells in under an hour. This approach has been used to rapidly tether NHS-DNA ligands to the surface of multiple mammalian cell types, including T cells, red blood cells and cardiac myoblasts without affecting their intrinsic cellular phenotypes. These specific cell coatings were then used to rapidly adhere cells to complementary DNA patterned on a glass surface [42]. Sulfonated NHS derivatives have increased water solubility and improve biocompatibility for cell surface modification, and this strategy is used to tether protein-signaling aptamers [43] or biotin [44-46] to the surfaces of MSCs.

Covalent biotinylation strategy using sulfonated NHS-LC-biotin was also utilized by Karp's group to coat biotinylated SLe^x ligand on MSCs for mimicking leukocyte extravasation through endothelium. With ligand coating, Karp et al. observed the reduction of MSC rolling velocity on P-selectin modified surface [44] and the increased MSC homing to inflamed ear in an inflammation-induced murine model after *in vivo* vein injection [45], in contrast to unmodified cells. For drug delivery applications, another study from Anderson's lab also employed NHS-ester biotin to load neutravidin nanoparticles on human mesenchymal stem cells (hMSCs) without changing their tumoritropic property [46].

The sulfo-NHS biotin strategy is particularly useful as an adaptable tool for additional cell surface functionalization. Of particular relevance, our lab demonstrated a cell encapsulation technique by covalent NHS ester biotinylation [23, 47]. Grafting of the streptavidin-conjugated photoinititator to a biotinylated cell interface rapidly facilitated polymerization around individual living cells, allowing the generation of polymer coating for different application such as cytoprotection [23] or tissue targeting [47].

1.3 Surface-mediated polymerization on individual cells

Building hydrogel thin film through surface initiation provides a great foresight in surface engraftment of polymeric materials (Figure 1.2). Prior study about individual cell polymerization has grafted nano-thin polymers on yeast cells by surface-activated ATRP polymerization to exhibit cytoprotective effects. While this uniformly formed polymer coating can prevent cell agglutination during E-coli introduction [48], the non-physiological operating conditions of ATRP system and the demand of transition metal catalyst $CuBr_2$ could lead to lethal DNA cleavage through the oxidative activation, making it not suitable for mammalian cell manipulation. Various works in thin film generation have established the local grafting of acrylate or methacrylic polymer on a photoinitiator-immobilized surface through radical propagation [49-54]. Previously, Seda Kızılel et al. designed an eosin-initiated photografting system in combination with co-initiator triethanolamine (TEA) and accelerator vinyl pyrollidinone (VP) to rapidly form a polyethylene (glycol) diacrylate (PEGDA) hydrogel film on an eosin-localized surface. By introducing photon energy from visible light, the excited eosin in triplet state promotes the formation of eosin radical and a cation TEA radical that is critical for polymer propagation

by cleaving acrylate double bond [50]. This eosin-based photocrosslinking system further provided a significant approach to greatly establish polymer-based amplification for multiple biological application, such as biodetection assay [51, 52], surface encapsulation or coating on proteins, living cells or tissues.

Our group has developed the generation of polymerized coating on an eosin-immobilized cell surface (Figure 1.3). Previously, we has demonstrated an antigen-targeted polymer coating on eosin-localized fixed fibroblast, suggesting the feasibility to create a dye-loaded film for protein signal amplification on each single cell [55]. This surface free radical polymerization consisting of PEGDA, TEA and VP was further developed to deposit an ultrathin hydrogel film on living mammalian cell encapsulation for different biological purposes. We also examined the feasibility of surface-coated gels to protect cells from immunoattack by evaluating the transport behavior of dextran particles with different molecular weights through the antigen-based polymer coating on individual Jurkat cells. Biotinylated antibody recognition on CD45-expressed Jurkats allowed surface localization of SAEITC to specifically photocrosslink the PEGDA hydrogel on the living cell membrane. The results from diffusion assay interpreted that either PEGDA575 or PEGDA3500 showed complete molecule exclusion of dextran particles with molecular weight higher than 10kDa, suggesting the ability of PEGDA-coated cells to effectively reject the immune attack by host antibody [25].

Through this size-dependent exclusion property, a degradable coating of PEG acrylate monomer was utilized to design an antigen-selective cell sorting system through antigen-specific lysis (ASL). The coating can protect antigen-positive cells from SDS surfactant lysis. By specially targeting EpCAM-positive A549 or CD45-positive Jurkat,

targeted cells can be collected in high purity (over 90%) and maintain their biological functions after coating removal [24]. To thoroughly understand the coating efficacy by this surface-initiated polymerization method, the yields of intact cells using both amine-conjugated and antigen-conjugated biotinylation were investigated after SDS lysing depletion. The cells modified through covalent amine-reacted biotinylation provided at least ten-fold higher eosin density than antibody-tagged cells, resulting in much higher yield (20%) than others (1% for antibody-labeled cells and 0.1% for untreated cells). This evidence clearly showed the role of surface-conjugated eosin is highly dependent on the polymerization efficiency for this cytoprotective coating [23]. In addition to eosin, fluorescein appears to be an alternative surface-conjugated photoinitiator in this photopolymerization coating system. Our lab previously established the PEGDA3500 coating on living A549s through SAEITC-based or FITC/antibody-based photopolymerization. Both coating approaches successfully present the cell protection property under hypotonic conditions [56]. Other than cytoprotective applications, recent work from us also used surface-polymerized cells to improve stem cell retention following myocardial infacrtion. A synthetic acrylate gelatin polymer which provides extracellular tissue adhesion property was generated on the bone marrow cell surface. It was proved that by creating this gelatin coating, we were able to enhance *in vivo* cell localization in the infarcted heart tissues [47]. Importantly, in this dissertation, we will take advantage of this surface-polymerized operation to create a membrane coating with specific functionality that cell itself doesn't possess.

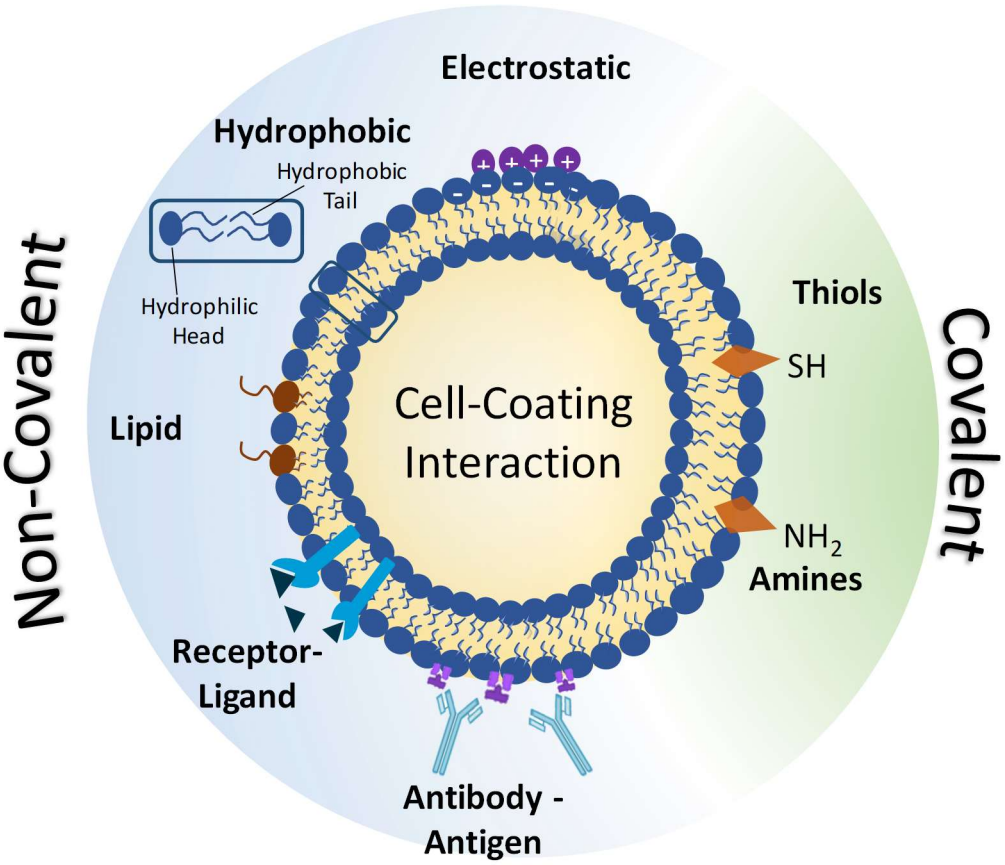

Figure 1-1. Common methods of anchoring coating to a mammalian cell surface. Reprinted from [57], Copyright 2019, with permission from Springer Nature. (https://doi.org/10.1186/s13036-018-0131-6)

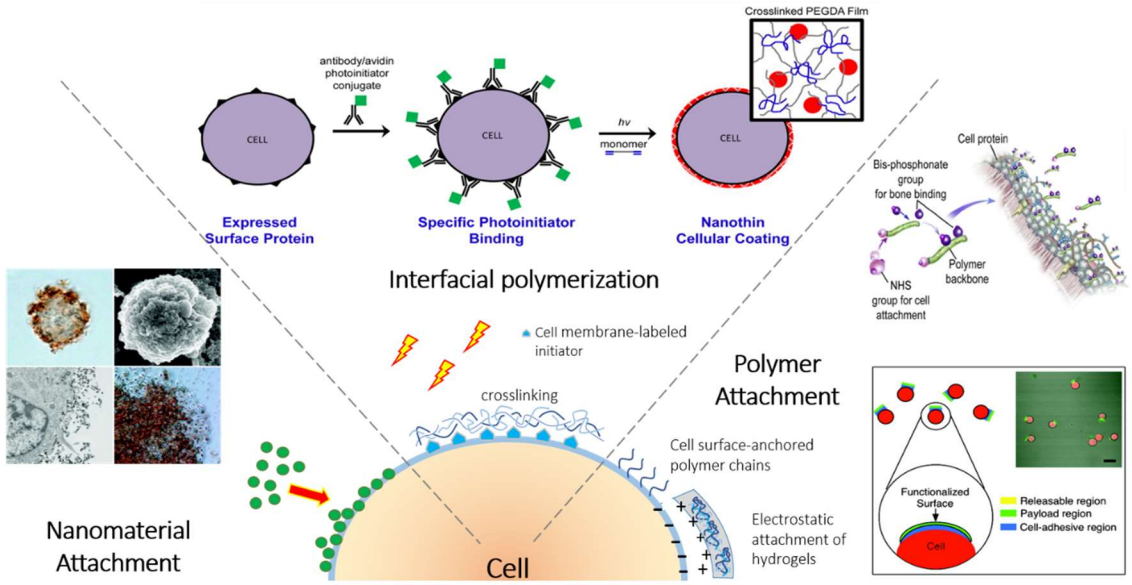

Figure 1-2. Material systems for coatings on mammalian cell surfaces. Reprinted from [57], Copyright 2019, with permission from Springer Nature. (https://doi.org/10.1186/s13036-018-0131-6)

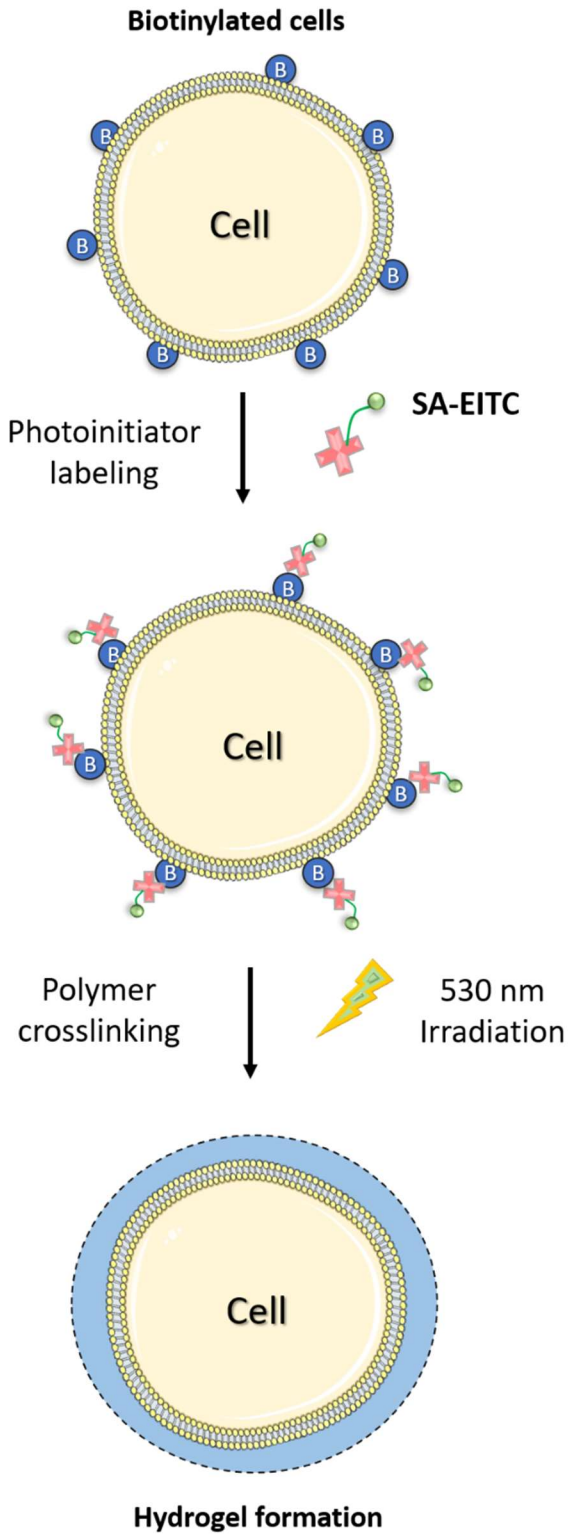

Figure 1-3. The generation of polymer coating on living cell surface through surface-mediated polymerization. The images were obtained from smart servier medical art (https://smart.servier.com/).

CHAPTER 2. CELL SURFACE COATING DESIGNED FOR DRUG DELIVERY

2.1 Introduction

The human body is a complex bioreactor where an intricate chemical balance is maintained through passive and active transport. Modern drug delivery systems have been successful in leveraging our passive transport mechanisms to deliver drugs through the airways, circulatory system, and diverse tissues. Only recently has the research community started to utilize the active transport mechanisms for cell-directed transport of species in the body. Cell-mediated delivery is a revolutionary approach to exploiting natural cell behaviors, which include migration across biological barriers and targeted homing to tumors or sites of inflammation [58-61]. Cellular coatings are emerging as a promising approach for the delivery of a therapeutic payload to a specific site. Therapeutic cargo is attached to the plasma membrane of tissue-targeting transporter cells to enhance site-specific delivery. Here, the chapter highlight the opportunities enabled by the recent clinical and preclinical studies which coated transporter cells are being used for drug delivery applications.

This section will focus on designing cell coatings for the specific applications in drug delivery. The following content presents a minor adjustment of our previously published review article on the journal of biological engineering.

Kara A. Davis,[#] Pei-Jung Wu,[#] Calvin F. Cahall, Cong Li, Anuhya Gottipati, and Brad J. Berron. Coatings on mammalian cells: interfacing cells with their environment. *Journal of Biological Engineering,* 2019. **13**(1): p. 5. (# equal contribution) (https://doi.org/10.1186/s13036-018-0131-6)

2.2 Coating designed to modulate the immune system

In many autoimmune diseases, immune cells mistakenly identify beneficial cells as a harmful species, resulting in chronic inflammation. In the case of multiple sclerosis (MS), cellular coatings have been designed to introduce immunologically-active substances, preventing the immune cells from attacking the normal nerve cells near the site of the brain and spinal cord [62]. A recent clinical study demonstrated the feasibility of antigen-specific tolerance therapy by intravenously transporting antigen-mimicking cells to T cell [63]. For MS, autologous peripheral blood mononuclear cells are coated with myelin antigens are used to stimulate antigen tolerance through interaction with myelin-specific T cells. For early stage patients treated with myelin coated cells, the vital signs and the blood cell composition of the patients were stable and no relapse occurred within 3 months of treatment.

Similar cell coatings were designed to target and deplete the specific T cell populations responsible for diabetic injury [64]. ERY1 peptide linkers were used to coat the surface of erythrocytes with a foreign ovalbumin species. Following intravenous injection, ovalbumin-coated erythrocytes were disproportionately targeted by the dendritic cells capable of indirect antigen specific tolerance. By also incorporating immune-induced antigens onto the surface of these erythrocytes, the cells promoted targeted depletion of the CD4 and $CD8^+$ T cells. These findings were further supported with a type I diabetic mouse model, where antigen-engineered erythrocytes induced clonal depletion of T cells, and the expression of IFN-γ-positive T cells was significantly reduced over ovalbumin-negative controls and ovalbumin alone.

Multiple cell types naturally migrate to the site of inflammation to serve a reparative function. Drug loaded coatings attached to these naturally-homing cells offer a new opportunity to target therapies to the inflamed region. However, the coverage of the entire surface of transporter cells with biomaterials would interfere with the migration and cellular activities of transporter cells throughout the body. Cellular patches were originally proposed by Rubner's group [37, 39] to partially cover the migratory cell with a surface anchored therapeutic material. In this strategy, polyelectrolyte multilayer (PEM) patches containing a magnetic nanoparticle payload were adhered onto the lymphocyte surface. These T cells were nearly 100% viable following patch modification and retained their migratory capacity with the magnetic PEM patch. This innovative idea of partial surface modification is appropriate to allow either T cell interactions involved in immunological responses or drug carrying potential for cell-based drug delivery.

Additional studies in the Mitragotri lab [38] found that PEM-modified multilayer patches on the surface of mouse macrophages had no adverse effects on cell viability, migration, or phagocytic activity towards polystyrene spheres. Optimization of PEM patch size, modulus, and shape enabled prolonged patch attachment on the macrophage surface without internalization. *In vitro* controlled loading of FITC-BSA from polymeric patches supports the feasibility of drug delivery with patch coated cells. Patch-coated and uncoated monocytes both undergo stimulation-induced differentiation into macrophages. The targeting of coated monocytes to inflamed skin and lung tissues was supported in mouse models [65]. Higher accumulation of patch-coated monocytes in inflamed tissue over the patch alone, illustrated that coated monocytes retained their ability to penetrate across barriers to target regions of inflammation.

2.3 Coating designed for cancer therapy

The irregular vessel organization, low oxygen supply, and high interstitial fluid pressure of large tumors impedes the delivery of drugs into large malignant tissues. Currently, the majority of tumor-targeting approaches use liposomes, micro- or nanoparticles, and polymers. However, their insufficient penetration into deep tumor tissues and rapid clearance limits therapeutic efficacy. The use of tumoritropic cells as drug carriers is a promising new approach to deeply penetrate tumor tissues and increase drug efficacy [61].

There are now multiple examples of drug-coated T cells used for tumor-specific targeting of a therapy [66, 67]. T cells, B cells, and natural killer cells all have some level of tumoritropic capacity [68-71]. These immune cells migrate across capillaries and blood vessels to tumor sites by targeting the cytokines released by the cancer microenvironment [66, 67]. Irvine et al coated T cells with liposomes loaded with cytokines promoting help T cell differentiation, growth, and endurance at tumor sites [72, 73]. The nanoparticle (NP) coatings were optimized to minimize any effect on cells' tumoritropic migration *in vitro* and *in vivo*. Later, this team also studied the cell-based delivery of phosphatase-encapsulated lipid nanoparticles to promote T cell expansion through the delivery of T-cell regulating phosphatases [73]. T cells were coated with these therapeutic NPs and used to treat mouse models of human prostate cancer. Mice treated with coated T cells had increased T cell expansion, reduced tumor size, and increased animal survival by 60 days over unmodified T cell groups.

Macrophages are also emerging as a useful tool for cell-mediated penetration into tumor masses. They effectively carry drug-encapsulated liposomes into tumors for

simultaneous imaging and therapeutic delivery [74]. After surface modification of doxorubicin (DOX)-loaded liposomes, these drug-loaded macrophages accumulated at the tumor site of an A549 xenograft tumor in a mouse model. 24 h after injection, accumulation of DOX was significantly higher in mice treated with of liposome-DOX-loaded macrophages when compared to PBS, macrophage, DOX and liposome-DOX-injected controls. The weekly intravenous injection of coated macrophages also decreased the tumor size by around 40% when compared to the DOX control group in the same study.

Many stem cell populations also naturally target tumor sites. Neural stem cells (NSC) are actively studied for the delivery of platinum-based therapies to ovarian tumors [75]. NSCs are coated with a nonporous silica that encapsulates platinum-based drugs and has minimal NSC toxicity. These platinum-loaded particles persisted deep inside in solid tumor masses 24 h following intraperitoneal injection into an ovarian cancer mouse model. These findings support NSCs as an alternative cell carrier for drug loaded coatings into the core of tumor masses. Finally, hMSCs are promising for the delivery of nanoparticle payloads into tumor masses [46]. In one study, NP patches were prepared through the attachment of NeutrAvidin-coated NPs to partially modify the surface of covalently biotinylated hMSCs. Coated MSCs targeted HEPG2 tumor spheroids *in vitro*, and this approach supports the use of nanoparticle-based coatings for cell-mediated tumor targeting.

CHAPTER 3. HYDROGEL PATCHES ON LIVE CELLS THROUGH SURFACE MEDIATED POLYMERIZATION

3.1 Introduction

Many naturally-occurring cells possess an intrinsic ability to cross biological barriers that block conventional drug delivery, and these cells offer a possible mode of active transport across the blood brain barrier or into the core of tumor masses. While many technologies exist to form complete, nanoparticle loaded coatings on cells, a complete coating on the cell surface would disrupt the interaction of cells with their environments. To address this issue, cell surface patches that partially cover cell surfaces might provide a superior approach for cell mediated therapeutic delivery. In this chapter, the goal of this study is to establish a simplified approach to produce polymeric patches of arbitrary shapes on a live cell via surface-mediated photopolymerization. Cell surfaces were nonspecifically labeled with eosin, and PEGDA coatings were directed to specific sites using a 530 nm irradiation through a chrome-coated photomask. These coatings may entrap drug loaded or imaging particles. The nonspecific formation of PEGDA hydrogel coatings increased with irradiation time, light intensity, and initiating species. 40 mW/cm^2 irradiation for 5 min delivered high-resolution patterns on the surface of A549 cells, and these cells remained viable for 48 h post-patterning with fluorescent nanoparticle loaded coatings. This work first demonstrated the feasibility to photo-pattern polymer patches directly onto the surface of cells. The work presented in this chapter has been published in the following peer-reviewed journal paper:

Pei-Jung Wu , Jacob L. Lilly, Roberto Arreaza, and Brad J. Berron*. Hydrogel Patches on Live Cells through Surface-Mediated Polymerization. *Langmuir*, **2017**, *33* (27), pp 6778–6784

3.2 Background

Targeted delivery seeks to minimize off target effects by localizing the therapeutic agent to the site of intended action [76, 77]. Much of the prior work focuses on modifying a therapeutic particle's surface chemistry, targeting ligands, shape, and size [78-80]. Recently, groups have begun loading a therapeutic cargo on the surface of a cell for a targeted effect [39, 81]. For example, stem cell-binding silica nanoparticles have been utilized for delivering doxorubicin to glioma tumor cells [78]. These cell carriers have also delivered encapsulated drugs through the blood-brain barrier and poorly accessible tumor tissues [46, 65] . A significant obstacle in these approaches is the adhesion of drugs to the surface of the transporter cell while not precluding the cell-directed transport throughout the body or interfering with nutrient transportation through the cell membrane [25, 37]. A coating that only covers part of a cell's surface would be capable of drug delivery while still allowing the cells to interact normally with the body. Swiston and Rubner attached polyelectrolyte multilayer patches on lymphocytes without altering their survival, proliferation rate, and normal cell functions [37]. This is the first evidence that cellular patches can confine a drug cargo to a region of a cell's surface. Since then, additional

applications of cell patches have been explored using stem cells for delivery of drug-loaded polymers to tumor tissue [46] or monocytes to deliver payloads to inflamed tissues [65].

A variety of techniques have been developed to produce drug loaded cellular patches. The PEM patches made by Rubner et al. were manufactured as pre-patterned films with a top layer conjugated with a cell binding ligand [37]. A similar concept was applied by Mitragotri to generate multilayered "backpack" on monocytes composed of poly (methacrylic acid), poly (vinyl-pyrrolidone), poly (allylamine hydrochloride) and anionic iron oxide magnetic nanoparticles for delivery to inflamed tissues [38, 65]. The production of cellular patches through these techniques requires multiple time-consuming steps of polymer film formation and conjugation. In an alternative approach, Anderson et al. used sulfosuccinimidyl-6-(biotinamido) hexanoate (sulfo-NHS-LC-biotin) to induce global biotinylation of cell surface protein on hMSCs, followed by high affinity of biotinylated cell surface with NeutrAvidin-labelled polystyrene nanoparticles [46]. A limitation of this technique is that they cannot control the size and shape of the patches, potentially interfering with robust interactions between the cell and the biological environment.

Here, we establish photolithographic patterning of a polyethylene glycol diacrylate (PEGDA) hydrogels as a simple technique to produce patches on cell surfaces. The cell patch approach is based on the eosin mediated photopolymerization of PEGDA, first demonstrated on cell surfaces by the Hubbell lab [82]. The irradiation of visible light (530 nm) on surface immobilized eosin Y in the presence of TEA initiates PEGDA gel formation adjacent to the cell surface. While the Hubbell lab loaded high levels of eosin through nonspecific eosin absorption, our lab has previously synthesized 100 nm thick, non-patterned PEGDA films on cells with lower eosin loadings. Low levels of eosin

conjugation (1,600 – 54,000 eosin/μm^2) are achieved by contacting a streptavidin-eosin conjugate with a cell surface specifically labeled with biotinylated antibodies or nonspecifically labeled with a biotinylated NHS species [24].

In this work, we pattern these coatings on a cell for the first time using standard photolithographic techniques. We first characterize PEGDA hydrogel formation on a microarray of biotinylated proteins on glass. The thickness, specificity, and spatial accuracy of PEGDA pattern formation was evaluated at different irradiation times, intensities, and mask positions. After pattern gelation trends are established on a glass substrate, we then apply nanoparticle loaded patches to A549 cells (adenocarcinomic human alveolar basal epithelial cells). As a potential application, the homing of tumor cells to pre-existing tumor sites [83, 84] offers an opportunity to direct the transport of drug-loaded cells to tumors. A549 cells have been frequently used as an invasive immortalized cell line for non-small cell lung cancer [85, 86]. The thickness and feature resolution of PEGDA patches deposited on the surface of A549 cells was characterized, and the effects of PEGDA pattern formation on cell viability were evaluated. In all, this study investigates the key parameters governing the formation of cellular patches through surface-mediated PEGDA photolithography. When compared to existing patch strategies, the simplicity of this approach decreases the aggregate time and complexity for cellular patch production.

3.3 Experimental section

3.3.1 Materials

Epoxy functionalized slides were obtained from CEL Associates. Bovine serum albumin (BSA), eosin-5-isothiocyanate, phosphate-buffered saline tablets,

triethanolamine, PEG diacrylate 575, 1-vinyl-2-pyrrolidinone and Whatman chip-clip were obtained from Sigma Aldrich (St Louis, MO). Poly (ethylene glycol) diacrylate 8000 was purchased from Alfa Aesar. Ethyl alcohol (200 proof) was purchased from Pharmco-aaper. Biotinylated bovine serum albumin, streptavidin, trypsin/EDTA, ethidium homodimer-1, yellow-green or nile red fluospheres, collagen I rat protein, sulfo-NHS-LC-biotin, 16% paraformaldehyde aqueous solution and DAPI were purchased from Thermo Fisher scientific. LED lamp with 530 nm wavelength (M530L2-C1) and neutral density filter (NE260B) were purchased from Thorlabs. Biotin anti-human EpCAM was purchased from BioLegend. The photomask used for surface patterning was a chrome-coated glass mask purchased from Louisville Photomask. RPMI-1640 cell culture media was purchased from Cellgro and supplemented with 10 v/v% fetal bovine serum (FBS, Gibco, Carlsbad, CA), 100 U/mL Penicillin, 10 mg/mL Streptomycin (Gibco) prior to use. Adenocarcinomic human alveolar basal epithelial cells (A549) were purchased from Lonza (Basel, Switzerland). 1X PBS was prepared by dissolving phosphate buffered saline tablets in ultrapure water according to the manufacturer protocol. Streptavidin-eosin was prepared as described previously[87]. PBSA was prepared by adding 1 mg/mL bovine serum albumin to 1X PBS.

3.3.2 Eosin conjugation of biotin-immobilized microarrays

Biotinylated microarrays consisted of an epoxide-coated glass substrate, and serial dilutions of biotinylated bovine serum albumin (bBSA, from 1000 to 0.105 μg per mL in PBS) were printed on array surface by GMS Affymetrix 417TM Arrayer. Each concentration of bBSA was duplicated into two spots. After array printing, the slides were dried overnight at room temperature and then were stored in a microscope slide storage

box until use. For each microarray experiment, the bBSA-printed slide was loaded in Whatman Chip-Clip slide holder, and each Chip-Clip array well was blocked with PBSA for 45 min to reduce non-specific interaction on unprinted sites. Array wells were then incubated in streptavidin-eosin (25 μg/mL in PBS) for 30 min.

3.3.3 Culture and eosin photo-initiator conjugation of A549 cells

The A549 cell line was cultured in RPMI-1640 medium containing 10v/v% FBS and 1% streptomycin/penicillin at 37ºC incubator with 5% CO_2. Cells were cultured between 80 and 90 % confluency, and trypsinized prior to use with 0.25% trypsin-EDTA (Thermo Fisher) in sterile PBS for 5 min. Glass microscope slides (25mm x 75mm) were sterilized in a conical tube by immersion in 200 proof ethanol overnight before cell culture. After drying and sterilization, slides placed in a 100 mm petri dish were rinsed with sterilized PBS twice and incubated with 415 μL collagen I rat protein solution in 20 mL PBS at room temperature for 1 h. Approximately 5 million cells were cultured on the collagen-covered slides within a cell culture dish. After cell attachment, cells were cultured until >90% confluency for polymerization studies.

A549-cultured slides were gradually lowered in temperature prior to incubations on ice. Specifically, slides in culture dishes were incubated in 25 mL fresh cold medium and placed at room temperature for 10 min and then on ice for 20 min, washed with ice cold PBS and then loaded into a Whatman slide holder. Each cell well on Whatman Chip-Clip was rinsed with 400 μL PBS three times. After rinsing, a freshly prepared biotinylation solution of 1 mM sulfo-NHS-LC-biotin was added to the cells for 30 min. Biotinylated cells were rinsed with cold PBS three times and incubated with 35 μg/mL streptavidin-

eosin in PBS for 30 min. After photoinitiator conjugation, cell slides were rinsed with PBS three times.

3.3.4 Non-patterned polymerization of PEGDA on biotin-immobilized microarrays

PEGDA monomer was composed of 25 w/v% PEG diacrylate 575, 21 or 210 mM triethanolamine, and 35 mM vinyl pyrrolidinone. Irradiation conditions were 20, 30, or 40mW/cm^2. The thickness of PEGDA hydrogel on microarray system was observed by Dektak 6M stylus surface profilometer. The estimation of PEGDA hydrogel thickness by fluorophore was performed by the addition of yellow green fluospheres (2.5 v/v%, Life Technology) into the PEGDA monomer solution. The fluorescence of yellow green fluospheres was obtained by Nikon Eclipse Ti-U microscope with filter set of 470/535 excitation /emission. Fluorescence intensity was quantified by image analysis using ImageJ software.

3.3.5 Photo-lithographic polymerization of PEGDA hydrogel patches on biotin-immobilized microarray or adherent live cells

For PEGDA hydrogel patches formation, bBSA-immobilized epoxy microarray or biotinylated A549 cell surface provided binding sites for streptavidin-eosin conjugation. For photolithographic polymerization, the slide (microarray or cell slide) was separated from the photomask with two 40 μm thick spacers, and this assembly was held together with binder clips. The photomask features consisted of 10 μm thick chrome stripes separated by 28 μm spaces. For microarray polymerization, a neutral density filter was attached under the glass slide to minimize reflection of the light, and the monomer solution was a solution of 25 w/v% PEG diacrylate 575, 21 or 210mM triethanolamine, 35 mM vinyl pyrollidinone and 2.5v/v% yellow green Fluospheres in deionized water. For patch

polymerization on live A549 cells, the monomer solution contained 10 w/v% PEG diacrylate 8000, 21 mM triethanolamine, 35 mM vinyl pyrollidinone and 2.5 v/v% yellow green fluospheres in PBS, and the pH was adjusted to 7.4 with the addition of 1.2 molar hydrochloride, as needed. Monomer solutions were bubbled with ultrapure nitrogen in the dark for 10 min before photopolymerization. For polymerization, the PEGDA monomer solution was pipetted into the space between the slide and photomask. The whole photomask assembly system was purged with nitrogen for 3 min. The photomask-assembled slide was then irradiated under visible-light exposure with peak wavelength of 530 nm with continuous ultra-pure nitrogen purge. The desired light intensity and irradiation time period was selected as a parameter for polymerization. After irradiation, microarray slides were gently rinsed with deionized water, blown dry with house air, and stored in a microscope slide box. Polymerized cell slides were gently removed from the photomask assembly, re-loaded into Whatman chip-clip, and rinsed with PBS three times. Images of hydrogel patches were obtained by epi-fluorescence microscopy (Nikon Eclipse Ti-U).

3.3.6 Statistical analysis for microarray hydrogel polymerization

The fluorescence intensity of nanoparticle-loaded hydrogel patterns was quantitated through image analysis using the Image J software. For determination of the hydrogel pattern accuracy, the normalized sum of squared error and mean peak intensity were calculated by a custom Matlab program. The experimental data of fluorescence intensity distribution was normalized and were input into a custom Matlab script to fit a Gaussian function to the fluorescence data. The midpoint of the Gaussian curve was considered the midpoint of the pattern. The mean peak intensity was determined by the

mean of the four data points closest to the pattern midpoint. The normalized ideal pattern is defined as a 10 μm wide step function with a magnitude equal to 1. The normalized pattern data was determined by scaling the fluorescent intensity data to a maximum of 1. The normalized sum of the squared error (Normalized SSE) is defined as the squared difference between normalized pattern data and normalized ideal pattern.

3.3.7 Membrane integrity assay after hydrogel patch polymerization on A549 cells

After polymerization and rinsing, photopatterned cells were incubated in 2 μM ethidium homodimer (Life Technologies) diluted in 3 v/v% FBS in PBS for 30 min. Single channel images were obtained by epi-fluorescence microscopy (Nikon Eclipse Ti-U) and merged by Image J software.

3.3.8 PEGDA hydrogel formation on fixed A549 cells

A549 cells were grown to ~90% confluency on sterilized glass microscopy slides. Cells were washed 3 times with cold PBS, then fixed with 1% paraformaldehyde for 10 min, then washed 3 times again with cold PBS. Slides were blocked with 1% BSA in PBS for 40 min. Cells were stained with 10 nM DAPI in PBS for 10 minutes and rinsed 3 times with PBS. Slides were then immersed in biotin anti-human EpCAM at 1:100 dilution in PBS+ 1%BSA for 40 minutes. Slides were rinsed 1 time with PBS+ 1%BSA then immersed in PBS+ 1%BSA with 25 μg/mL SA-EITC for 30 minutes. The slides were then rinsed 3 times with PBS and clamped to a chromium/glass photomask with a 40 μm spacer. A monomer precursor solution was injected into the photomask setup which consisted of 420 mM PEG-diacrylate (Mn ~575), 210 mM triethanolamine, 35 mM vinyl pyrrolidinone, and 0.05 wt% nile red Fluosphere nanoparticles. The entire setup was then exposed to 10 mW/cm^2 green LED light (Thorlabs) for 10 minutes and rinsed 3 times with

DI water. After drying, the slides were imaged with an inverted epifluorescent microscope at 20X objective.

3.4 Results and discussion

Cellular patch fabrication typically consists of patterned layer-by-layer coating fabrication, adhesion onto the cell surface, and release of the assembly from the substrate.[37, 46] In this study, we provide a unique approach for the formation of a drug-loaded polymer patches through direct photopolymerization of a nanoparticle-loaded polymer depot on the surface of a live cell. We expect the photo-polymerization of hydrogel cellular patch to have the following attributes: (a) patch fabrication in a physiologically-compatible environment; (b) direct hydrogel production onto a portion of cell membrane without multistep coating prefabrication; (c) highly controllable patch geometry fine-tuned by irradiation conditions and photomask features. To create geometrically-controlled polymeric film on the cell's surface, we take advantage of the high affinity between biotin and streptavidin to localize eosin on the cell surface. Cell surface biotinylation is attained through labeling surface proteins with sulfo-NHS-biotin, and the biotinylated cell surface is contacted with streptavidin-eosin to immobilize low concentrations of eosin on the surface. A photomask with striped chrome features is placed above adherent A549 cells, and the gap between the cells and the photomask is filled with a PEGDA monomer solution. The surface-mediated photopolymerization of PEGDA hydrogel patches proceeds with green light irradiation at a wavelength of 530 nm (Figure 3.1).

3.4.1 Characterization of PEGDA film polymerization parameters

The fabrication of PEGDA cellular patches requires a careful balance of gelation in irradiated regions with soluble macromolecular species in dark regions. The surface-mediated photopolymerization of PEGDA is controlled by multiple key parameters: the wavelength and intensity of light for photoinitiator excitation, irradiation period, composition of monomer and co-initiator, and the density of photoinitiators on the cell surface. These parameters alter the rate of polymer gelation on the cell membrane. In addition to the complex parameters which govern PEGDA film formation, cells have irregular geometries which limit our capacity to directly measure PEGDA pattern thickness on cells. To better characterize PEGDA film formation for eventual use on live cells, we first utilized an epoxy microarray system without a photomask to characterize how these same parameters dictate PEGDA film formation. Based on these results, we identify target conditions for cellular patch construction.

Biotinylated bovine serum albumin (bBSA) microarrays were prepared with serial biotin concentrations from 0 to 1000 μg/mL bBSA, where these surfaces were made to represent the possible biotin concentrations on our target cell surfaces [24]. These microarray surfaces were treated with precursor solution (25 w/v% PEGDA575, 21 or 210 mM TEA, 35 mM VP and 2.5 w/v% yellow-green nanoparticles in deionized water), and exposed to green light (530 nm) under different irradiation conditions (20, 30, and 40 mW/cm^2 for 2.5, 5, and 10 min). The profilometric thickness of PEGDA film generated based on bBSA concentration gradient was described in Figure 3.2 A With different irradiation conditions, PEGDA hydrogels were thickest (250 ± 8 nm) under 10 min, $40mW/cm^2$ irradiation using 210 mM TEA (Figure 3.2 B). With the same TEA

concentration and irradiation time, lower irradiation intensity (30mW/cm^2 and 20mW/cm^2) produced lower peak thickness (182 ± 4 and 177 ± 4 nm, respectively). Despite the similar peak thickness at high bBSA, 20mW/cm^2 irradiation had consistently lower hydrogel thickness with lower bBSA concentration. Furthermore, under 21 mM TEA, same irradiation conditions produced lower hydrogel compared to 210 mM TEA (Figure 3.2 C). Taken together, these results supported that the thickness of the polymer are predictably controlled by all controllable parameters of the initiation system: the density of eosin conjugation, the irradiation energy, and the amine coinitiator concentration [50, 52, 53].

3.4.2 Fluorophore-labeled PEGDA for thickness estimation

For the measurement of PEGDA photopatterned coatings, our profilometer lacks adequate resolution for PEGDA film features that are less than 1 μm wide because of stylus tip radius is ~12 μm. To overcome this limitation, we correlated the fluorescence of embedded nanoparticles to the thickness of a PEGDA films on large features [24], and we used this correlation to determine submicron feature geometries by epifluorescent microscopy. We included 2.5 v/v% of yellow-green nanoparticles to become nonspecifically embedded into the hydrogel during polymerization. Fluorescence was highly proportional to the actual PEGDA film thickness from 20 to 150 nm (Figure 3.2 B). This is consistent with our previous report which used fluorescent intensity to estimate of hydrogel thickness [24]. Furthermore, the fluorescence of yellow green was sufficient to detect polymer thickness below 50 nm, supporting the feasibility of quantifying PEGDA pattern height over the relevant thickness scales for surface mediate polymerization of PEGDA coatings.

3.4.3 Parameters governing the specificity of gelation in irradiated and non-irradiated regions

To better describe the relationship between the irradiation parameters and localized gelation via surface mediated polymerization, a chrome photomask was used to restrict the irradiation to 10 μm stripes on microarrays of biotinylated surfaces (1000 μg/mL). Figure 3.3 schematically describes the photomask system, and a photograph of the system is provided as Figure A.3. The spacers separating the photomask from the microarray were 40 μm thick for all data shown, while preliminary studies with thicker spacers had lower feature resolution (60, 80 and 100 μm, Figure 3.4). Fluorescence microscopy was used to observe the spatial distribution of the fluorescence of yellow-green NPs labeled hydrogel patches in a 1 mg/mL bBSA printed microarray spot. Both brightfield and fluorescence (ex/em 470/535 nm) microscopy confirm that 10 μm green striped hydrogel patterns were confined to regions within the photoinitiator-bound array spots (Figure 3.3). The localization of polymer stripes to circular regions confirmed the polymerization was driven by specific binding of eosin to the microarray spots.

The intensity of fluorescence in both irradiated and non-irradiated regions of the array spot was analyzed by imageJ. The intensity was then converted to an estimated thickness based on the fluorescence-thickness relationship curve described in Figure 3.2 C. The thickness at non-irradiated regions was consistently < 5 nm and was not dependent on light intensity and irradiation period (Figure 3.5). To reduce the light reflection at the back side of the glass substrate, a neutral density filter was applied to decrease polymer formation in non-irradiated regions of array spots (Figure 3.6).

For the irradiated region of the array spot and a 2.5 min irradiation period, there was extremely low thickness (<5 nm) showing that no observable polymerization occurred for intensities up to and including 40 mW/cm^2 (Figure 3.7B). For the irradiated regions using light intensities of 30 and 40 mW/cm^2 with times of 5 or 10 min, the thickness was considerably higher (>30 nm). In contrast, when light intensity was lowered to 20 mW/cm^2, almost no polymer film was generated. The polymer thickness increased with both light intensity and irradiation time, and these trends are consistent with unpatterned coatings (Figure 3.2B). In all, there is a strong relationship between coating thickness and irradiation intensity and time within the irradiated area (Figure 3.7B), while the non-irradiated area is largely independent (Figure 3.5). However, there was lower polymer formation under neutral density filter compared to polymerization without the neutral density filter (Figure 3.2 and Figure 3.7). The lower thickness is consistent with a lower contribution of reflected light to the irradiation regions, creating a compromise between improved feature sharpness and overall polymer thickness. In all, these trends support a parameter space for successful pattern formation: 5-10 min irradiation at 30-40 mW/cm^2.

3.4.4 Analysis of coating feature edge sharpness

To quantify the accuracy of the pattern transferred from the photomask to the polymer patch, a normalized sum of square error (SSE) was calculated between the experimental topography and an ideal step pattern (Figure 3.7A and 3.7B). The SSE of the patterned PEGDA film increased with both irradiation intensity and duration (Figure 3.7C). In general, the polymer features were larger than the ideal dimensions, and this excess polymerization is attributed to the diffusion of oligomers and actively polymerizing chains into adjacent non-irradiated areas. Our data shows 40 mW/cm^2, 5 min of irradiation

generated the PEGDA film with over 50 nm thickness, which is sufficient to load nanoparticles [54], but also with modest SSE compared to 40 mW/cm^2, 10 min or 30 mW/cm^2, 10 min. In all, high irradiation intensities coupled with low exposure times are supportive of thick polymer coatings and high feature accuracy.

3.4.5 Parameters governing PEGDA pattern formation and viability on A549 cells

To generate PEGDA film on cell surface, A549 cell surfaces were first biotinylated with sulfo-NHS-biotin. Then, slides with biotinylated A549 cells were inserted into the same apparatus described in Figure 3.3A. To minimize monomer toxicity, we used PEGDA 8000 as the monomer unit for cell surface PEGDA hydrogel photopatterning. PEGDA monomers with higher molecular weights have shown to generate less stress and more biocompatible [88]. A lower concentration of TEA (21 mM) was used for cell surface PEGDA hydrogel formation because higher concentrations (210 mM) are toxic to the cells [25]. PEGDA hydrogel are successfully patterned onto A549 cells with monomer solution 25 and 15 w/v% PEGDA 8000 polymerized under 40 mW/cm^2 for 5 min, but these conditions also correlated with significant amount of cell death in the irradiated region where PEGDA polymer was generated (Figure 3.8). 10 w/v% of PEGDA 8000 was sufficient to polymerize PEGDA patterns as evidenced by fluorescence signal of yellow green nanoparticle loading, but with much lower cell death rate (Figure 3.9). Most importantly, A549 cell survival rate was not affected after 48 hours of incubation followed by PEGDA patch generation. As such, photopolymerization is capable of generating partial polymer coatings onto live cells in a rapid manner. Furthermore, the shape of the patch is modified through the selection of an appropriate photomask. Stripes of 10, 20, and

40 μm pitch and circles of 5 and 20 μm are easily achieved on cellular substrates (Figure 3.10).

3.5 Conclusions

This study provides a feasible approach to control the shape of PEGDA hydrogel films on live cells. Also, in contrast to existing methods, our approach avoids multiple, time-consuming fabrication processes required in advance of the patch deposition. Most importantly, PEGDA patches formed through photomask-governed photopolymerization does not impact the survival of cells, suggesting the potential use of these coatings as biologically-guided, drug delivery vehicles. Further investigation is justified to determine the effects of these patches on cell biological functions and to conjugate therapeutic nanoparticles into these cell patch matrices for therapeutic applications.

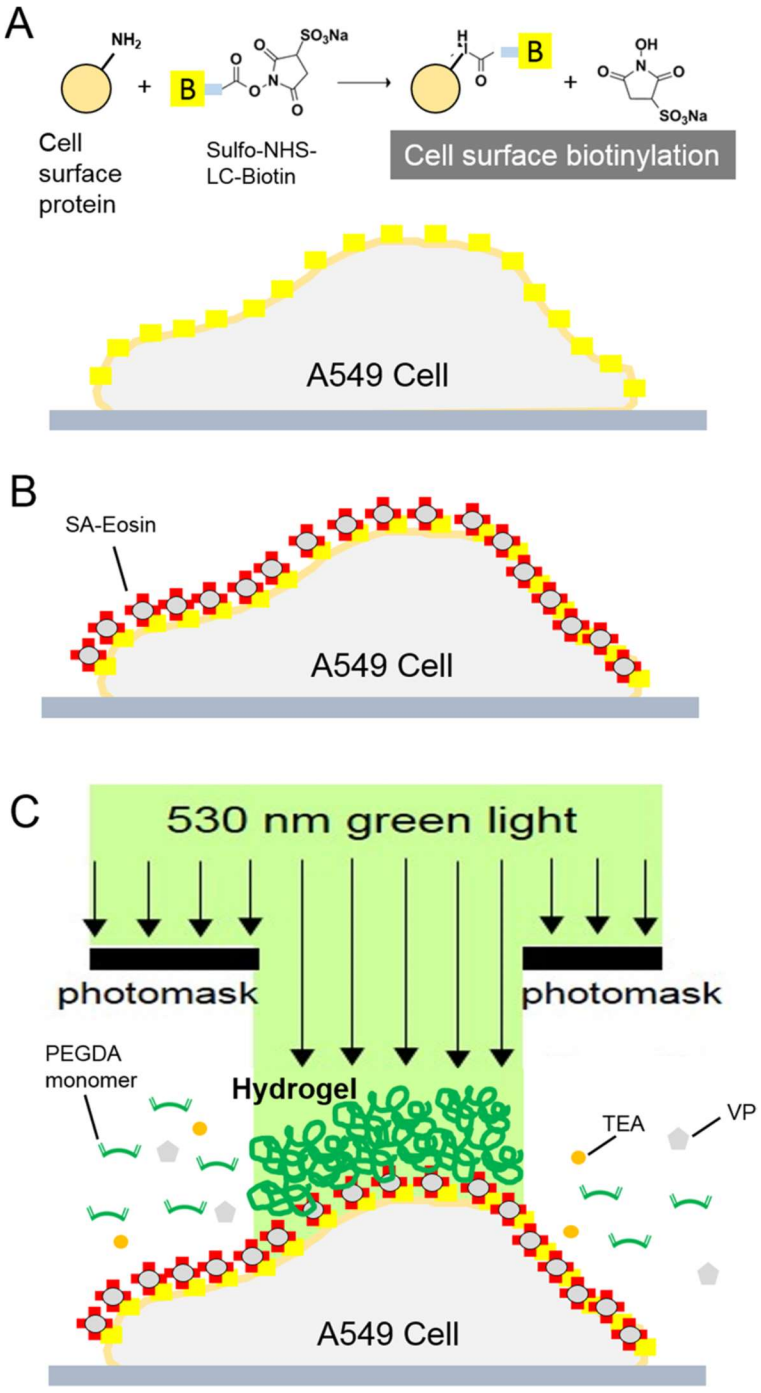

Figure 3-1. Schematic description of A549 cell surface patch photopolymerization. (A) Cells are cultured on the collagen-coated slide, and cell surface proteins are targeted and biotinylated by sulfo-NHS-biotin. (B) Cell surface biotin is conjugated with the streptavidin− eosin conjugate. (C) The PEGDA monomer solution is injected into the gap between the photomask and cell slides. Formation of PEGDA hydrogel patches is photopolymerized in the presence of the photomask, which allows only light passing through the restricted irradiation region to trigger photopolymerization. TEA denotes triethanolamine, and VP denotes 1-vinyl 2-pyrrolidinone.

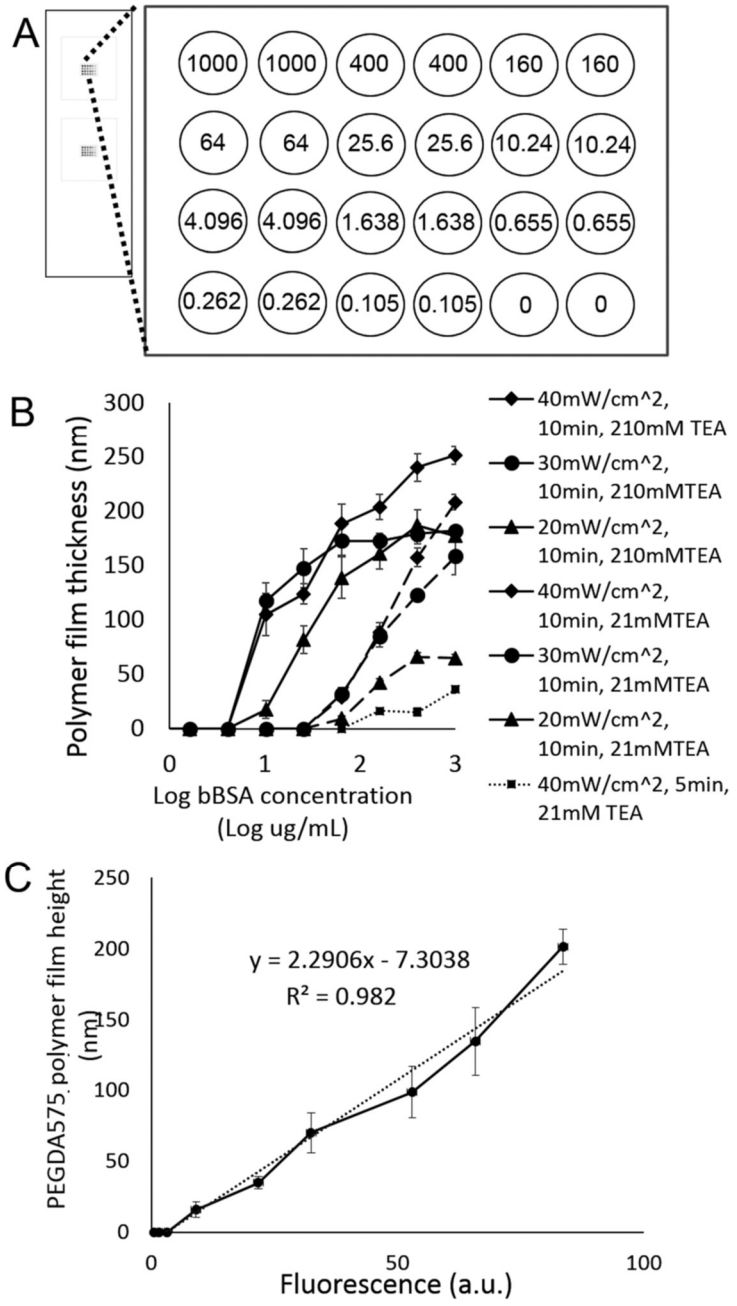

Figure 3-2. Epoxy microarray system for characterizing PEGDA hydrogel formation via photopolymerization. (A) Arrangement of the bBSA microarray on an epoxy microscope slide. Twelve concentrations of bBSA were printed from 1000 to 0 μg/mL, and each concentration has two replicates. (B) Relationship between the log bBSA concentration and the PEGDA 575 hydrogel thickness under various light intensities, TEA concentrations, and irradiation times. Data are given as means ± the standard error of the mean (SEM). (C) Relationship between fluorescence and polymer film thickness. Data are given as means ± SEM. The fluorescence was contributed by yellow-green nanoparticle loading in a PEGDA 575 hydrogel.

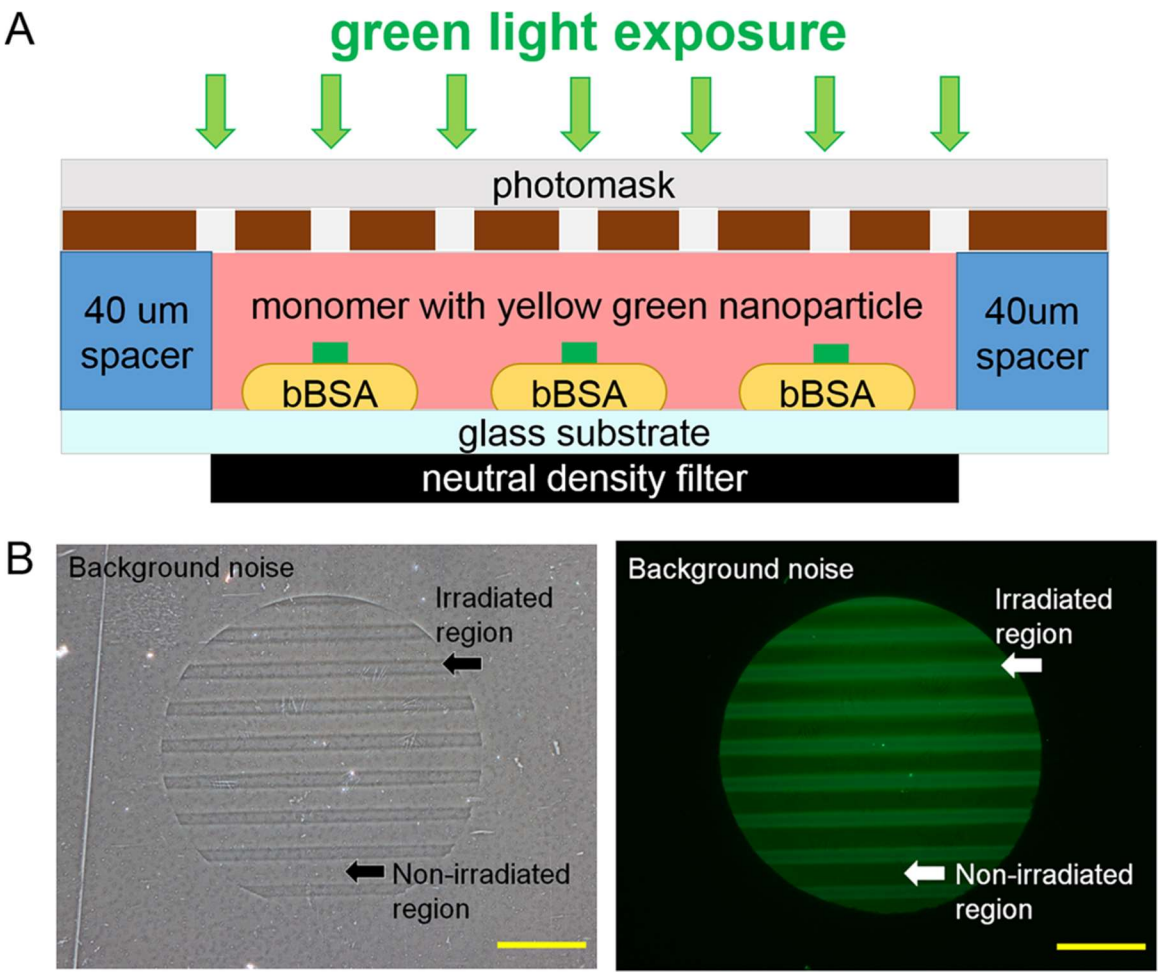

Figure 3-3. Photopatterned PEGDA hydrogels in a microarray format. (A) Schematic diagram of the experimental setup of the photomask covering a biotinylated BSA-printed epoxy microarray. (B) Bright field image of patterned PEGDA hydrogels (left) and epifluorescent image of patterned PEGDA hydrogels stained with green fluorescent particles (right). The photomask had 10 μm wide irradiated regions. The spacer thickness is 40 μm. The scale bar is 100 μm.

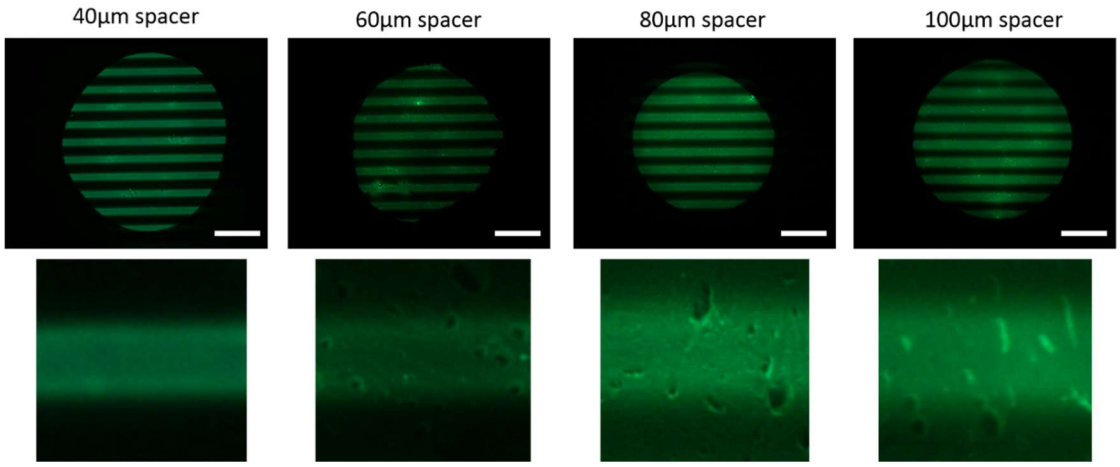

Figure 3-4. PEGDA 575 stripe patch polymerized with different thickness of spacers. The spacers used for photomask setup are 40, 60, 80 and 100 µm, respectively. Scale bar is 100 µm.

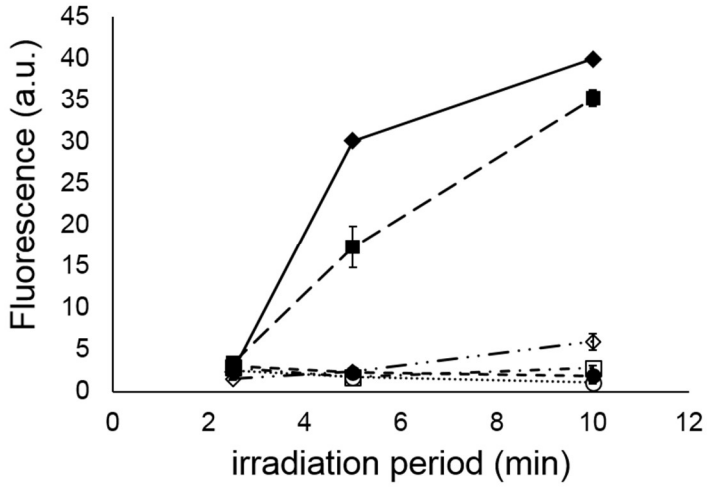

Figure 3-5. Relationship between fluorescence intensity of PEGDA 575 pattern and irradiation period. For fluorescence at irradiated regions, close diamond: 40 mW/cm^2; close square: 30 mW/cm^2, and close circle: 20 mW/cm^2) and irradiation period (2.5, 5 and 10 min). For fluorescence at non-irradiated regions, opened diamond: 40 mW/cm^2; opened square: 30 mW/cm^2, and opened circle: 20 mW/cm^2) and irradiation period (2.5, 5 and 10 min).

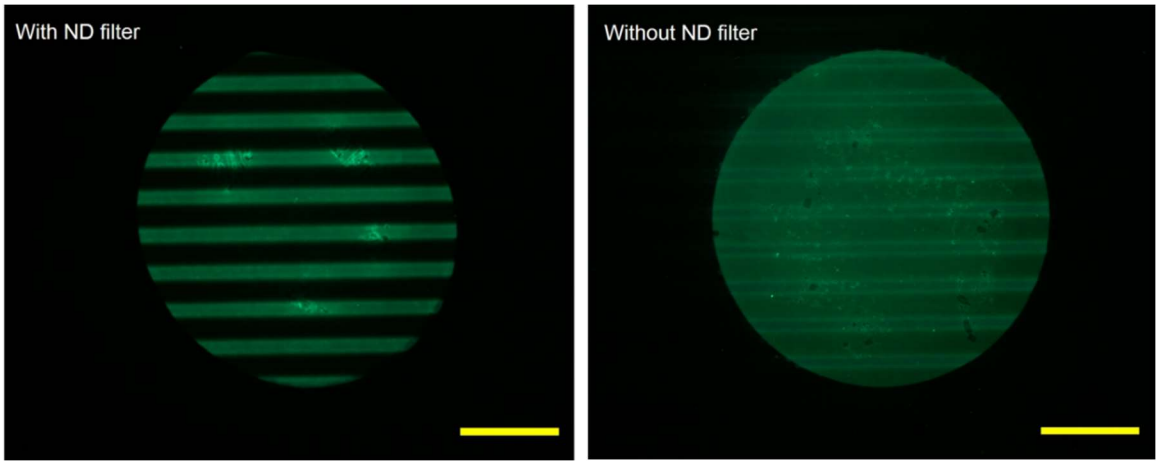

Figure 3-6. PEGDA 575 photopatterned patches on microarray spots with and without the use of neutral density filter. Scale bar is 100 μm.

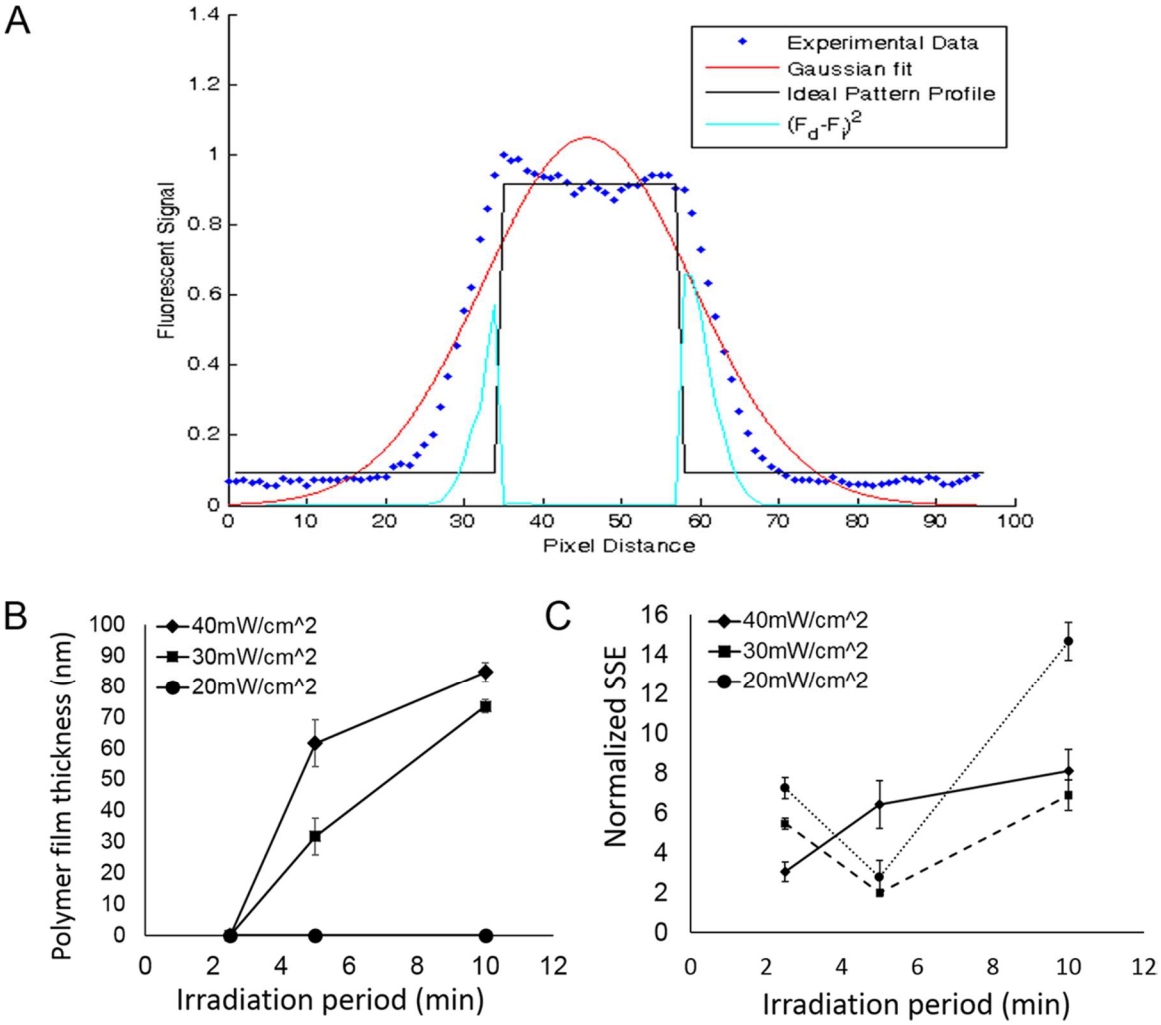

Figure 3-7. Analysis of PEGDA hydrogel formation rate and accuracy. (A) Schematic graph from Matlab analysis of the sum of the square error for PEGDA of photopatterning. The dark blue dots are input data of normalized pattern fluorescence. The Gaussian fit (red curve) was used to fit the data to obtain the midpoint of experimental results. Four data points near the center were averaged to determine the normalized fluorescence value of the ideal pattern profile. SSE was calculated by the square difference between experimental data and ideal pattern value. The light blue line presents the value of SSE for each data point. (B) Relationship of PEGDA 575 gel pattern thickness and irradiation period under different light intensities. The nanoparticle-loaded PEGDA hydrogel was polymerized under various light intensities [(◆) 40, (■) 30, and (●) 20 mW/cm^2] for various irradiation periods (2.5, 5, and 10 min). The fluorescence of the hydrogel pattern was analyzed by imageJ and then converted to polymer thickness according to the relationship between fluorescence and polymer film height. (C) Relationship between normalized SSE and irradiation period under different light intensities. The normalized SSE of the hydrogel pattern was analyzed by Matlab: (□) 40, (···) 30, and (---) 20 mW/cm^2.

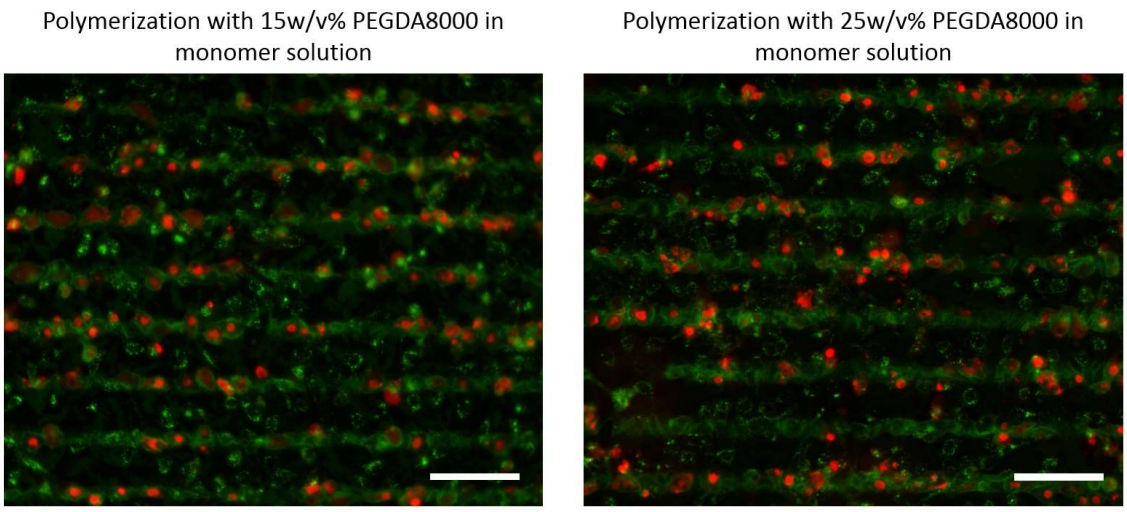

Figure 3-8. Cell viability after hydrogel patch formation with 15 and 25 w/v% PEGDA8000 loading. After polymerization, cells were immediately stained with ethidium homodimer. The red fluorescence showed that large number of cells at irradiated region were dying with higher concentration of PEGDA 8000 monomer.

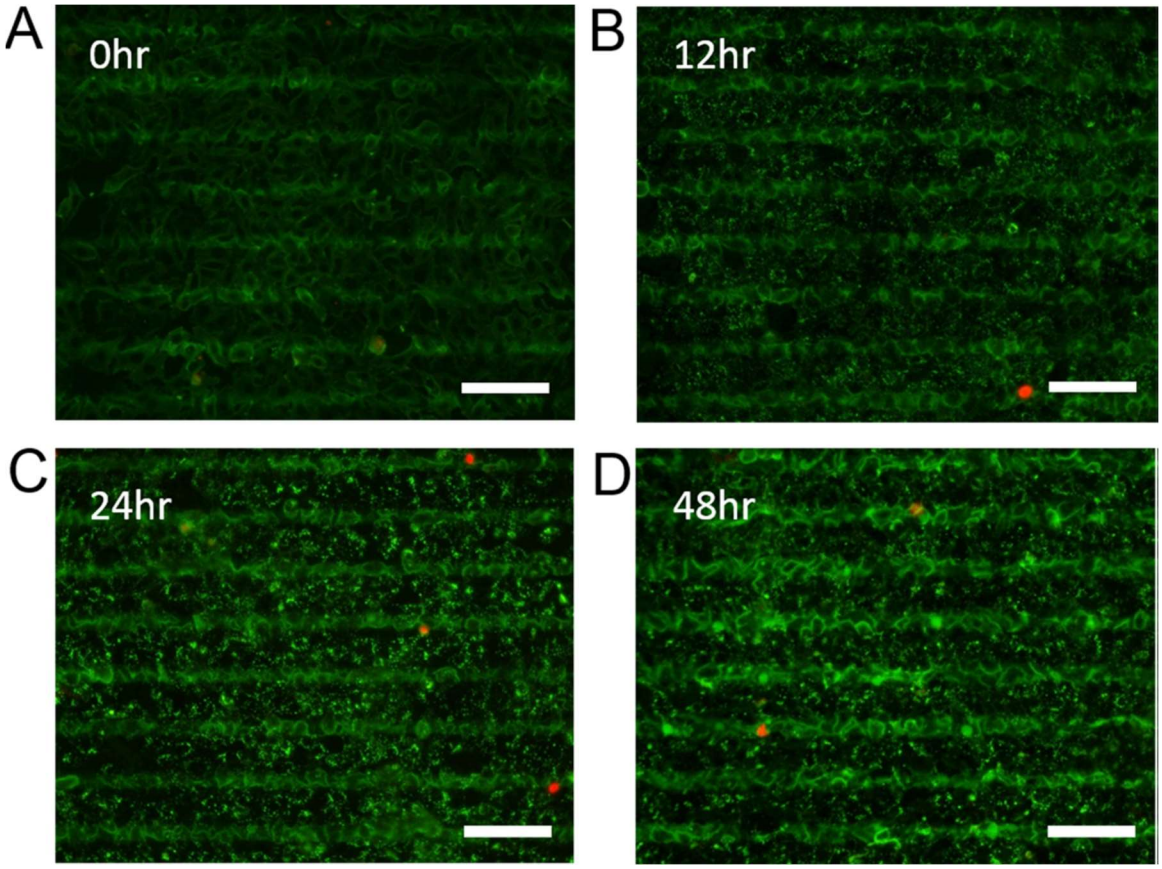

Figure 3-9. Cell membrane permeability following hydrogel patch formation. The PEGDA 8000 hydrogel patches were polymerized under 40 mW/cm^2 for 5 min. The TEA concentration was 21 mM. After polymerization, cells were (A) stained with ethidium homodimer immediately or incubated in medium at 37 °C with 5% CO_2 for (B) 12, (C) 24, or (D) 48 h. The green fluorescence resulted from the yellow-green loaded hydrogel patches on the surface of adherent A549 cells. The red fluorescence indicates the complexation of the ethidium homodimer with cellular DNA in the nucleus of a compromised cell. The scale bar is 100 μm.

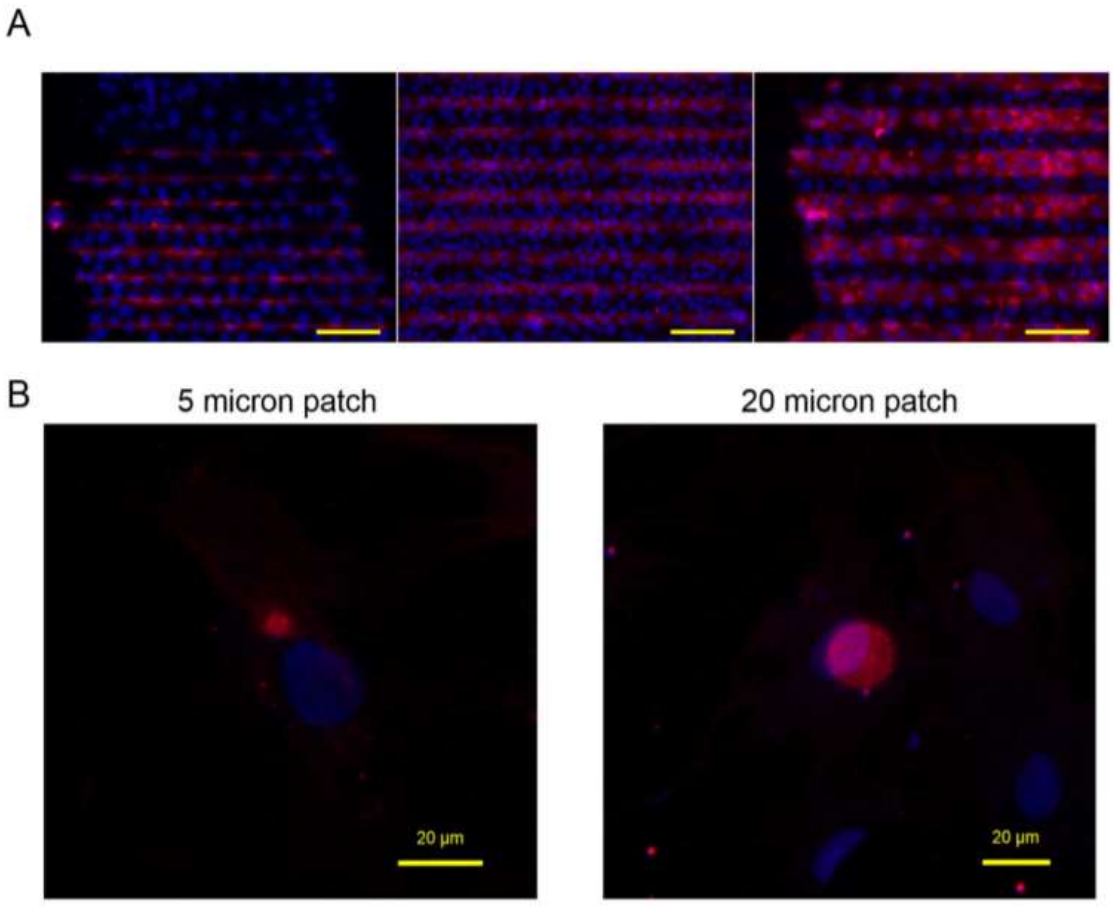

Figure 3-10. Hydrogel patch formation with different photomask geometries. Under fixed cell system, nuclei were stained using DAPI, and nile red fluorosphere-loaded PEGDA hydrogels were patterned based on different features of photomask: (A) stripe shape with width of 10, 20 and 40 µm; scale bar is 100µm; (B) circular shape with diameters of 5 and 20µm; scale bar is 20µm.

CHAPTER 4. BIO-INTERACTIVE COATING FOR MSC-BASED MYOCARDIAL INFARCTION THERAPY

4.1 Introduction

Myocardial infarction (MI) is a global mortal and morbid disorder that can lead to a series of cardiac abnormalities, such as reduced left ventricular (LV) ejection fraction, abnormal LV volume, cardiomyopathy and scarring formation, or, even worse, other acute systemic diseases, such as kidney failure, stroke, or angina. MI occurs when blood clots acutely block the coronary artery, resulting in the lack of oxygen and nutrient supply to local tissues. The decreased oxygen level chronically present in the cardiac environment seriously endangers functional myocardium, negatively affecting their viability and contractibility for preserving regular cardiac activities. At present, long-term cardiac treatment has only been through passive strategies by either controlling multiple cardiac risk factors such as the level of blood glucose, blood pressure and cholesterol to regulate cardiac functions, or offering some anti-thrombotic and anti-platelet drugs to prevent blood clots. Although these therapeutic methodologies can moderately relieve the burden on the heart, they still cannot repair damaged myocardial functions, reduce scarring formation or rejuvenate necrotic cardiomyocytes. Therefore, the use of regenerative stem cells has led to new generation of regenerative therapy, especially for therapeutic homing to damaged tissues.

While stem cells allow specialized cell differentiation, local adherence of these therapeutic cells to a targeted tissue location after transplantation is highly limited due to the absence of homing ligand on cell surfaces. Thus, tailoring stem cell membranes with specific targeting reagents can provide functional characteristics which actively direct

modified cells to the targeted destination. This chapter will first discuss therapeutic roles of MSCs through either immunomodulation or differentiation methods in MI therapy. Secondly, current surface coating techniques with targeting materials such as antibody or ligands will be discussed to localize inflamed or infarcted tissues for MI treatment, providing a basic understanding of material selection and targeting parameters to assist tissue targeting efficacy. At last, the chapter will also focus on present cell surface coating techniques that simultaneously satisfied the need of disease targeting effects and the retention of intrinsic therapeutic functions on treated cells.

4.2 Stem cell-based therapy for myocardial infarction

Occlusion to cardiac blood flow creates acute ischemia and a persistent hypoxic environment. Based on the cardiomyocyte's inability to self-regenerate and repair, cardiac ischemia leads to severe necrosis and a permanent decrease in contractility. While various reperfusion efforts showed reduced infarct size and modestly improved vascular endothelial functions [89], there is no effective clinical methodology to compensate the irreversible loss of cardiomyocytes after MI. As a result, therapies which protect or regenerate tissues post MI are of the utmost urgency.

Several stem cell therapies are promising for the treatment ischemic heart diseases due to their capacity for differentiation, regeneration, and modulation of inflammation. Several types of stem cells, such as hematopoietic stem cells [90], skeletal muscle stem cells [91, 92], bone marrow cells [93, 94], cardiac stem cells [95]and MSCs [96], have been broadly utilized in cardiovascular therapy. The infusion of progenitor cells, bone marrow-derived stem cells and MSCs to damaged tissues have been proposed to support

normal biological functions of the heart following an ischemic event. Moreover, the delivery of therapeutic MSCs effectively improve the contractility and functionality of cardiac muscles, encouraging future use of MSCs for protection of heart function.

4.3 Mechanism of MSC-based cardiac protection

4.3.1 MSC-induced Immunosuppression effects

Accumulating evidence supports the use of MSC-based cardiac therapies in an immunosuppressive role to protect health myocardial tissue. The introduction of MSCs in buffer to an infarcted heart reduces the scar size and increases cardiovascular function over the introduction of buffers alone [97, 98]. Excessive immune responses cause persistent damage to heart tissues. The biological functions and actions of activated immune cells are closely correlated to MSC interactions (Figure 4.1) [99, 100]. Most significantly, MSC-macrophage communication drives macrophage polarization and function. The macrophage secretion of anti-inflammatory cytokine IL-10 is modulated by MSCs to drive a phenotypic change of macrophages toward an anti-inflammatory state. This presence of anti-inflammatory macrophages is critical, as the addition of MSCs with the complete depletion of the macrophage population significantly increased cardiac adverse remodeling and mortality *in vivo* [100]. Taken together, the introduction of MSCs acts as an immunosuppressive mediator to defense overresponsive inflammation [101].

MSCs modulate many species in the post-MI environment to modulate inflammation beyond interaction with macrophages. IFN-γ and other proinflammatory cytokines are secreted from activated T cells, and in combination with TNF-α, IL1-α and IL-1β, these factors drive MSC-associated immunosuppressive functions [101-103].

Following a T cell-triggered phenotype shift, MSCs secrete multiple biological molecules that directly participate in immune cell pathways, including IDO enzyme, HLA-G5, iNOS/NO, prostaglandin E2 (PGE2), HGF or IL-6, to alter the state of immune cells, including cytotoxic T cells, T regulatory cells, natural killer cells, dendritic cells, monocyte or macrophage [101]. Immunocyte activities are also suppressed by MSC through direct and indirect pathways [104-106]. Furthermore, the proliferation of CD4 and CD8 T cells can be inhibited by nitric oxide [104] or HLA-G5 [107] production, cellular division and IL-2 generation from T cells can be delayed by PGE2-stimulated pathway [108], and intracellular apoptosis signaling can be processed by secreted IL-6 [109].

4.3.2 Mechanism of MSC differentiation into cardiac-related cell lineages

The multipotency of MSC also offers the potential for differentiation into multiple cardiac cell lineages. The elevated expression of VEGF and FGF in an infarct environment supports MSC reprogramming into several types of vascular-phenotypic cells, including endothelial cells (EC) and smooth muscle cells, which are essential and fundamental components to structurally and physiologically support vasculature reconstruction [110-114]. In heart, the abundance of laminin proteins in extracellular matrix could induce FOX2 upregulated pathway that promotes the EC marker expression and EC-like tubular network formation on MSCs [115].

MSCs are also inducible into a cardiomyocyte lineage. Specific paracrine growth signals will drive MSCs towards a cardiomyocyte-like state [114, 116]. IGF-1 pushes the MSC to increase myocardial marker expression through the PI3k/Akt pathway. Alternatively, the cardiomyocyte differentiation efficacy of engrafted MSCs can be effectively enhanced by reacting bFGF in ischemic environment [116]. Other than growth

factors, the exposure of chemical modifier 5-Azacytidine stimulates MSCs' cardiomyogenesis through extracellular signal related kinases (ERK) activation pathway [117] from the evidence of increased cell beating actions and ventricular morphology shift [118].

4.3.3 Other protective mechanisms of MSCs

Several other beneficial mechanisms of action have been proposed to explain the therapeutic effects of MSCs in the post-MI myocardium. It has been proposed that MSCs inhibit the activties of proteolytic cathepsins that degrade extracellular matrix (ECM) during heart remodeling [99, 100]. Additionally, MSCs mediate blood coagulation and further clotting-associated heart damage [119-121] through the upregulation of urokinase plasminogen activator and plasmin activators to block thrombus formation [120]. Finally, MSCs excrete fibrinolytic enzymes to inhibit scar formation by cleaving the fibrin matrix formed during cardiac remodeling state [121].

4.3.4 The role of endothelium as a pathological target in MI

Endothelium is a defensive interface which plays an essential role in regulating vascular functions, such as clot reduction, oxidative species production and inflammation stimulation. This protective endothelial cell-aligned layer also serves as a significant pathological target of various diseases, such us MI, cancers or other inflammatory-related diseases, when multiple biological events simultaneously occurs near vessel regions, including recruitment of immune cells, diffusion of excess oxidative stresses and induction of thrombosis triggered by serious damages near injured tissues [122].Typically, healthy endothelial cells are prominent hallmarks to regulate cardiac metabolism, contractility and maintain basic cardiac functions. In MI, persistent ischemic injury in infarct sites,

however, occurs with severe necrosis, apoptosis and metabolic dysfunction of cardiac cells, initiating destructive degradation processes of intracellular matrix. Continuous stimulation and generation of degraded cellular contents as well as reactive oxidative stress to adjacent extracellular components induces upregulation of pro-inflammatory chemokines that can significantly change endothelium phenotypes. TNF-α is a pro-inflammatory protein that is highly upregulated after acute ischemia. As TNF-α is released into inflamed heart, the binding interaction between endothelial surface receptor TNFR and its ligand cytokine TNF-α results in a series of upregulated protein transcription of cell adhesion molecules (CAMs) on endothelial surfaces by triggering NF-κB-based signaling pathway [123, 124]. This inflammatory mediator-induced phenotypic alterations on endothelial cells is so called "endothelium activation".

With elevated biological marker presence on cell surfaces following MI-induced inflammation, this activated, antigen-overexpressed endothelium layer can be recognized as a highly adhesive interface to attract circulating immunocytes, such as leukocyte, monocyte and neutrophil. When inflammation takes place at a site of injury, inflammatory cytokines release recruiting signals for leukocyte surface activation. The cause of activated leukocyte extravasation is the conjunction of sequential biomechanical processes near vascular endothelium, including slow radial motion (rolling), ligand-receptor capture, tethering, firm adhesion and then transendothelial migration (Figure 4.2). The surface receptor B2-integrins, LFA-1 and Mac-1, highly expressed on activated leukocytes have strong affinity toward corresponding ligands such as selectin glycoproteins, ICAM1 or VCAM1 on antigen-elevated endothelial alignment [125, 126]. Once the contact between leukocyte surface integrin and endothelial surface CAMs occurs, this ligand-receptor

affinity promotes the deceleration of leukocyte flowing speed (rolling) through the interface of inflamed microvasculature and then lead to leukocyte adhesion, allowing leukocyte penetration through the gap between adjacent endothelial cells for further leukocyte infiltration into deep tissue area. By understanding cell recruitment behavior through inflammation targeting, we will coat MSC membrane with specific targeting materials to assist MSC migration to ischemic heart by mimicking leukocyte adhesion on inflamed endothelium.

4.4 Surface coating techniques for targeting endothelium

Vessel interfaces where endothelium locates are always bearing shear stress from peripherical blood, making endothelial cells difficult to be targeted. Thus, several cell surface markers of endothelium containing selectins and CAMs were revealed as primary targeting sites to deliver drugs, like antioxidant and anti-thrombotic molecules, to endothelium layer [127]. To successfully transport drug carriers to targeted tissues, a variety of biomaterials has been surface-coated with specific ligands or antibodies. Early research from Steinberg's lab first established the delivery of immunoconjugate beads for cell targeting. The coating of lysosomal-targeted antibody on the surface of polystyrene Latex spheres was used to examine the lysosomal-mediated actin differentiation activities after macrophage phagocytosis [128]. This IgG-coated bead technique was further developed for the surface loading of endothelium-targeted antibodies to target CAM-overexpressed or activated endothelial cells.

Multiple studies using anti-ICAM1 coating for endothelium targeting has been widely applied in different disease treatment. For example, the anti-ICAM1 coated

nanobeads with a payload of lysosomal enzyme, which can metabolize excess lysosomal stored in tissues, has been utilized for enzyme replacement therapy of Niemann-Pick disease [129, 130]. Compared with non-anti-ICAM1-coated group, significantly decreased lysosomal accumulation was observed in endothelial cytoplasm [130] or microvasculature [129]after the delivery of anti-ICAM-coated drug vehicles without tissue injury. Another example is to coat ICAM1 antibody on the surface of catalyze-loaded latex microbeads to protect endothelial cells from H_2O_2-induced oxidative stress. With the coating of targeting antibody and loading of H_2O_2-degradable enzyme, anti- endothelial cells were successfully targeted and able to survive under H_2O_2 shock after the internalization of catalyze-loaded beads [131].

While multiple studies broadly displayed the use of anti-endothelium beads in different disease targeting purposes, key parameters that are responsible for endothelium binding has been deeply explored to understand optimized coating design for adhesion efficacy improvement. Importantly, Eckmann et al. has indicated that the density of surface-coated ICAM1 antibody on polystyrene beads is highly dependent on material association with ICAM1-expressed endothelium under shear flow, providing the facts that antigen-targeted adhesion property can be precisely tuned by surface coating characterization [132].

4.5 Cell surface coating for targeting endothelium

Stem cells are known to lack homing ligands that target specific cell surface markers present on inflamed tissues. Engineering cell membranes with tissue-targeting molecules is a promising strategy to assist the orientation of ligand-deficient stem cells

toward the inflamed endothelium. For instance, by modifying cell surface with selectin-targeted ligand sLe^x, Karp et al. successfully mediate leucocyte-mimicking MSC rolling on *in vitro* selectin-localized surfaces [133] and *in vivo* inflammation-promoted tissues [45]. They demonstrated two different coating techniques to associate sLe^x ligands with MSCs. The first cell surface coating strategy is achieved by using biotin-streptavidin affinity to conjugate biotinylated sLe^x onto streptavidin/lipid-bound cells. The second method demonstrated the anchorage of nanosized polymer- sLe^x chain onto MSC surfaces. For both SLe^x-coating studies, reduced rolling velocities of sLe^x-coated cells on P-selectin-modified surfaces were observed under a flow chamber assay, designed to simulate cell movement behavior through inner blood vessel wall [45, 133]. Compared to the uncoated cells, *in vivo* nanosized polymer-sLe^x-coated MSC rolling was also discovered under a dynamic real time microscopy and around 35-fold increased sLe^x-coated cells were found in LPS-induced inflamed ear [45]. Instead of applying a coating of natural cell surface ligand, Kong's group used cell coating technique to apply VCAM1-associated material on MSC surfaces. Nanoscale coating of synthetic VCAM-binding peptide (VBP) was hydrophobically embedded on MSC membranes to target activated endothelium and vasculature. This group used surface plasmon resonance to detect the adhesion efficacy of VBP-coated cells or VBP peptides on VCAM-expressed endothelium and VCAM1-containing surfaces. The hyper branch-structured polyglycerol chain that contains VBP was proved to have increased association rate constant and lower dissociation rate constant than only polyglycerol-coated cells, indicating the implication of surface-coated VBP is a key element to cause cell rolling in lower speed and enhance cell attachment on an endothelial layer [134].

The other way to specifically bind activated endothelium is the MSC surface coating with artificial antibodies that have high affinity with endothelial surface CAMs (Figure 4.3). Palmitated protein-G-(PPG)-associated lipid was hydrophobically intercalated on MSCs by In Kap Ko et al., allowing the capture of IgG-type antibodies on cell membranes by PPG-guided absorption. To determine if cell surface coating of PPG-anti-ICAM1 enhances MSC retention, a physiological flow assay showed the significant increase of MSC resistance to shear stress on anti-ICAM1-coated groups [135]. In the same lab, they also established the first animal study to deliver antibody-modified MSCs for *in vivo* treatment of inflammatory bowel disease (IBD) in which cell surface addressin is highly expressed on intestinal endothelial layers as a targeting aim. The goal of this study is to examine MSC immunosuppressive effects on inflamed colon tissues and mesenteric lymph nodes to inhibit immunoactivities following the targeted delivery of antibody-engineered MSCs. It was proved that the increased retention of PPG-MSCs, incorporated either VCAM1 or addressin antibody, is able to delay spleenocyte proliferation, induce the presence of T regulatory cells, and enhance the survival rate of IBD-induced mice [136]. While antibody-PPG incorporation exhibited great endothelium targeting efficacy in both *in vitro* and *in vivo* studies, this protein-G coating technique that only has ability to absorb immunoglobin highly restricts the selection of cell-targeting materials that can be incorporated on the cell surfaces.

4.6 Cell surface coatings for targeting myocardial infarcts

In addition to inflammation targeting, cell surface coating through other targeting aims are also employed in cardiovascular diseases. For instance, magnetic nanoparticles

have been widely used in various bioimaging and biomedical applications because of their responsive properties under magnetic stimuli. Cheng's group deposited an FDA-approved FHP (Feraheme, heparin and protamine) magnetic nanocomposite for cardiosphere-derived stem cell (CDC) membrane coating to provide cell targeting and imaging potentials [137]. The study showed this cell surface deposition with ferromagnetic particles had no change in several cellular activities, such as differentiation, proliferation, migration, and no oxidative stress was generated in the FHP-coated CDCs. Besides, this iron-contained cell coating could be magnetically regulated *in vivo* to effectively examine the mobility of coated cells under an external magnetic field and caused increased retention at the infarcted heart region only with coated cell group. Although FHP cell coating on CDC cells was loaded through natural cellular uptake, this strategy might accumulate in non-infarcted region and affect long-term intracellular activities due to the lack of cell ability to metabolize this uptake materials in the cytoplasm. Additionally, SPIONs (superparamagnetic iron oxide nanoparticles) are also a popular nanomedicine applied on stem cells because of their imaging, tracking and targeting potentials for MRI or magnetic-based diagnostic assays. However, significant obstacles exist due to their poor metabolism and body clearance, unfavorable release to extracellular environment and long-term oxidative stress production [138].

Following an ischemic shock, a variety of chemokines were recruited near oxygen-deficient infarcts and play an important role in regulating anti-apoptosis and angiogenesis effects [139]. Importantly, the low oxygen level triggers the production of HIF-1α, resulting in the upregulation of a stem cell recruited chemokine, SDF-1 (stromal cell-derived factor-1) in the infarct site [140]. Thus, to enhance stem cell migration and

recruitment to myocardium infarcts, the presence of SDF-1 under hypoxia condition has been considered as a significant target by using the interaction between SDF-1 and its receptor CXCR4. The cell modification work from Bull's lab demonstrated the CXCR4-conjugated lipid coating on MSC membranes significantly enhance cell migration toward SDF-1 containing environment [12]. The migration feature of CXCR4-coated cells is highly dependent on the dose of SDF-1. This ligand-incorporation work indicated MSC recruitment potentials to hypoxia myocadiac regions by cell membrane engineering.

Cardiomyocyte necrosis accompanying with myofilament remodeling causes substantial release and degradation of proteins, vasculature fragment, proteinases and enzymes. Elevated breakdown of damaged cardiac molecules has been clinically identified as one of important diagnostic indicators of cardiac dysfunction following MI. During ischemia, the release of myosin light chain (MLC), a cleavage form of contractile cardiac myosin, can be stimulated by MMP-2-guided proteolysis, leading to huge loss of contractility and mobility of cardiac muscles [141, 142]. Importantly, it has been clinically found that MLC quickly accumulated and reached peak concentration near injured heart several days post MI and is closely related to the size of infarct scarring [143], suggesting this ventricular myosin fragment can be a significant targeting marker of MI. Similar to previously mentioned antibody incorporation for endothelium targeting, antibody coating on stem cells was also utilized to target MLC in damaged heart. A bifunctional antibody that has dual targeting abilities was designed by Lee RJ et al. to act on both transporting therapeutic cells and targeted cells. To create an antibody hybrid, two distinct antibodies (anti-CD45 and anti-MLC) were modified by amine-reacted Traut's reagent and sulpho SMCC, respectively, to present sulfhydryl and maleimide groups on each IgG chain for

dual antibody conjugation [144, 145]. The delivery of bispecific antibody-coated hematopoietic stem cells (HSCs) was used to target myosin-exposed cardiac cells, showing improved ventricular biofunctions with the increased HSC retention 5 weeks post MI [144]. The group using biospecific antibody coating strategy also proved therapeutic effects in a Langendorff-perfusion mice heart model. The *in vivo* intravenous administration suggested the ability of antibody-coating to restore biological functions of cardiac vasculature and to reduce myocardial degradation and fibrosis formation [145]. Unfortunately, this anti-MLC coating methodology might mislead surface-coated MSC toward undesired destination, since the increased release of myosin fragment into circulating blood serum several days following heart failure [143] makes this pathological cardiac maker difficult to be specifically targeted only in the ischemic region. Although the incorporation of bispecific antibody has high specificity for dual cell targeting, the efficacy of cell surface coating by antibody-antigen recognition can be limited. The insufficient and restricted marker density and diversity of cell surface antigen expression on different cell types make antibody-based coatings less competitive and less adjustable than other cell surface modification techniques.

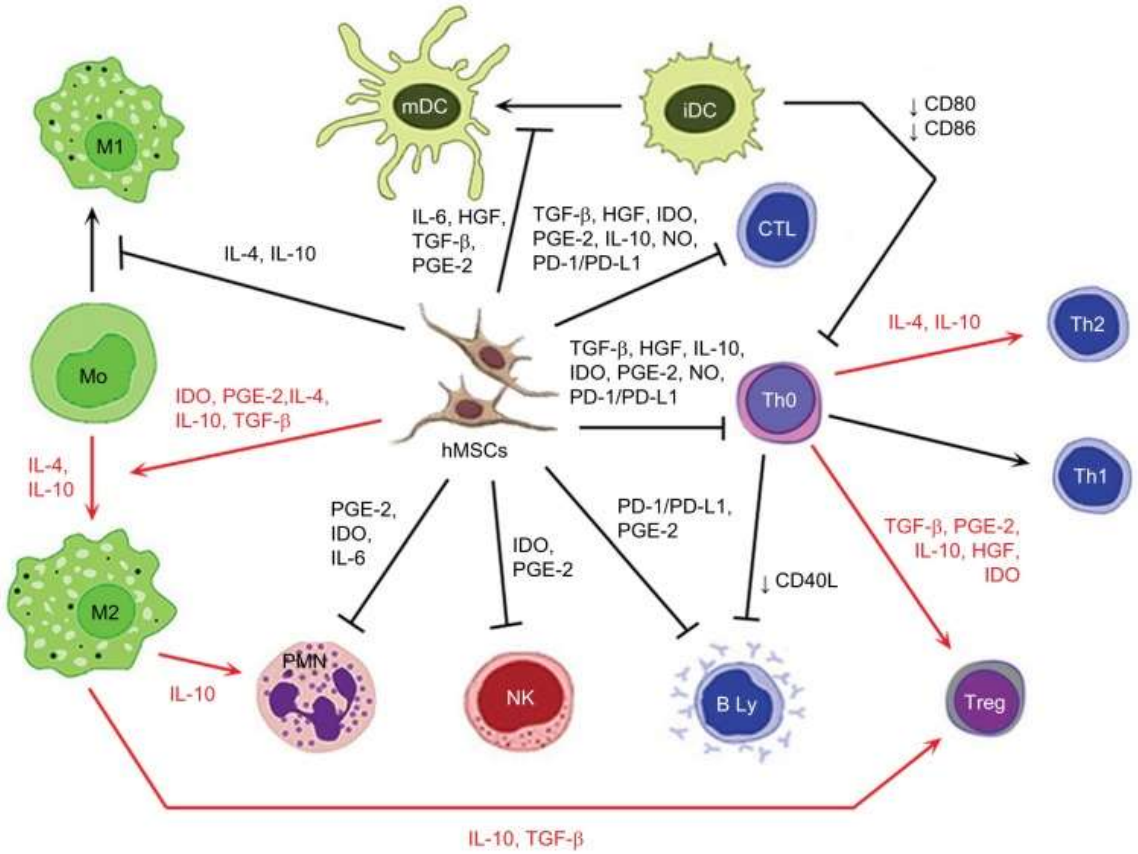

Figure 4-1. Immunomodulation strategies of mesenchymal stem cells. Reprinted with permission from [146], Copyright 2016. (https://www.ncbi.nlm.nih.gov/pmc/articles/PMC5170601/?report=reader)

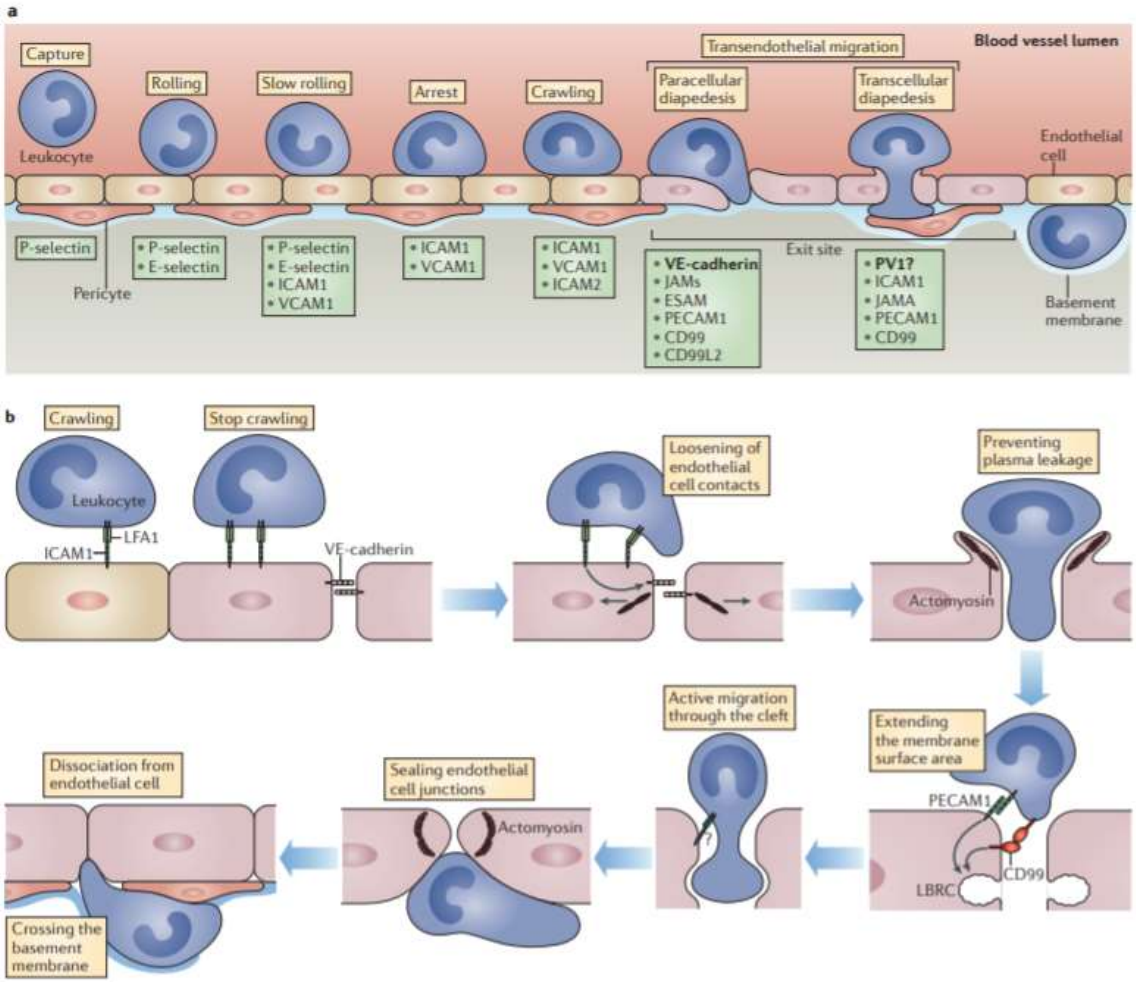

Figure 4-2. The mechanism of leukocyte transendothelial migration. Reprinted with permission from [147], Copyright 2015, with permission from Springer Nature.

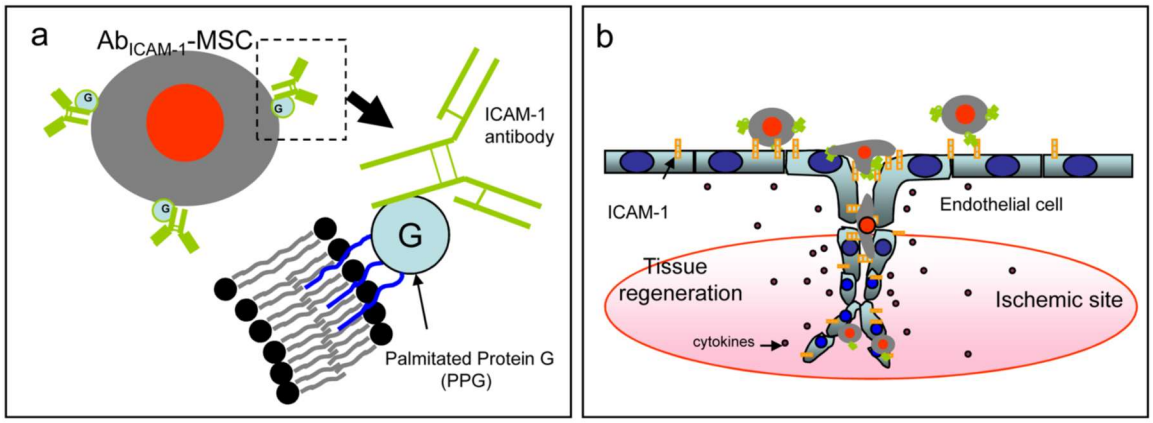

Figure 4-3. MSC surface coating of ICAM1 antibody for endothelium targeting. Reprinted with permission from [135], Copyright 2009, with permission from Elsevier.

CHAPTER 5. ICAM1-ADHESIVE MSC FOR ENHANCED CELL RETENTION VIA INTRAMYOCARDIAL DELIVERY

5.1 Introduction

Intramyocardial delivery is a direct route for placing MSCs into an inflamed heart to regulate the local inflammation response. The retention of MSCs at the injection site is severely limited by the fluid flows that rapidly wash cells away and minimize their capacity to modulate cardiac inflammation. To prevent this loss of MSCs and their function, this chapter will focus on the development of an anti-ICAM1 coatings on the plasma membrane of MSCs to enhance their adhesion to their inflamed environment. Covalently biotinylated MSCs were tethered to biotinylated anti-ICAM1 through an intermediate deposition of streptavidin layer with unsaturated biotin binding domains. MSC surfaces were modified with ~7,000 biotin/μm^2 and ~23 antibodies/ μm^2. The intramyocardial injection of antibody-coated MSCs offered a 3-fold increase of cell retention in the heart over the injection of uncoated MSCs. The mechanism of adhesion was supported through analysis of MSC adhesion to activated HUVECs and surfaces of purified ICAM1 glass under microfluidic shear flow.

5.2 Background

MIs are severe cardiovascular events where the occlusion of the blood supply damages local tissues. Without access to oxygen and essential nutrients, cells within the infarct zone become necrotic and release waves of cytokines driving local inflammation to recruit additional inflammatory cells and alter the phenotype of local cells. The spike in inflammation drives the spread of damage to tissue outside the initial infarct site, and this

wave of inflammation-driven damage continues to spread out into healthy heart tissue for weeks following the initial occlusion. As a result, MI-associated damage is dramatically worsened by unchecked inflammation following the initial injury.

MSCs are potent modulators of inflammation and have been effectively utilized *in vivo* to promote immunomodulatory effects of immunocytes, including CD8 T cell, T lymphocyte, natural killer cells, dendritic cells and macrophage [104, 107-109]. Additionally, MSCs that are pre-stimulated by macrophage-secreted TNF-α and IFN-γ release immunosuppressive factors, such as IDO enzyme [148-150], PGE2 and TSG6 [151], and these factors drive pro-inflammatory monocytes towards an anti-inflammatory M2 state [152, 153]. Beyond their immunomodulatory effects, MSCs are effective at driving angiogenesis [154, 155] and multilineage differentiation [156, 157] to further promote repair to damaged tissues. Through the cooperative action of these mechanisms for MSC action, the introduction of MSCs into the heart has been effective in promoting cardiovascular function and limiting the expansion of the scarred tissue following MI [158, 159].

Direct MSC injection into the healthy tissue surrounding the infarct concentrates these therapeutic cells at the site of injury to promote a localized therapeutic effect [160]. Unfortunately, the injected cells are rapidly cleared from the injection site, limiting their opportunity to modulate the infarct environment. For most injected cell therapies, the vast majority of the injected cells are rapidly lost from the injection site [161-164] owing to the injected cells and buffer swelling the tissue. The elastic recovery of the heart tissue drives fluid escape from the tissue, and the injected cells are swept away [164]. This pressure driven flow is further exacerbated by heart muscle contractions and other tissue dynamics

in a pumping heart [165-168]. In MSC therapies for MI, these factors combine to yield as little as 0.44% of the injected MSCs remaining in the heart 4 days after injection [169]. Since a larger MSC dose carries a greater risk of mortality [170, 171], the maximum number of MSCs present in the heart post-MI is fundamentally limited by the retention of these cells in the peri-infarct tissue. The loss of cells from the infarct site is a critical challenge for the future of MSC-based cardiovascular therapies [164].

We seek to increase the number of MSCs retained in the peri-infarct tissue through engineering of the MSC peripheral membrane. Our strategy is to present artificial ligands on the MSC plasma membrane to increase adhesion of the MSC to the peri-infarct tissue. The inflammatory response to ischemia drives the secretion of proinflammatory factors which alter the endothelium to recruit leukocytes and other immune cells. The inflamed endothelium overexpresses CAMs, making these CAM-exposed endothelium sheets important pathological targets [122-124].

Here, we developed a cell surface coating to present antibodies against ICAM1 to adhere to the endothelium of infarcted hearts (Figure 5.1a). Through intramyocardial injection, we confirmed that the delivery of antibody-coated MSCs provides 3-fold higher retention in infarcted heart tissues when compared to uncoated MSC injection. The ICAM1 adhesion mechanism is supported through the increased cell adhesion of coated MSCs to activated endothelial cells and ICAM1-coated glass under physiological shears. Interestingly, we found that the adhesion of cells was improved with lower concentration of our biotinylation reagents. Lower concentration of NHS-ester biotin (0.1mM) retained 50% of the cells under wall shear stresses of 150 dyne/cm^2 while no cells were retained with 1.0 mM biotinylation. In all, this straightforward coating design significantly

enhances the adhesion of MSCs to an infarcted heart through specific targeting of overexpression of endothelial ICAM1 in response to local inflammation.

5.3 Experimental section

5.3.1 MSC isolation and culture

Mouse MSCs isolated from C57BL/6 or C57BL/6-Tg (CAG-EGFP)131Osb/LeySopJ mice (Jackson Laboratory, BarHarbor, ME). Mice were sacrificed, femurs, tibias and hip bones were collected and then flushed with PBS supplemented with 10% FBS. MSCs used in this study were of a passage less than 10. MSCs were cultured in pre-warmed mouse MesenCult^{TM} basal medium, supplemented with MesenCult™ 10X Supplement (STEMCELL Technologies), 10% USDA Approved Origin FBS (VWR), 1% 200mM L-glutamine (Gibco) and 1% streptomycin/penicillin (Gibco). MesenPure^{TM} (STEMCELL Technologies) was added in MSC medium at 1:1000 dilution right before cell seeding. MSCs were cultured under hypoxic conditions (less than 5% O_2 supply) for MSC cultivation was needed by introducing ultrapure nitrogen into a 37ºC humidified incubator, with 5% CO_2. For cell collection, cells were rinsed with sterile PBS (Corning) and treated with 0.25% trypsin/EDTA (Gibco) for 5 min in 37ºC. Serum-containing medium was added to neutralize the trypsin. Cells were centrifuged at 300 g for 5 min and the supernatant was removed by pipetting. The cell pellet was washed once and resuspended in ice-cold DPBS before use.

5.3.2 Preparation of anti-ICAM1 coated MSCs

All incubation steps for cell membrane antibody incorporation were processed on ice. MSCs were rinsed twice with cold PBS. 0.1 mM or 1.0 mM sulfo-NHS-LC-biotin was

prepared in PBS immediately before cell incubation, 2 mL of biotin solution per 106 cells is added for 1 h. Cells were then rinsed twice with PBS, and 2 mL of 25 μg/mL streptavidin in PBS was added for every million cells for 1 h. The streptavidin coated cells were then incubated for 1h in 30, 50, or 100 μg/mL biotinylated monoclonal mouse antibody against human ICAM1 (clone IH4, Invitrogen) or 100 μg/mL biotinylated monoclonal rat antibody against mouse ICAM1 (clone YN1/1.7.4, Invitrogen) in PBS.

5.3.3 MTT viability assay

Metabolic activity detection depending on mitochondrial function was evaluated by using MTT (3-(4,5-Dimethylthiazol-2-yl)-2,5-Diphenyltetrazolium Bromide) reagents (M6494, Invitrogen). A 12mM MTT solution was prepared in PBS (5mg/mL). 50,000 cells were diluted in 1mL MSC culture medium. 200 μL of cell solution was pipetted into 96 well plate and then incubated with 20 μL of MTT stock for 4 h at 37 °C. Cell supernatant was removed after centrifuge (1 rpm, 5 minutes) and 200 μL of DMSO was added to dissolve the reacted product. A plate reader (Biotek, Winooski, VT) was used to examine the sample absorbance at 570 nm. The percentage of cell viability was determined by normalizing the sample absorbance with the positive control.

5.3.4 Myocardial infarction surgery and intramyocardial cell transplantation.

Myocardial infarction was induced by permanent left anterior descending artery (LAD) ligation in 8-10 week female C57BL/6 mice under 1-3% isoflurane anesthesia using a small animal vaporizer system. Immediately after ligation, the animals were randomized to receive 25μL of either PBS, MSCs, or anti-ICAM1 modified MSCs (125,000 cells per 25uL injection per mouse) via intramyocardial injection to the peri-infarct region. Pain medications were administrated after surgery for 24-48 hours.

5.3.5 Immunohistochemistry analysis

The hearts were harvested 3 days after MI and MSC injection. Immediately after cervical dislocation, the hearts were perfused with cold PBS with 4% paraformaldehyde and fixed for 24 hours prior to embedding in a paraffin block. 4 μm thick heart tissue sections were used for immunofluorescent analysis of heart for evidence of the GFP^+ MSCs. Briefly, heart tissue sections were exposed to pH 6.0 antigen retrieval buffer (Vector Laboratories, Burlingame CA) following the company protocol. Slides were blocked with normal goat serum for 16 hours at 4°C and stained with primary rabbit anti-GFP antibodies (Abcam, Cambridge, United Kingdom) following by incubation with Alexa 488 secondary goat anti-rabbit antibodies (Abcam, Cambridge, United Kingdom).

5.3.6 Flow Cytometry

Single-cell suspensions were prepared from digested cardiac tissue as previous described [47]. Briefly, hearts collected 3 days after MI were minced then digested using a collagenase B (Roche, Indianapolis, IN) and dispase II (Roche, Indianapolis, IN) solution for 30 minutes at 37°C with mixing every 5 minutes. The heart cell suspensions were strained using 40 μm strainers (VWR, cat#10199-654) to remove tissue debris and undigested tissue. Cells were washed with flow buffer with centrifugation (400×g for 10 min at 4 °C) and suspended in Flow Buffer. Cells were stained with eFluor 660 conjugated anti-GFP antibody (eBioscience, Thermo Fisher Scientific, Waltham MA) and analyzed using an LSR II (Becton Dickinson) in the University of Kentucky Flow Cytometry Core.

We utilized FlowJo v10 (FlowJo, FlowJo Ashland OR) software to generate dot plots and analyze the data.

5.3.7 Macrophage cytokine secretion assay

BMDMs (Bone marrow-derived macrophage) were isolated and differentiated using previously published protocols [172]. Primary macrophages were derived from bone marrow cells and cultured for 7 days in DMEM (with 10% L929 cell-conditioned medium, and 10% fetal bovine serum). For co-culturing, $5x10^5$ BMDMs were seeded into a twelve-well plate. The next day, 20,000 unmodified MSCs or anti-ICAM1 coated MSCs were placed into the twelve-well plate with the BMDMs. Co-culture were incubated for 3, hours with or without 100 ng/mL lipopolysaccharide (LPS-B5, Invivogen) and IFN-γ (20 ng/ml).

Conditioned media were obtained from BMDMs alone, co-cultured with BM-MSCs, or anti-ICAM1-coated BM-MSCs as described above. The secreted TNF-α and IL-10 in the conditioned media were evaluated using enzyme-linked immunosorbent assay ELISA kits (BD OptEIA™) according to the manufacturer instructions.

5.3.8 Endothelial cell culture, activation and shear assays

Human Umbilical Vein Endothelial Cells (HUVEC) (#00191027) was purchased from Lonza. HUVEC culture medium was prepared by adding 1% streptomycin/penicillin and EGM™-2 SingleQuots™ Supplements (CC-4176) into EGM™-2 Basal Medium (CC-3156). The EGM™-2 SingleQuots™ Supplements include 2% FBS, 0.2 mL hydrocortisone, 2 mL hFGF-B, 0.5 mL VEGF, 0.5 mL IGF-1, 0.5 mL ascorbic acid, 0.5 mL hEGF, 0.5 mL GA-1000, and 0.5 mL heparin. Cells were cultured in a 37ºC incubator with 5% CO_2. Cells were rinsed with sterile PBS and detached by TrypLE treatment for 5

min at 37ºC. The trypsin was neutralized with culture medium and centrifuged at 300 g for 5 min. The supernatant was removed, and cells were resuspended in pre-warmed medium or PBS before use or next passage.

To create a HUVEC monolayer on glass slides, attachment factor was used to enhance HUVEC attachment to the glass. Microscope slides (25mm x 75mm) were placed in a 50 mL conical tube and pre-sterilized overnight in 70 vol% ethanol and dried before use. Each sterilized slide was loaded into a well (3x8cm) in a 4-well rectangular dishes and rinsed twice in PBS. Each slide was incubated with 4 mL 1X attachment factor at 37ºC for at least 3 h. Excess solution removed and $1x10^6$ of HUVEC in 4 mL EGM™-2 medium was seeded directly onto each slide. Each HUVEC-seeded slide was used for MSC adhesion studies after reaching 95% confluency.

HUVECs were activated through the addition of 4 mL of 10 ng/mL TNF-α in growth factor and serum-suppled EGM-2 medium directly onto a HUVEC-adhered microscope slide in a 4 well dish at 37ºC incubator for 5 or 20 h.

ICAM1 expression on adherent HUVECs was qualitatively labeled with 25 µg/mL biotinylated mouse antibodies against human ICAM1 in PBS for 45 min, rinsed twice with PBS and stained with 2 µg/mL Alexa647-labeled secondary antibodies against mouse IgG (Invitrogen) for 45 min. Cells were rinsed in PBS and imaged in the far-red channel of a Nikon Ti-U Epifluorescent microscope.

In cell-cell adhesion studies, HUVEC cells were stained with calcein red for tracking. HUVECs were rinsed with serum-free (SF) EGM-2 medium twice. Calcein-red orange powder was dissolved in 63 µL pure DMSO and stored in -20 ºC before use. HUVEC slides were incubated with in a 1:1000 dilution of the calcein-red orange stock in

SF-EGM-2 for 3 min and rinsed twice with SF-EGM-2. Cell slides were blocked with 5% BSA in SF-EGM-2 at least for 1 hour. For the *in vitro* shear assays of GFP MSCs on calcein red stained HUVECs, one milliliter of $0.5x10^6$ cells/mL pipetted onto a slide of 95% confluent HUVEC cells blocked with BSA. The coculture was incubated for 5min at 37ºC. Cells were sheared using a rectangular parallel plate flow chamber from Glycotech (#31-010) with a 0.01-inch-thick gasket. A vacuum pump was used to seal the device to a cell-coated slide immersed in PBS. The flow rate of fluid through the chamber was controlled with a syringe pump (NEWERA, #4000-US) and two 60 mL syringes withdrawing fluid to pull PBS from a reservoir through the chamber at the indicated flow rate for 15 s. The fluorescence images of attached GFP-positive MSCs under different shears and the number of retained cells were counted with ImageJ analysis.

Shear stress acting on the cell was calculated as the wall shear stress under Newtonian flow in a rectangular cross section based on the following equation (Q= flow rate, μ= fluid viscosity, H= gap height, W= gap width, τ_w= shear stress at wall).

$$\tau_w = \frac{6Q\mu}{H^2 w}$$

5.3.9 Quantitation of cell surface group density

Covalent biotinylation of cell surface proteins was achieved by treating cells with various concentration of sulfo-NHS-LC-biotin (0.025; 0.1; 0.5; 1; 2 mM). Two milliliters of sulfo-NHS-LC-biotin solution was used to treat $1x10^6$ cells for 1 hour on ice and rinsed with ice-cold DPBS twice. One milliliter of 0.5 μg/mL streptavidin-phycoerythrin (SAPE) mixed with extra streptavidin protein (0, 20, 60, 80 or 90 μg/mL) was used to label $1x10^6$ of biotinylated cells for 1hr on ice. After rinsing with ice-cold PBS twice, the fluorescence of PE-labeled cells was analyzed by flow cytometry in FL2 channel.

QuantiBRITE^{TM} PE was purchased from BD Biosciences is a phycoerythrin (PE) fluorescence quantitation kit and includes PE calibration beads of known quantity of PE conjugated per bead. Red PE fluorescence was collected in FL2 channel (585/40 nm bandpass filter) by flow cytometry. The mean FL2 fluorescence per PE was correlated from a linear regression and was used for quantitation of PE fluorophore bound to each cell. The number of available biotin groups on each cell event was calculated through PE calibration curve (Figure 5.2).

Activated or naïve HUVECs were trypsinized as before and rinsed twice with PBS. 100 µL of 2.5 µg/mL biotinylated human ICAM1 antibody in ice-cold PBS was added for every 10^6 HUVECs and incubated for 30 min on ice. After rinsing twice with PBS, cells were incubated in 500 µL of 0.5 µg/mL SA-PE in PBS. After PBS rinsing, the fluorescence of surface-anchored PE was analyzed through flow cytometry in FL2 channel, and a relative measure of ICAM1 per cell was determined using the PE calibration curve (Figure 5.2).

After coating with antibody against human ICAM1, coated MSCs were incubated with 350 µL of PE-conjugated secondary antibody against mouse for 45 min. The PE fluorescence acquired by FL2 channel of flow cytometry was compared with calibration PE curve to determine the number of ICAM1 antibody coated on a cell by the assumption of 1:1 binding ratio between anti-ICAM1 and secondary antibody.

5.3.10 Preparation of hICAM1-coated slides

Human recombinant ICAM1 protein was reconstituted at 250 µg/mL in sterilized PBS and stored at 4 ºC before use. The density of hICAM1 protein was estimated by specifically fluorescent targeting on hICAM1 molecules coated on protein-reactive glass

surfaces. Eleven concentrations of hICAM1 protein (250; 150; 100; 50; 25; 12,5; 6.25; 4; 2; 1 μg/mL and PBSA negative control) were tested in this study. Epoxide slides were placed in a lid-covered petri dish, coated with 30μL of hICAM1 protein solution in a 1cm^2 area for 3hr, and then rinsed twice with 0.1% BSA in PBS. ICAM1-immobilized slides were loaded into a Whatman Chip Clip, blocked with 0.1% BSA for 30 min, and washed with 1X PBS twice. Each ICAM1-coated area was labeled with 50 μL of 30 μg/mL biotinylated human ICAM1 antibody for 1 h and rinsed twice with PBS. Biotinylated immobilized sites were fluorescently tagged through the incubation of 70 μL diluted SA-Cy3 (1:40 in PBS) in each well for 30 min. After rinsing with PBS three times, slides were dried in a stream of air and scanned in an Affymetrix 428 Microarray Scanner at 30 dB gain in the Cy3 channel. The number of Cy3 molecules were estimated by Cy3 calibration curve (Figure 5.3) prepared using a Cy3 calibration slide from Full Moon Biosystems and image analysis using ImageJ software.

5.3.11 *In vitro* adhesion of anti-ICAM1 coated MSCs on ICAM1-immobilized surfaces under shears

A 1 cm by 1 cm region of an epoxy slide was treated with 30 μL of human ICAM1 protein in PBS at 6.25 for 3 h at room temperature in a sealed dish. The protein-coated slides were blocked with 1 mg/mL BSA in PBS for 30 min. 50 μL of 0.5x10^6 MSCs were added onto the ICAM1-coated surface for 5 or 45 min at room temperature. Cells were sheared and counted for 30 s using a rectangular parallel plate flow chamber as described above.

5.4 Results and discussion

The direct injection of MSCs into the heart wall has been effective in improving the function of hearts post-MI. The effective dose of MSCs present in the heart tissue after injection is a critical limitation, and this study tests the hypothesis that the synthetic incorporation of antibodies against ICAM1 onto the peripheral membrane of the injected MSCs will increase the number of MSCs retained at the site of injection. Our strategy is to first biotinylate MSCs through incubation in 1 mM sulfo-NHS-LC-biotin (NHS-biotin), then coating the MSC surface through incubation in 25 μg/mL streptavidin, and finally using the excess biotin binding sites of streptavidin to bind a biotinylated-antibody against mouse ICAM1 (100 μg/mL) (Figure 5.1b). Since this method targets the post-MI inflammatory environment, we induced MI in our mice with an established infarct model where the left anterior descending coronary artery is sutured. The animals are then injected with either $1.25x10^5$ MSCs in PBS or $1.25x10^5$ anti-ICAM1 coated MSCs in PBS. There was one injection per heart, 25 μL per injection site, and all injections were into the peri-infarct heart wall, and the infarct zone was determined through visual tissue discoloration. Three days following MI and MSC injection, the mice were sacrificed, and the resident heart cells were dispersed and analyzed by flow cytometry (Figure 5.4a). Our utilization of GFP-labeled MSCs injected into a non-GFP host allows for simple determination of the number of injected cells remaining in the host. The number of the injected MSCs remaining in the heart on day 3 were significantly higher ($p=0.02$) for the MSCs coated with antibodies against ICAM1 (16 ± 3.7 cells/mg) than for the unmodified MSCs (4 ± 1.4 cells/mg, Figure 5.4c). This finding is qualitatively supported through the analysis of tissue sections from other animals in the study, where GFP^+ cells are more frequent in peri-infarct tissue sections from the anti-ICAM1 coated MSCs than the uncoated MSCs (Figure 5.4b).

In related studies, inflammation-adhesive cell coatings have also been designed on MSCs by incorporating functional ligands that target endothelial antigens [16-20]. Coatings with a CAM-specific peptide also allowed MSC to target an inflamed endothelium [134], while surface incorporation of an ICAM1 antibody enhanced MSC homing to the site of inflammation by MSC adhesion on ICAM1-upregulated endothelium [135]. Finally, antibodies against VCAM and addressins have also been used to target inflamed tissues in a mouse model of inflammatory bowel disease [136]. In all, our study strongly supports for the first time that the ICAM1 coated MSC are retained in the heart wall more than the established treatment using unmodified MSCs.

Therapeutic MSCs play multiples biological roles in regenerating new cardiac tissues, regulating extracellular immune responses, secreting angiogenesis-induced paracrine factors. Therefore, it is essential that our MSC coating strategy preserves the biological functions required for MI therapy. We coated MSCs with anti-ICAM1 through 1mM ester-biotin treatment and the viability of coated cells is preliminarily supported through MTT assays as well as MSC expansion in culture. As compared with uncoated cells, the MSC viability is not significantly impacted by the anti-ICAM1 coatings (Figure 5.5).

Uncoated MSCs or MSCs coated with anti-ICAM1 were prepared using 0.1 mM or 1 mM NHS-biotin and seeded onto pre-coated tissue flasks in media. After 30 minute of cell culture, all groups exhibited similar numbers of attached MSCs and similar morphologies, and these groups were indistinguishable two days after treatment (Figure 5.6), suggesting the minimal interference on MSC expansion. In addition, the intensity of

the GFP signal in the cells is correlated to viability and protein production, and the GFP signals were also similar across these groups.

The immunoregulatory function of MSCs is proposed as a dominant mode of cardioprotection post-MI. Near an infarct, ischemia-induced apoptotic and necrotic cardiomyocytes secrete pro-inflammatory cytokines which drive macrophages into a pro-inflammatory phenotype. As demonstrated *in vivo* and *in vitro*, the introduction of MSCs to pro-inflammatory macrophages will reduce the level of pro-inflammatory factors secreted from macrophages. Here we specifically assay the capacity for our anti-ICAM1 coated MSCs to modulate the inflammatory cytokine secretion through an *in vitro* coculture assay with BMDM macrophages.

The macrophage was directly contacted with uncoated MSCs, anti-ICAM1 coated MSCs or serum alone in LPS/IFN-γ supplemented medium for 3 h. Under LPS and IFN-γ stimulation, macrophages can be stimulated to M1 phenotypes for proinflammatory TNF-α secretion [173]. Either the uncoated or anti-ICAM1 coated MSCs cocultured with inflammatory macrophages showed significant decreased TNF-α secretion profile when compared to macrophage alone (Figure 5.7a). We also investigated the anti-inflammatory factor secretion following MSC-macrophage crosstalk. The level of immunosuppressive IL-10 in the conditioned medium exhibited higher concentration in both macrophage-interacted groups compared with non-MSC-interactive macrophage (Figure 5.7b). Hence, we can conclude that the immunosuppression effects of MSCs are not adversely influenced by the coating, and the cytokine section from macrophages can be regulated in an immunosuppressive manner in a presence of anti-ICAM1 coated MSCs.

In addition to the preservation of the innate functions of MSCs, we have the power to tune the biotin density on the surface of the cell and the density of antibodies against ICAM1 presented on our MSCs. The NHS-biotin molecule non-specifically tethers biotin groups to amine groups on the MSC's peripheral membrane. The biotin labeling was determined by pairing accessible biotins with a streptavidin molecule labeled with phycoerythrin (PE), and comparing flow cytometric fluorescence of each cell to a calibration bead of known PE loading (Figure 5.2). By simply controlling the concentration of the NHS-biotin in buffer, up to ~7,000 biotin/μm^2 (Figure 5.8a). This magnitude compares favorably to our previous reports of loading up to 10,000 molecules/μm^2 using a similar NHS-biotin approach [23]. To confirm that there are not inaccuracies in the magnitude of fluorescence value based on energy transfer between adjacent molecules [174, 175], we competed out the labeled streptavidin with an unlabeled streptavidin and found comparable biotin densities as the undiluted streptavidin-PE labeling.

Antibody density on the MSC surface was estimated using PE-labeled secondary antibodies against mouse IgG. For an MSC treated with 1 mM NHS-biotin, incubations in 30, 50, or 100 μg/mL of biotinylated antibodies against ICAM1 resulted in up to 23 antibodies/μm^2 (Figure 5.8b). While ~1 PE is bound per secondary antibody, each primary antibody will be tagged by multiple secondary antibodies [176]. As a result, the actual density of anti-ICAM1 groups is likely several fold lower. The biotin density (~7,000 biotin/μm^2) represents an upper limit for number of antibodies loaded onto the MSC surface. Given the larger size of the antibody (150kDa) [177] over the streptavidin (53

kDa) [178] and inefficiencies of sequential binding, it is reasonable there are order several orders of magnitude fewer antibodies than accessible biotin groups.

Our overall MSC retention hypothesis is based on the expectation that the anti-ICAM1 coated MSCs adhere strongly to the ICAM1 presented by the inflamed endothelium present near the infarct site (Figure 5.1b). To support these proposed mechanisms, we contrasted the force of adhesion between anti-ICAM1 coated MSCs and an activated endothelial cell with the shear stress exerted by a flowing buffer (Figure 5.9a). A near-confluent layer of HUVECs were grown on a microscope slide and were activated with a 5 or 20h exposure for TNF-α, and activation was confirmed with fluorescent labeling of ICAM1 on HUVECs (Figure 5.10 and 5.11). MSCs were treated with 0.1 mM NHS-biotin, streptavidin, and 100 μg/mL biotinylated antibodies against human ICAM1. MSCs were allowed to settle on the HUVECs for 5 minutes and then subjected to wall shear stress up to 31 dyne/cm^2. While greater shear stresses than 31 dyne/cm^2 delaminated the HUVECs, the chosen shear range captures most of the physiological wall shear stress range observed in human arteries (10-70 dyne/cm^2), veins (1-10 dyne/cm^2) and capillary beds (<1 dyne/cm^2) [168, 179-181]. For all shear stresses studied, a greater number of the anti-ICAM1 coated MSCs were retained on the activated HUVEC cells than unmodified MSCs (Figure 5.9b and 5.9c). The retention of anti-ICAM1 coated MSCs was comparable with 5 or 20 h exposure to TNF-α. This is attributed to the surface density of ICAM1 on the activated HUVECs being in large excess (>500 ICAM1/μm^2, Figure 5.11) compared to the surface density of the anti-ICAM1 ligands on the MSCs (<23 antibodies/μm^2). In the absence of TNF-α induced ICAM1 activation, neither the anti-ICAM1 coated MSCs or the unmodified MSCs were retained on the HUVEC surface under flow. This is

expected as MSCs do not typically interact with endothelial cells through direct physical interactions. The statistically insignificant increase in mean retention of the anti-ICAM1 coated MSCs over uncoated MSCs on non-activated HUVECs is potentially attributed to the low basal expression of ICAM1 on HUVECs is <10 ICAM1/μm^2, Figure 5.11). While specificity is not required for this application, the antibody-driven mechanism of retention is expected to be specific. These *in vitro* shear studies on activated HUVECs support the proposed antibody-antigen mode of retention as the driver for the increased MSC retention *in vivo*.

To further confirm the proposed mechanism for MSC retention, we evaluated cell adhesion to an ICAM1-coated surface under shearing flow (Figure 5.12a). Epoxy coated glass slides were incubated in human ICAM1, and the density of ICAM1 on the glass surface was determined through fluorescent labeling of ICAM1, and correlation of fluorescent intensity to a calibration slide in a microarray scanner. This approach provided surface densities of purified protein to 5,000 ICAM1/μm^2 (Figure 5.12b), and this range encompasses the surface density of ICAM1 on non-activated and activated HUVEC cells (Figure 5.11). In particular, we focused on incubations of 6.25 μg ICAM1/mL to give a surface density of 2,400 ICAM1/μm^2 to replicate the surface density of HUVECs activated with 20 h exposure to TNF-α (1,500 ICAM1/μm^2). MSCs were added to the ICAM1 surfaces, incubated for 5 minutes at 37ºC, and subjected to shearing flows. For all groups of anti-ICAM1 coated MSCs, the majority of the cells remained adhered for the expected physiological range of wall shear stress (<70 dyne/cm^2). Increasing the contact time between the MSC and the ICAM1 surfaces to 45 minutes did not have a significant increase in the fractional retention of cells, suggesting the adhesion is dominated by rapid

binding events, including the expected antibody-antigen interactions. Importantly, the fractional retention of anti-ICAM1 coated MSCs on the purified ICAM1 surface compares favorably with the fractional retention of for anti-ICAM1 coated MSCs on the activated HUVECs. These two systems were run using the same MSC-surface contact times, antigen type, and antigen density. The quantitative agreement in MSC retention supports the antibody-antigen mode of retention in the HUVEC study, and by extension supports the role of antibody coatings in the increase in anti-ICAM1 coated cell retention *in vivo*. We were unable to retain any uncoated MSCs on the ICAM1 coated surface under the most minimal shear (Figure 5.13 and 5.14), and this supports our significant differences between coated and uncoated cells *in vivo*, and in the *in vitro* assay of MSC attachment to activated endothelial cells.

Throughout our *in vitro* shear assays, MSCs that were biotinylated using 1 mM NHS-biotin were retained to a lesser degree than the MSCs that were biotinylated using 0.1 mM NHS-biotin (Figure 5.9c and 5.12c). This is counter intuitive, given the higher ligand density resulting from the 1mM NHS-biotin treatment. Given the necrosis associated with >1 mM NHS-biotin [182], we suspect this higher concentration is causing damage to the MSCs which we are not able to detect through viability, proliferation, or function assays. It is reasonable to think that excessive conjugation of cell surface proteins will have a significant impact on the function of these proteins. The shear assays of coated cells on purified surfaces of ICAM1 (Figure 5.12c) still support the antibody-antigen mechanism, but the magnitude of the effect is lower with the 1 mM NHS-biotin than for the 0.1 mM NHS-biotin.

5.5 Conclusions

Direct injection of cells is commonly thought of as a reasonable method of directly controlling the position of cells *in vivo*. But on its own, direct injection is not capable of retaining the majority of these cells at the injection site across multiple clinical applications [164, 183-186]. While other studies have demonstrated ICAM1 based retention of cells in inflammatory bowel disease [136], this study is the first direct evidence that anti-ICAM coatings increase the number MSCs retained in the heart tissue following a heart attack. We support the *in vivo* retention phenomenon with a mechanistic study of the adhesion of the cells when subjected to fluidic shears. The anti-ICAM coating significantly increases the number of cells retained on activated endothelial cells. To eliminate other cellular processes, we further supported this mechanism by coating microscope slides with ICAM1 protein and demonstrated the enhanced retention of the anti-ICAM1 coated MSCs over unmodified MSCs. In all, we connected the design of a cell's surface can significantly increase the number of MSCs remaining in a post-infarct heart by promoting strong adhesion between the MSC and ICAM1 presented by the inflamed endothelium. More broadly, this study is additional evidence that the intentional engineering of a cell's peripheral membrane is an effective strategy for improving the localization of injected cells in the ever-expanding range of emerging cell-based therapies proposed in modern medicine.

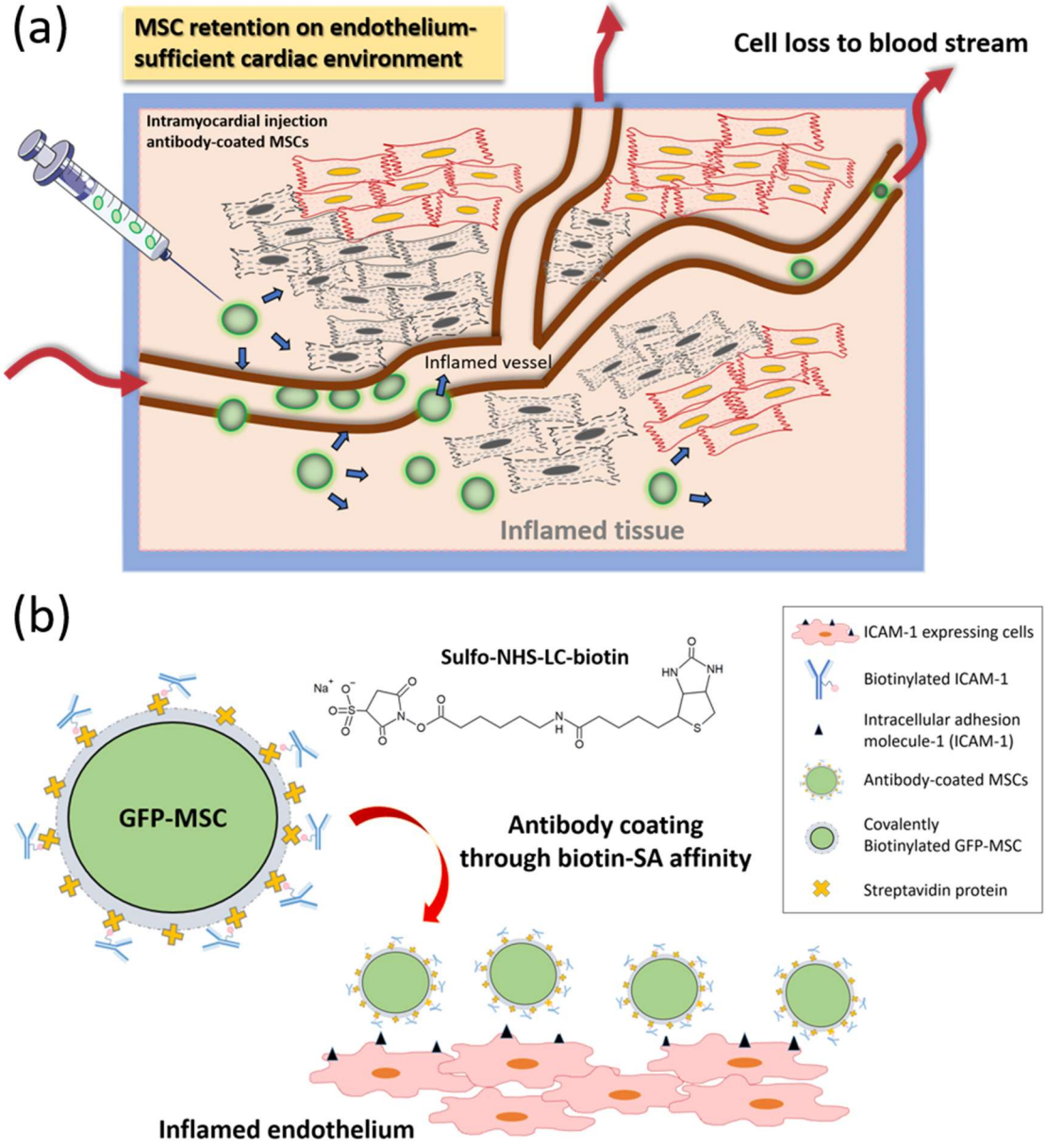

Figure 5-1. Scheme of intramyocardial delivery of antibody-coated MSCs. (a) Direct intramyocardial injection of antibody-coated MSCs and subsequent interaction of MSCs with inflamed endothelium. (b) Incorporation of inflammation-targeted antibody on MSCs through biotin-streptavidin affinity.

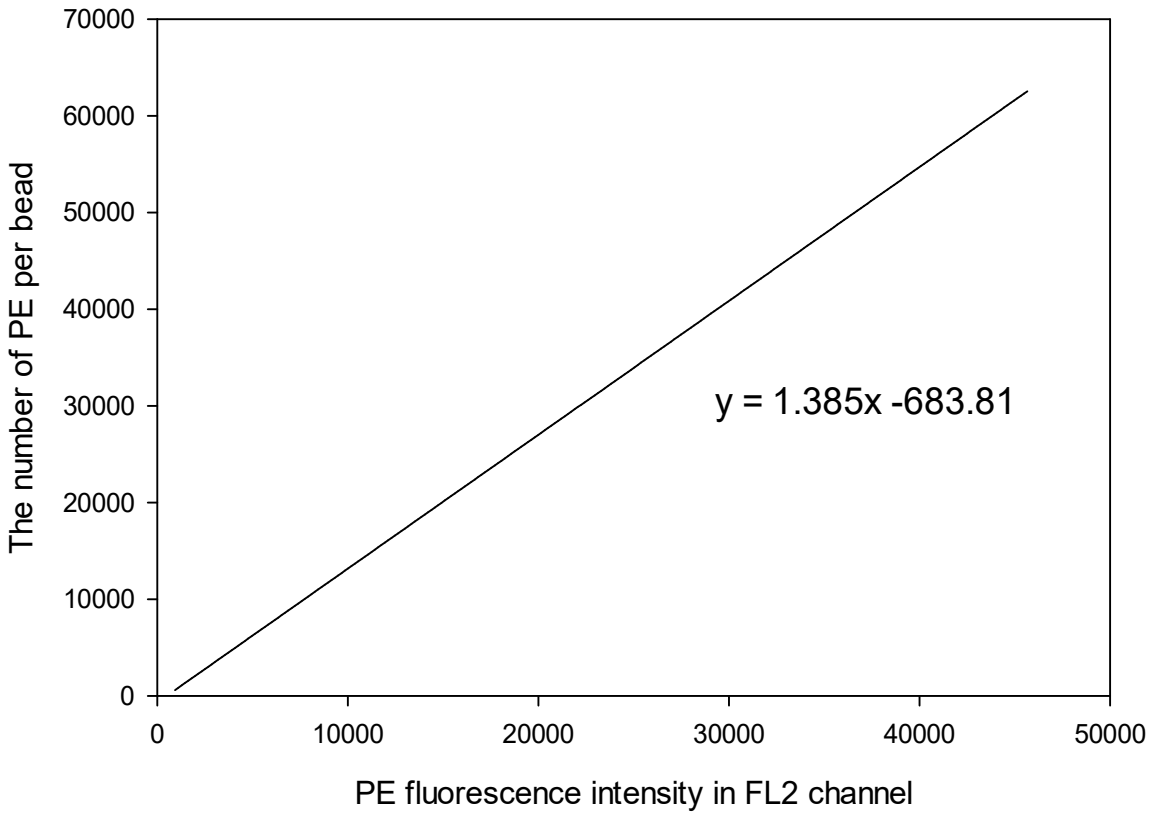

Figure 5-2. Standard calibration curve of PE quantitative beads.

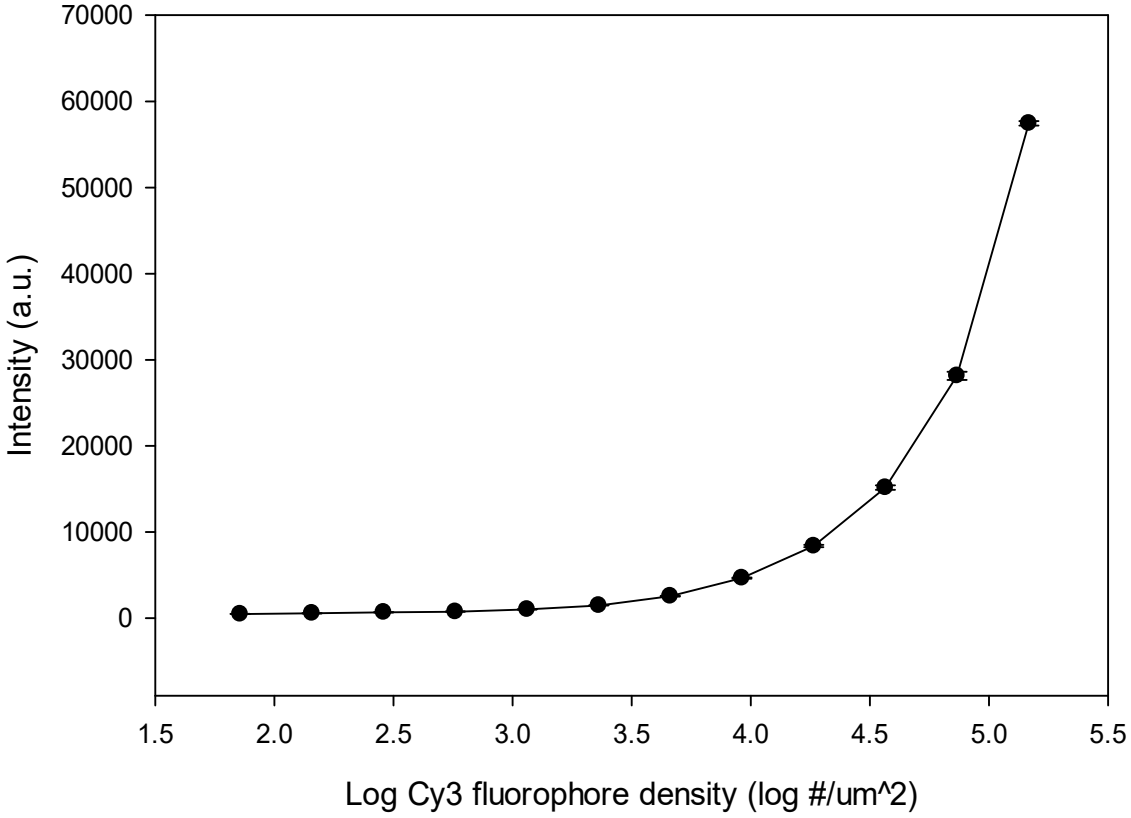

Figure 5-3. Calibration curve of Cy3 fluorophore number.

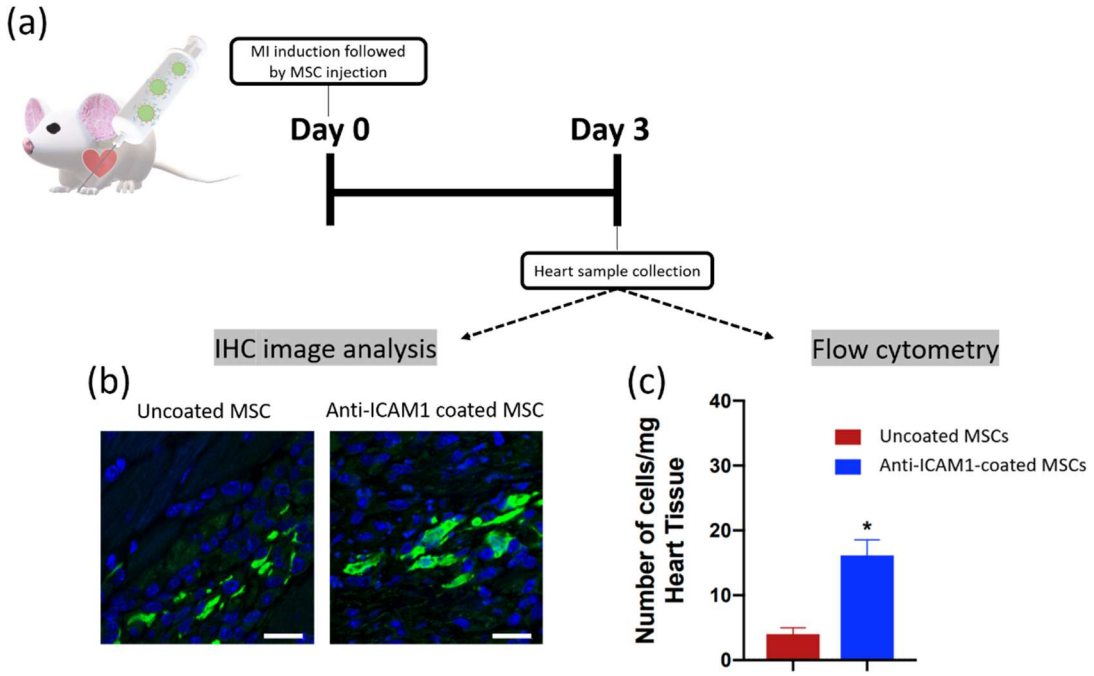

Figure 5-4. *In vivo* Intramyocardial delivery of ICAM1 antibody-coated MSCs in infarcted mouse model. (a) Timeline of MI induction, MSC injection and sample collection. The coated or uncoated cells were directly injected into peri-infarct area immediately after left anterior descending artery ligation. At day 3, the heart sample was collected and digested for flow cytometry and immunohistochemistry analysis. (b) Representative immunofluorescent analysis of uncoated and anti-ICAM1 coated GFP-MSCs retention in infarcted heart tissues. The scale bar is 20 μm. (c) Quantitative retention analysis of uncoated MSCs and anti-ICAM1-coated MSCs through flow cytometry. Data are presented as mean number of retained MSCs with stand errors (n=4 for uncoated cells and n=3 for anti-ICAM1 coated MSCs).

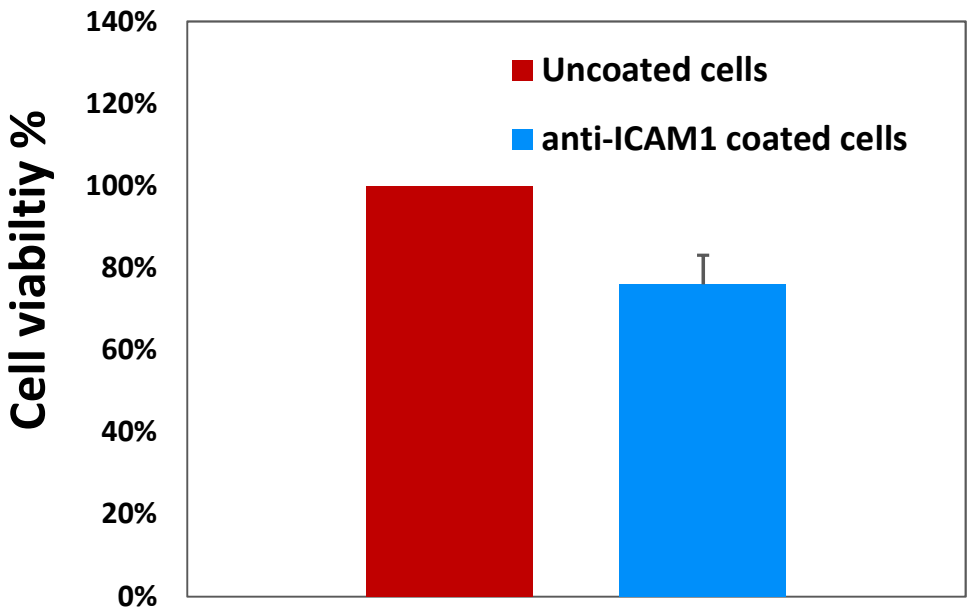

Figure 5-5. Cell viability of anti-ICAM1 coated cells (n=4).

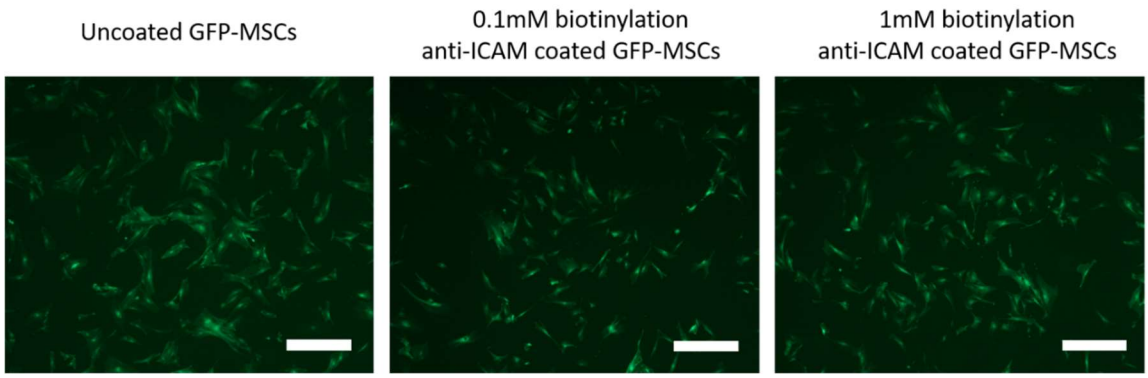

Figure 5-6. Cell attachment after anti-ICAM1 coating on GFP$^+$ MSCs. The scale bar is 100 µm.

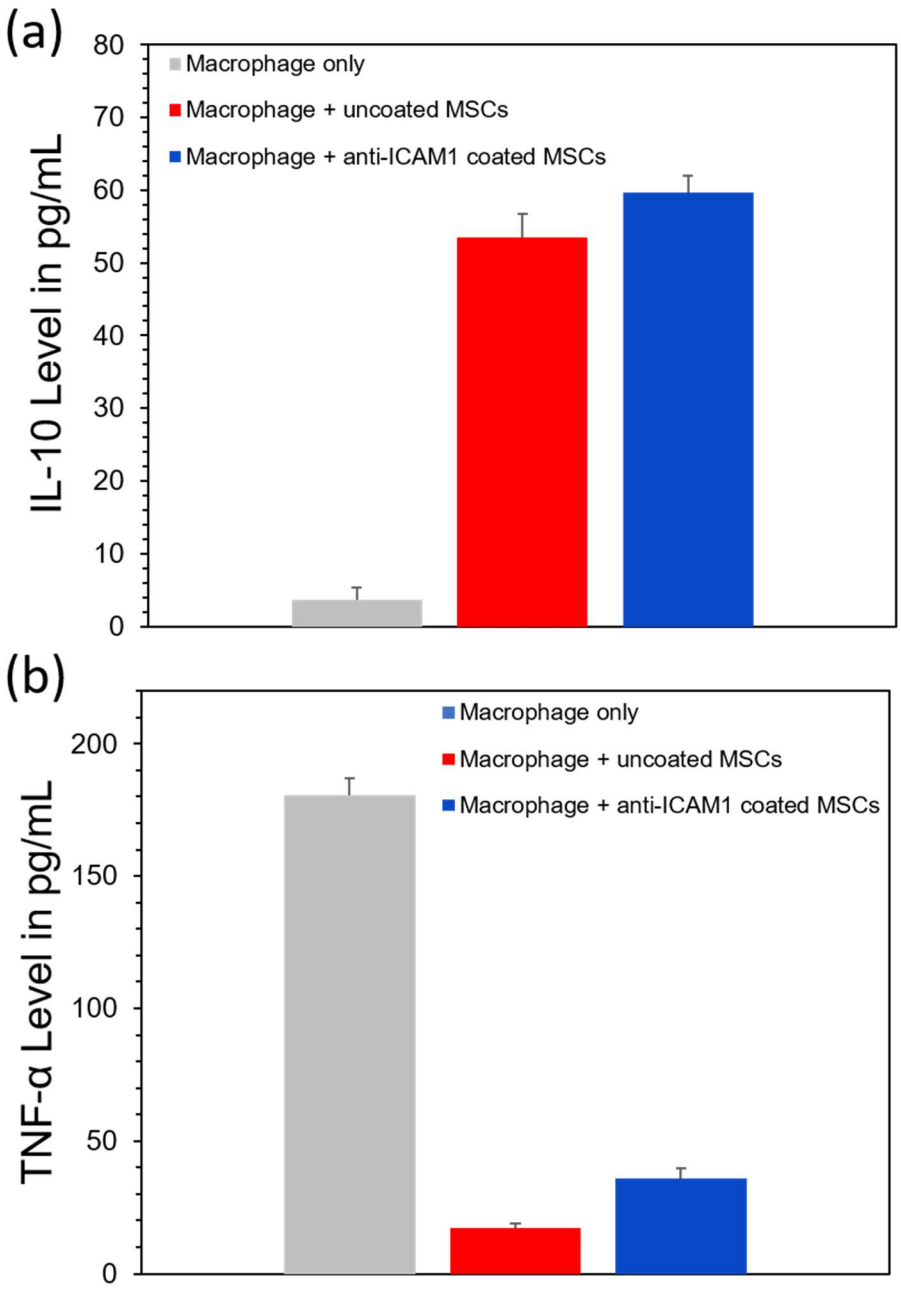

Figure 5-7. Immunosuppressive cytokine secretion from macrophage-interacted MSCs.

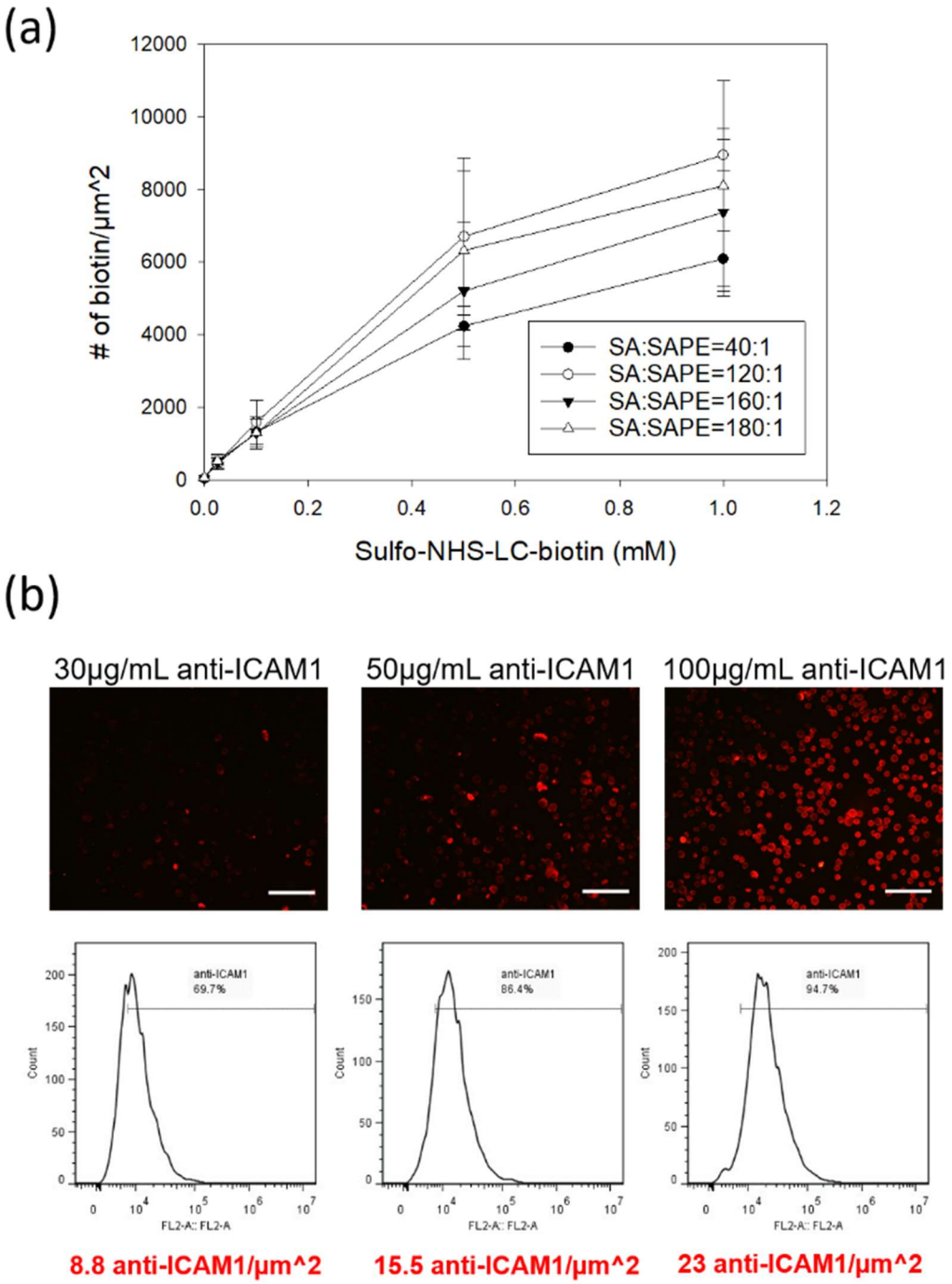

Figure 5-8. Quantitation of surface biotin density on biotinylated MSCs. (a) Quantitation of biotin groups through competitive binding of SA/SAPE on biotinylated cells. The ester-biotin treated cells were stained with four different ratios of SA to SAPE (n ≥3). (b) Quantitation of ICAM1 antibodies on the MSC surface with different antibody concentrations (30, 50 and 100 μg/mL) through secondary PE labeling (n ≥3). The scale bar is 100 μm.

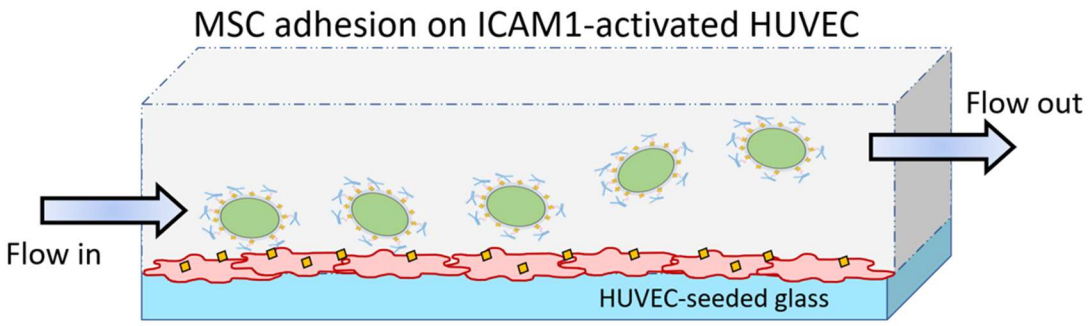
MSC adhesion on ICAM1-activated HUVEC
Flow out
Flow in
HUVEC-seeded glass

(b)

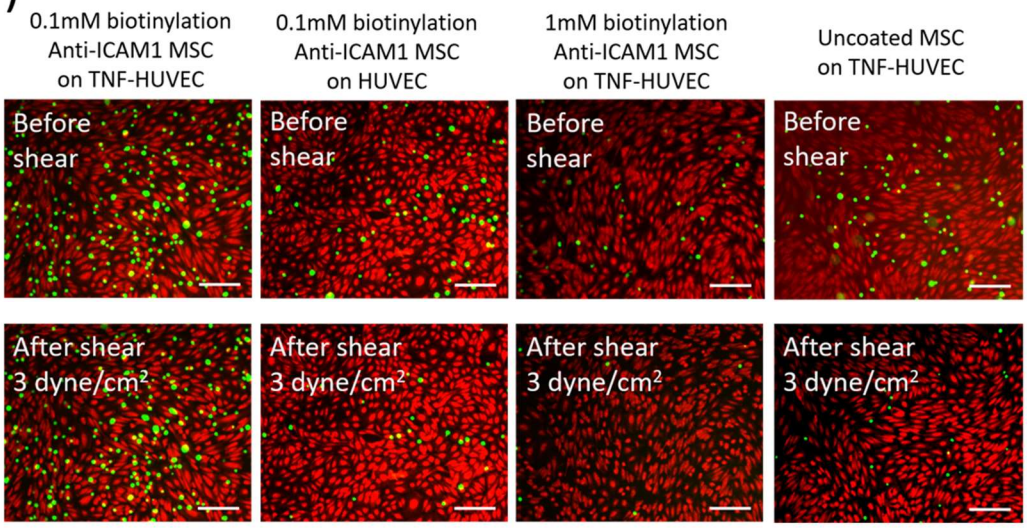
0.1mM biotinylation Anti-ICAM1 MSC on TNF-HUVEC
0.1mM biotinylation Anti-ICAM1 MSC on HUVEC
1mM biotinylation Anti-ICAM1 MSC on TNF-HUVEC
Uncoated MSC on TNF-HUVEC
Before shear
After shear 3 dyne/cm²

(c)

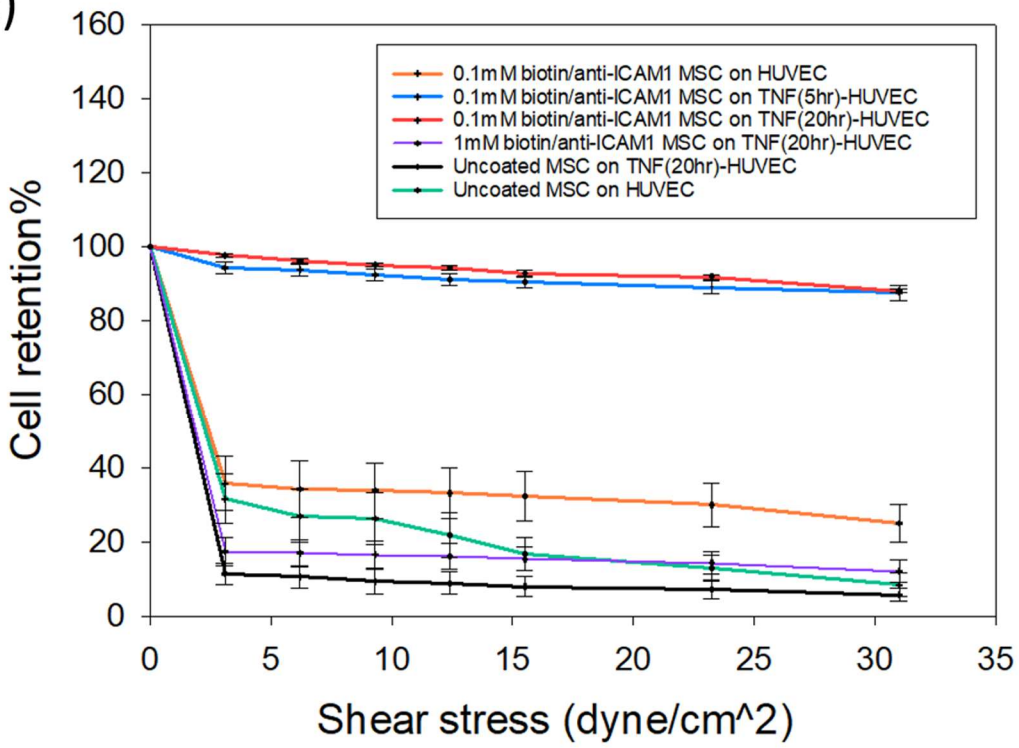
0.1mM biotin/anti-ICAM1 MSC on HUVEC
0.1mM biotin/anti-ICAM1 MSC on TNF(5hr)-HUVEC
0.1mM biotin/anti-ICAM1 MSC on TNF(20hr)-HUVEC
1mM biotin/anti-ICAM1 MSC on TNF(20hr)-HUVEC
Uncoated MSC on TNF(20hr)-HUVEC
Uncoated MSC on HUVEC
Cell retention%
Shear stress (dyne/cm^2)
0
20
40
60
80
100
120
140
160
0
5
10
15
20
25
30
35

Figure 5-9. Cell adhesion on ICAM1-expressed endothelium and cell detachment under the presence of shear flow. (a) Schematic diagram of experimental setup of shear-detached cells on HUVEC monolayer. (b) Fluorescence images of adhesion behavior of uncoated or anti-ICAM1 coated MSCs (GFP^+) on untreated or TNF-α-treated HUVECs (calcein-red staining) under shear flow. The anti-ICAM1 coated cells were treated with 0.1mM or 1mM ester-biotin, respectively. Cell adhesion behavior was observed before and after shear (3dyne/cm^2). The scale bar is 100 μm. (c) Relationship between cell retention % and shear stress under different cell adhesion conditions ($n \geq 5$).

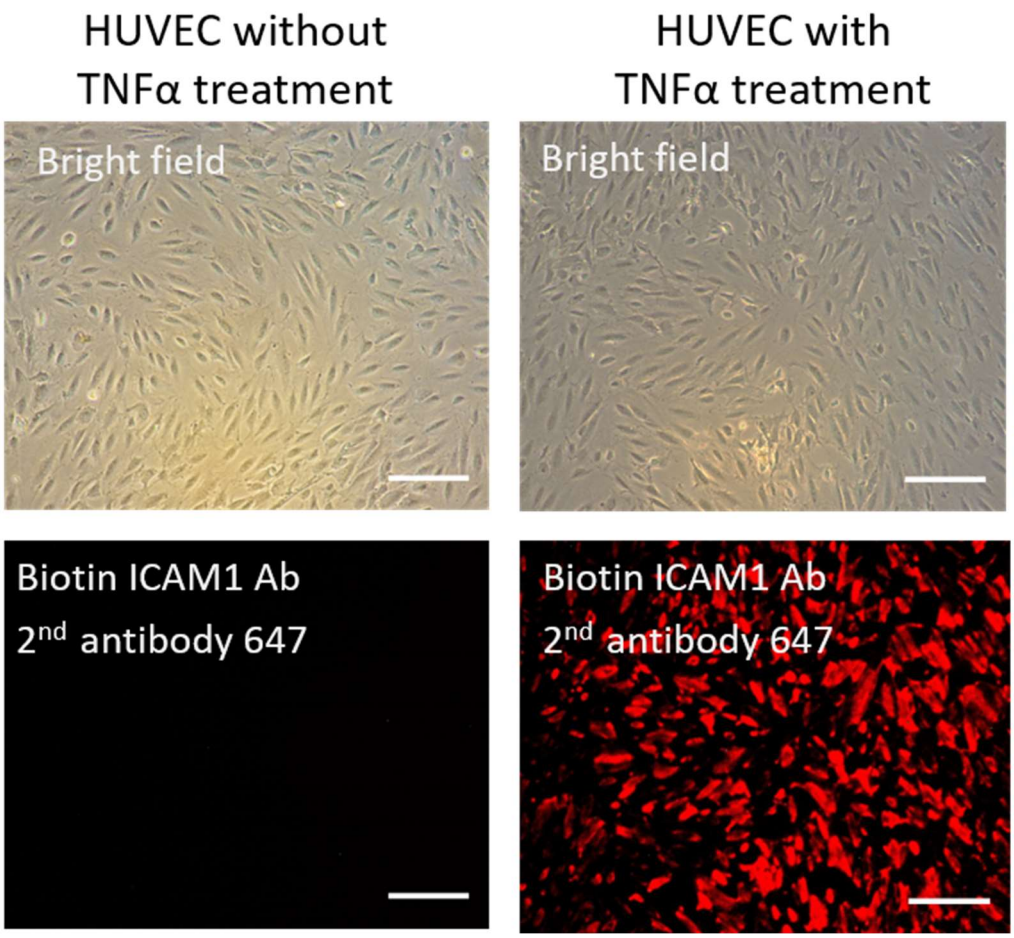

Figure 5-10. Immunostaining of human ICAM1 protein on non-treated or TNF-α treated HUVECs. The scale bar is 100 μm.

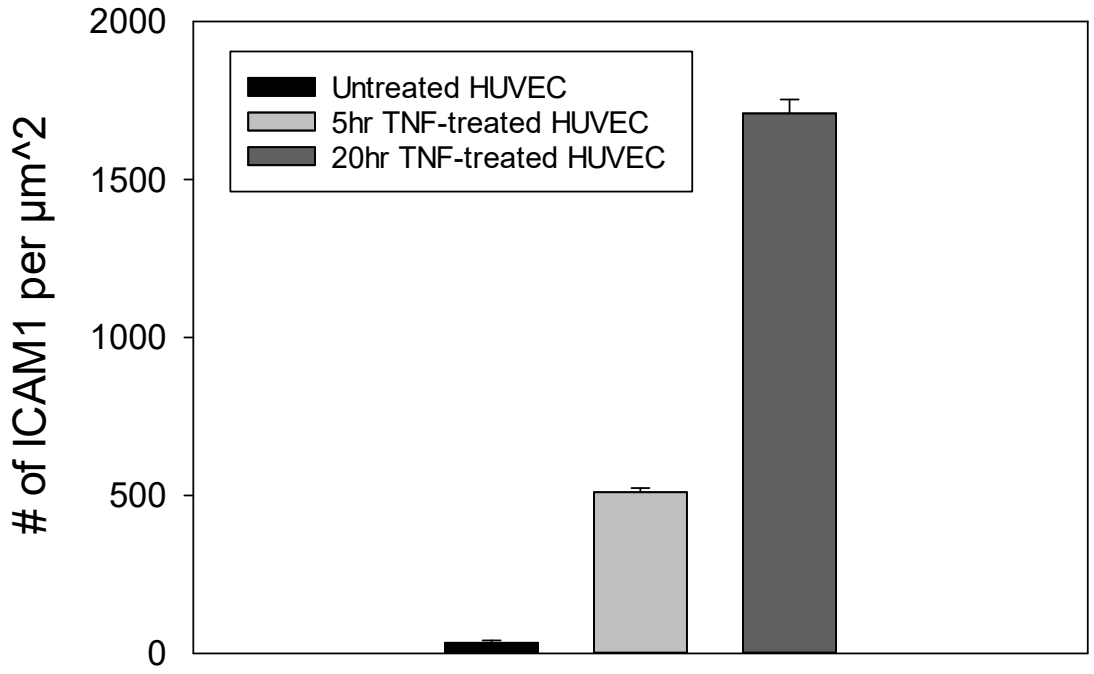

Figure 5-11. Quantitative analysis of ICAM1 surface density on non-treated, 5hr TNF-α-treated, or 20hr TNF-α-treated HUVECs by flow cytometry (n=3).

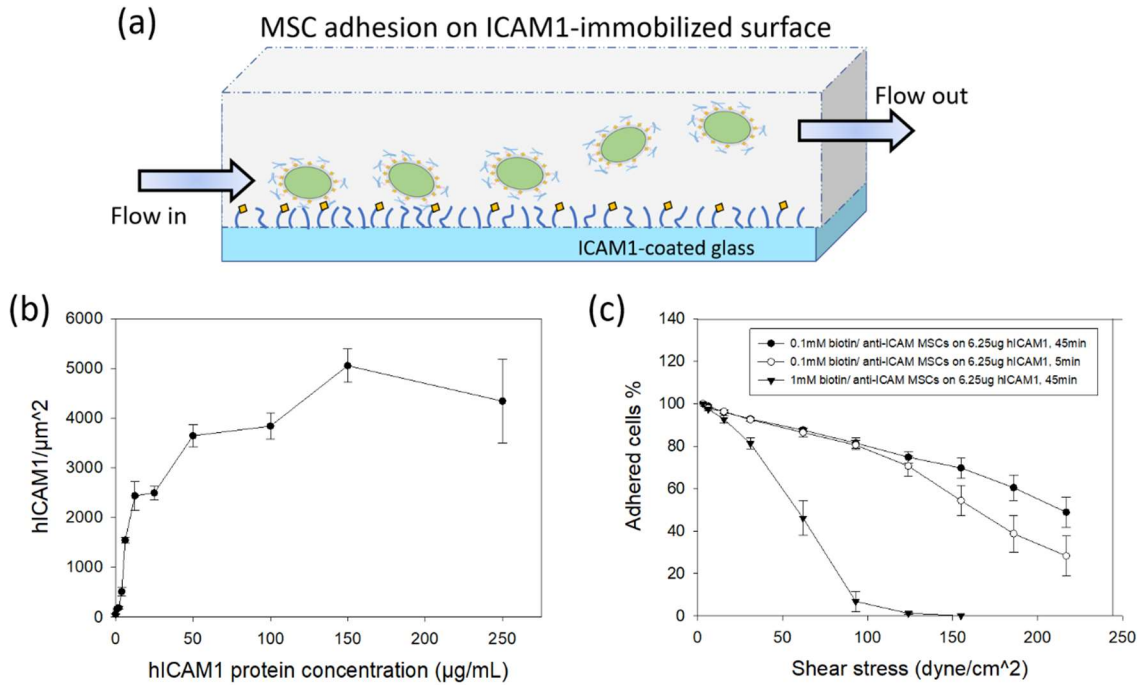

Figure 5-12. Cell adhesion on ICAM1-modifed glass and cell detachment under the presence of shear flow. (a) Schematic diagram of experimental setup of shear-detached cells on ICAM1-modifed glass. (b) Relationship of human ICAM1 protein density and protein concentration used for epoxide glass modification (n=3). (c) Relationship between attached cells % and shear stress under different cell adhesion conditions (n ≥4).

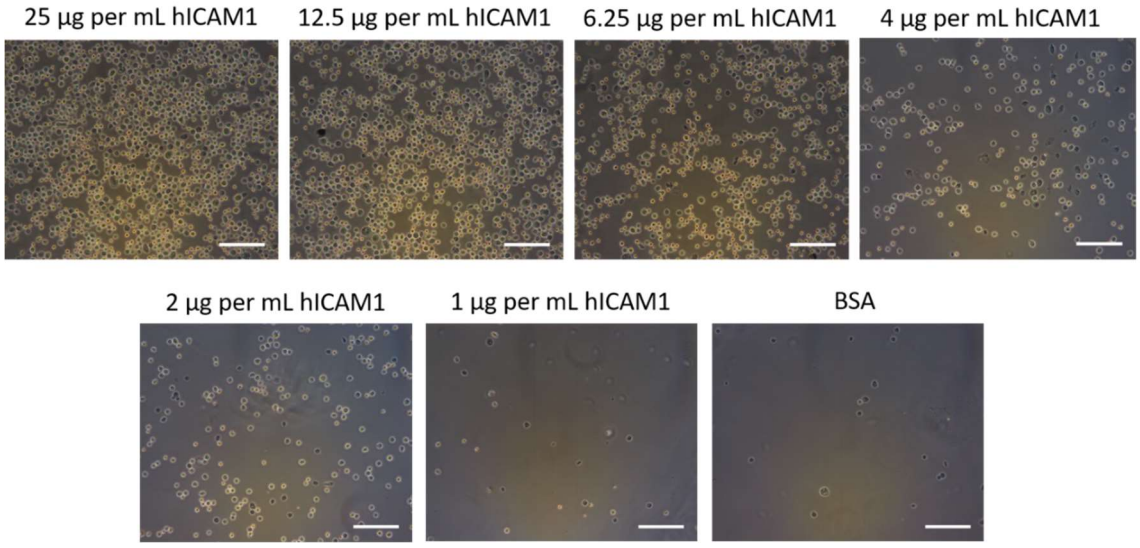

Figure 5-13. Stationery adhesion of anti-ICAM1 coated MSC on hICAM1-modified glass. The scale bar is 100 µm.

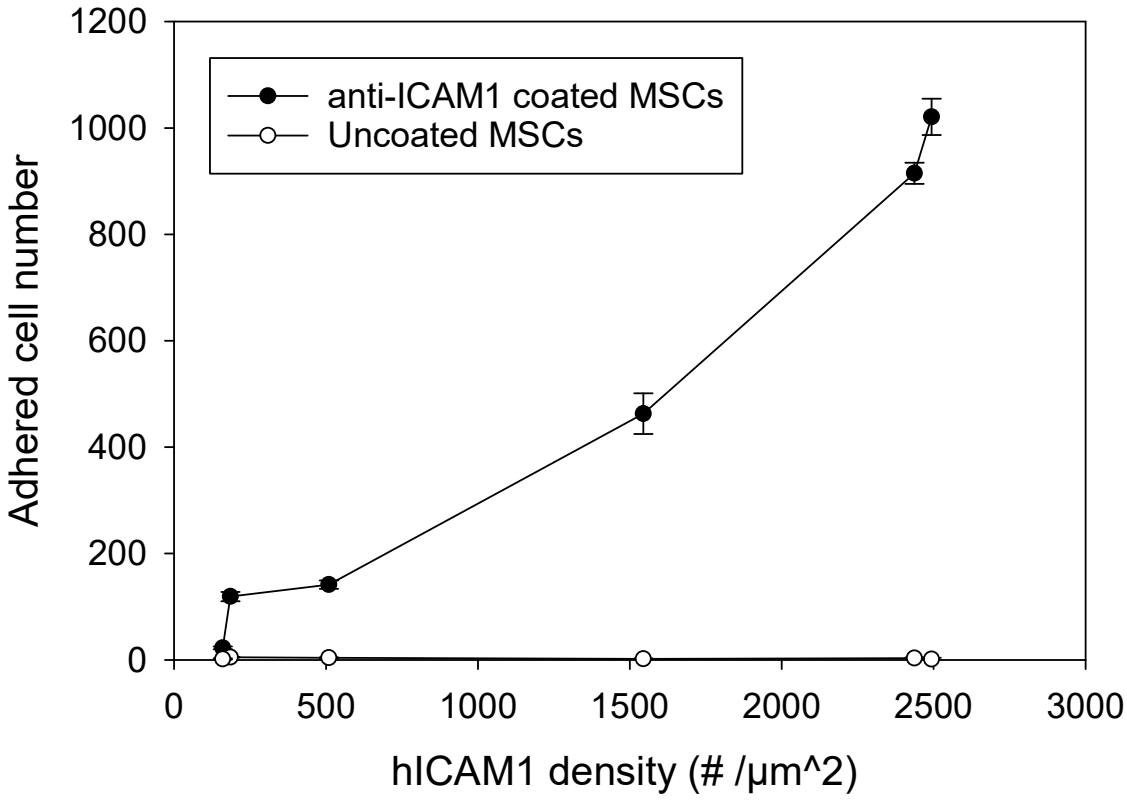

Figure 5-14. Stationery adhesion of anti-ICAM1 coated or uncoated MSCs on ICAM1-modified glass. Data are mean adhered cell numbers with stand errors (n ≥10).

CHAPTER 6. INTRAVENOUS TARGETING OF MSCS TO MODULATE POST-INFARCT INFLAMMATION

6.1 Introduction

Insufficient MSC homing to targeted inflammation in AMI-induced heart represents one of the most critical challenges in regenerative therapy. Targeted cell delivery appears to be a promising solution for MSC retention in the heart. Herein, the section will demonstrate a cell surface antibody coating on immunosuppressive MSCs for inflamed tissue targeting. Initially, by using flow cytometry, the feasibility to coat cells with ICAM1 antibody was evaluated by surface group quantitation. The adhesion efficacy of coated cells is correlated to antigen presence on ICAM1-modified surfaces. By introducing shear flow, I examined the adhesion force present by this antibody-coated cells. The optimal adhesion efficacy of coated cells was proposed in this study by biotinylating cells with 0.1mM sulfo-NHS-LC-biotin. One day after the cell injection through retro-orbital vein, the flow cytometry results showed higher coated MSC accumulation in the heart, spleen and lung, as compared to uncoated MSCs. By quantifying immune cells such as neutrophil, monocyte, leukocyte and macrophages in the heart tissues, the intravenous delivery of anti-ICAM1 coated cells exhibited the dramatically reduced post-MI inflammation responses.

6.2 Background

Despite significant advances in rapid clinical interventions, acute myocardial infarction (AMI) is still plagued by high prevalence, morbidity and mortality. The majority of clinical progress centers on the rapid clearance of obstruction and the prevention of

restenosis. Critically, the processes responsible for the progressive loss of functional heart tissue have already initiated. This initial site of damage kicks off a cascade of inflammation that gradually expands the infarct to encompass large sections of the myocardium, resulting in tissue fibrosis, ventricular remodeling, heart dilation [187, 188]. Infarct expansion and heart's negligible capacity for regeneration leads to an irreversible loss of function and an increased risk of heart failure.

The prevention of infarct expansion is an exciting path to improve cardiovascular function post-AMI. Apoptotic cells release many factors which activate inflammatory cells and lead to the abundant production of pro-inflammatory cytokines. This inflammation damages nearby healthy tissue and expands the infarct. Mesenchymal stem cells (MSCs) are potent modulators of inflammation[189-191]. The inflammatory signal cascade triggers the MSCs to release immunosuppressive factors and growth factors [189, 192-194]. The implantation of MSCs near infarcted tissue has slowed the progression of infarct expansion and improved cardiovascular function. Additionally, implanted MSCs have some capacity for regeneration through differentiation into endothelial cells, smooth muscle cells, and cardiomyocytes [111, 112, 118, 169, 195-201]. In all, the implantation of MSCs is promising for protecting the heart from damage post-AMI and repairing cardiovascular tissue.

The most effective mode of MSC implantation post-AMI is the direct injection of cells into the heart wall adjacent to the infarct. The precision of an intramyocardial injection is unsurpassed for localized MSC delivery, and this strategy has been effective in numerous animal studies [91, 202, 203]. Critically, direct injection into the wall of a beating heart in humans requires opening of the chest cavity, and the risk associated with

this invasive procedure is clinically prohibitive. As a result, most clinical studies sacrifice the localization of intramyocardial injection for intravenous (IV) injections with minimal targeting of MSCs to the target tissue [160, 161, 204-206]. With IV injections, MSCs typically distribute to the lungs and spleen [161, 163, 204].

Here, we demonstrate a simple cell surface engineering strategy to home IV injected MSCs to an infarct site through inflammation targeting (Figure 6.1). The inflammation that drives unfavorable expansion of the infarct actively recruits leucocytes through the expression of ICAM1 on endothelial cells. We create MSCs that are coated with antibodies against ICAM1 to mimic leucocyte recruitment and support the retention of MSCs in the inflamed myocardium. To create a cell with an ICAM1-targeting capacity, we covalently biotinylated cell surface proteins with sulfo-NHS-biotin, and then deposited a layer of streptavidin to anchor subsequent additions of biotin mouse ICAM1 antibody onto the MSC's peripheral membrane. We hypothesize that the antibody coated cells will adhere to ICAM1 and that more IV administered ICAM1 cells when coated with antibodies against ICAM1. We test these hypotheses using an established mouse model of AMI, and then support the *in vivo* findings with microfluidic *in vitro* analysis. The antibody coated MSCs are retained on surfaces of mouse ICAM1 and in the infarcted mouse heart more than unmodified MSCs. Further, there is a decrease in the number of neutrophils, leukocyte, macrophage and monocytes in the infarcted hearts when antibody coated cells were administered over unmodified MSCs. While targeting of cells has been applied to other inflammatory conditions [135, 136], this work is the first ICAM1 targeting of cells to effectively modulate the immune environment of the post-AMI heart.

6.3 Experimental section

6.3.1 MSC isolation and culture

Mouse mesenchymal stem cells (MSCs) isolated from C57BL/6 or C57BL/6-Tg (CAG-EGFP)131Osb/LeySopJ mice (Jackson Laboratory, BarHarbor, ME). After the mice were sacrificed, femurs, tibias and hip bones were collected and then flushed with PBS supplemented with 10% FBS. MSCs used in this study were of a passage less than 10. MSCs were cultured in pre-warmed mouse MesenCult^{TM} basal medium, supplemented with MesenCult™ 10X Supplement (STEMCELL Technologies), 10% USDA Approved Origin FBS (VWR), 1% 200mM L-glutamine (Gibco) and 1% streptomycin/penicillin (Gibco). MesenPure^{TM} (STEMCELL Technologies) was added in MSC medium at 1:1000 dilution right before cell seeding. MSCs were cultured under hypoxic conditions (less than 5% O_2 supply) for MSC cultivation was needed by introducing ultrapure nitrogen into a 37ºC humidified incubator, with 5% CO_2. For cell collection, cells were rinsed with sterile DPBS (Corning) and treated with 0.25% trypsin/EDTA (Gibco) for 5 min in 37ºC. Serum-containing medium was added to neutralize the trypsin. Cells were centrifuged at 300 g for 5 min and the supernatant was removed by pipetting. The cell pellet was washed once and resuspended in ice-cold phosphate buffered saline (PBS) buffer (Gibco) before use.

6.3.2 Preparation and surface group quantitation of anti-ICAM1 coated MSCs

All incubation steps for cell membrane antibody incorporation were processed on ice. MSCs were rinsed twice with cold PBS. 0.1 mM or 1 mM sulfo-NHS-LC-biotin was prepared in PBS immediately before cell incubation, 2 mL of biotin solution per million cells is added for 1 h. Cells were then rinsed twice with PBS, and 2 mL of 25 μg/mL streptavidin in PBS was added for every million cells for 1 h. The streptavidin coated cells were then incubated for 1h in 30, 50, or 100 μg/mL biotin monoclonal rat antibody against

mouse ICAM1 (clone YN1/1.7.4, Invitrogen) in PBS. For intravenous injection, cells were treated with 0.1 mM sulfo-NHS-LC-biotin, 25 μg/mL streptavidin and then 100 μg/mL anti-ICAM1.

QuantiBRITE^{TM} PE tubes purchased from BD Biosciences is a phycoerythrin (PE) fluorescence quantitation kit and includes PE quantitative beads presenting different fluorescence intensity levels with the given information of corresponding number of PE conjugated per bead. PE fluorescence was collected in the FL2 channel (filtered by 585/40 bandpass wavelength) by flow cytometry. The calibration curve of mean FL2 fluorescence per PE was plotted, and the linear regression equation was used for quantitation of PE fluorophore bound to each cell (Figure 6.2).

MSC-associated antibody was stained by 2 μg/mL of mouse PE-conjugated secondary antibody against rat (clone R2B-7C3, Invitrogen). PE fluorescence was acquired by FL2 channel in flow cytometry. By assuming the binding ratio of PE, secondary antibody and primary ICAM1 antibody is 1:1:1, the number of ICAM1 antibody coated on each MSC is estimated by the calibration curve (Figure 6.2).

6.3.3 Cell attachment and MTT viability assay

After anti-ICAM1 coating, $0.1x10^6$ coated cells were cultured in a 12.5 cm^2 tissue culture flask with MSC expansion medium for 2 days. Attachment behavior, cell expansion and GFP fluorescence of coated GFP^+ MSCs was observed with epifluorescent microscopy.

Metabolic activity detection depending on mitochondrial function was evaluated by using MTT (3-(4,5-Dimethylthiazol-2-yl)-2,5-Diphenyltetrazolium Bromide) reagents (M6494, Invitrogen). A 12mM MTT solution was prepared in PBS (5mg/mL). 50,000 cells

were diluted in 1mL MSC medium. 200 μL of cell solution was pipetted into 96 well plate and incubated with 20 μL of MTT stock for 4 h at 37 °C. Cell supernatant was removed after centrifuge (1 rpm, 5 minutes) and 200 μL of DMSO was added to dissolve the reacted product. A plate reader (Biotek, Winooski, VT) was used to examine the sample absorbance at 570 nm. The percentage of cell viability was determined by normalizing the sample absorbance with the positive control.

6.3.4 Preparation and ICAM1 quantitation of mouse ICAM1-coated slides

Recombinant mouse ICAM-1/CD54 Fc chimera protein (796-IC, R&D systems) was reconstituted at 250 μg/mL in sterilized PBS and stored at 4 ºC before use. The density of mouse ICAM1 protein was estimated by specifically fluorescent targeting on mICAM1 molecules coated on protein-reactive glass surfaces. Twelve concentrations of mICAM1 protein (100; 50; 25; 12,5; 6.25; 4; 2; 1; 0.5; 0.25; 0.1 μg/mL and PBSA negative control) were tested in this study. Epoxide slides were placed in a lid-covered petri dish, coated with 30 μL of mICAM1 protein solution in a 1cm^2 area for 3 h, and then rinsed twice with 0.1% BSA in PBS. ICAM1-immobilized slides were loaded into Whatman Chip Clip, blocked with 0.1% BSA for 30 min, and washed with 1X PBS twice. Each ICAM1-coated area was labeled with 50 μL of 30 μg/mL biotinylated mouse ICAM1 antibody for 1 h and rinsed twice with PBS. Biotinylated immobilized sites were fluorescently tagged through the incubation of 70 μL diluted SA-Cy3 (1:40 in PBS) in each well for 30 min. After rinsing with PBS three times, slides were dried in a stream of air and scanned in an Affymetrix 428 Microarray Scanner at 30 dB gain in the Cy3 channel. The number of Cy3 molecules were estimated by Cy3 calibration curve (Figure 6.3) prepared using a Cy3 calibration slide from Full Moon Biosystems and image analysis using Image J software.

6.3.5 Laminar flow chamber assay

A 1 cm by 1 cm region of an epoxy slide was treated with 50 µL of mouse ICAM1 protein in PBS (0.1; 1; 6.25; 100; 250 µg per mL) for 3h at room temperature in a sealed dish. The protein-coated slides were blocked with 1 mg/mL BSA in PBS for 30 min. 50 µL of $0.5x10^6$ coated or uncoated MSCs were added onto the mICAM1-coated surface for 45 min at room temperature.

To assemble the flow chamber system, a parallel laminar flow chamber from Glycotech (#31-010) was flipped upside down with a 0.01-inch-thick gasket tightly mounted on the chamber bottom. In this microfluidic chamber, tubing is connected to the inflow port from a PBS-filled reservoir. The tubing from the outflow port was connected to two 60 mL syringes on a two-channel syringe pump (NEWERA, #4000-US). Additional tubing was connected to a vacuum pump to secure the device to the sample slide. The entire gasket area on the slide was covered with PBS, the sample slide was then gently and parallelly covered, to avoid bubble formation in the device. The vacuum pump then secured the slide to the microfluidic device. To introduce laminar flow, the syringe pump was turned on to pull the liquid into the system at various flow rates. GFP-cells were sheared for 30 s, and the number of cells remaining on the slide were counted using ImageJ.

6.3.6 Myocardial infarction surgery and Intravenous MSC delivery

MI surgery was performed as previously described [47]. Briefly, 8-10-week female C57BL/6 mice were anesthetized under 1-3% isoflurane using a small animal vaporizer system. MI was induced by permanent left anterior descending artery (LAD) ligation. Two hours after MI surgery, mice were randomized to receive 100uL of either PBS, MSCs, or

anti-ICAM1 modified MSCs ($1x10^6$ cells per injection per mouse) via intravenous injection. Pain medications were administrated after surgery for 24-48 hours.

6.3.7 MSC in heart, spleen and lung and inflammatory cells in infarcted heart

Single-cell suspensions for flow cytometry analysis were prepared from digested cardiac tissue as previous described [47]. Briefly, hearts and lungs collected 1 day after MI were minced then digested using a collagenase B (Roche, Indianapolis, IN) and dispase II (Roche, Indianapolis, IN) solution for 30 minutes at 37°C with mixing every 5 minutes. The cell suspensions in the heart, lung and spleen were strained using 40 μm strainers (VWR, cat#10199-654) to remove tissue debris and undigested tissue. Cells were washed with flow buffer with centrifugation (400×g for 10 min at 4 °C) and suspended in Flow Buffer. Retained GFP^+ MSCs were stained with eFluor 660 conjugated anti-GFP antibody (eBioscience, Thermo Fisher Scientific, Waltham MA) and analyzed using an LSR II (Becton Dickinson) in the University of Kentucky Flow Cytometry Core. For cardiac inflammatory cells, antibodies against Ly6G/C (BD Pharmingen), CD45 (Biolegend), CD115 (Biolegend), CD11b (Biolegend), and F4/80 (Biolegend) were used to identify inflammatory neutrophils, macrophage, leukocyte and monocytes. We utilized FlowJo v10 (FlowJo, FlowJo Ashland OR) software to generate dot plots and analyze the data.

6.4 Results and discussion

IV injection is a simple and minimally invasive route for MSC delivery, but the poor recruitment of MSCs to the heart limits the efficacy of IV administration. Our strategy to increase the MSC population in the heart is to coat the MSCs with antibodies against

vascular inflammation associated markers (ICAM1) and allow these cells to naturally home to the ICAM1 upregulation surrounding the infarct.

Our approach for anti-ICAM1 cell coatings is to use the multivalence of streptavidin to connect a biotinylated cell surface to a biotinylated antibody. The cell surface is biotinylated with incubation of MSCs in 0.1 mM or 1 mM sulfo-NHS-biotin for 1 hr. The biotinylated cells are then incubated in 25 μg/mL streptavidin, and then in biotinylated antibodies against mouse ICAM1. The number of antibodies on the cell surface was estimated by fluorescently tagging the anti-ICAM1 with secondary antibodies and relating the measured PE fluorescence to a calibration curve of fluorescence per PE. The resulting number of PE per cell are considered an order of magnitude estimate of the number of anti-ICAM1 on the cell surface and dividing by a mean cell surface area provides an estimate of antibody density in our coatings. We first modified cells with 0.1 mM or 1 mM NHS-ester biotin, and then examined coating efficiency by using three biotinylated anti-ICAM1 concentration (30, 50 and 100 μg/mL) after streptavidin deposition. Interestingly, cell coating through 0.1 mM biotinylation had higher anti-ICAM1 surface density than 1 mM biotin coated cells. The process using 0.1 mM biotinylation delivered up to 74 ± 6.38 anti-ICAM1/μm^2 when streptavidin coated cells are incubated with 100 μg/mL biotinylated antibody (Figure 6.4a). There is a positive trend of antibody density with the concentration of the biotinylated antibody between 30 and 100 μg/mL for both 0.1 mM or 1 mM biotinylated groups (Figure 6.4a), and this trend is also supported qualitatively through epifluorescent imaging (Figure 6.4b).

These coatings do not have a negative impact on the viability, proliferation, attachment to tissue culture polystyrene, morphology, and immunosuppressive function of

MSCs. After anti-ICAM1 coating on GFP^+ MSCs, the coated and uncoated cells were re-cultured into medium-contained tissue culture plastics respectively. Under 2 days observation, all the cell groups showed no difference on cell attachment, morphology, and cell expansion rate. Additionally, the GFP fluorescence remains the same on both coated and uncoated cells (Figure 6.5). Moreover, cell viability is the second important indicator of normal cellular function. In this study, MTT assay was used to evaluate cell health after coating. The coated MSCs were treated with 0.1mM sulfo-NHS-biotin, 25 μg/mL streptavidin and 100 μg/mL antibody against mouse ICAM1. As positive control, uncoated cells were mixed with mitochondrial reactive reagents for metabolic activity determination. After 4 h MTT incubation, the anti-ICAM1 coated cells showed no significant influence in cell viability (Figure 6.6), which suggests the feasibility for cells to maintain their cellular functions after modification.

To support the proposed mechanism of targeting through differential adhesion to endothelial ICAM1 expression, we quantified adhesion of coated and uncoated MSCs to surfaces coated with BSA or mouse ICAM1. To mimic the inflamed endothelial surface, we coated epoxy functionalized microscope slides with purified mouse ICAM1 protein. The density of ICAM1 that is available for antibody binding was determined with primary antibodies against-ICAM1 and Cy3-labeled secondary antibodies (Figure 6.7a). Based on this analysis, up to ~9,000 ICAM1 are available for binding. We tested our system with a surface marker density as low as 300 ICAM1/ μm^2, which is slightly lower than we expect the ICAM1 density to be on an activated endothelium. While direct analysis of ICAM1 density on the inflamed mouse endothelium is not available, surface marker densities on endothelial cells rarely reach 10^4 markers/μm^2 [207]. These ICAM1-coated surfaces were

contacted with anti-ICAM1 coated MSCs treated with two different biotinylation conditions (0.1 mM and 1 mM biotin) and then subjected to laminar shear flow using a microfluidic chamber. By anti-ICAM1 coating with 0.1 mM biotinylation, the majority of the antibody coated MSCs were retained on the ICAM1 surfaces with antigen density higher than 5000 ICAM1/ μm^2 for wall shear stresses up to our system limit of 217 dyne/cm^2, while very few cells retained with ~300 ICAM1/ μm^2 (Figure 6.7b). On the other hand, as compared to 0.1 mM biotin-treated cells, the coated cells through 1 mM biotinylation exhibited overall lower retention efficacy (Figure 6.7c), which also agreed with the evidence of lower incorporated antibody number on MSC surfaces (Figure 6.4b). For our target application, around 90% of anti-ICAM1 coated cells were retained under the 15 dyne/cm^2 wall shear stress expected in microvessels adjacent to the infarct site (Figure 6.7b and 6.7c) [179, 181]. In support of inflammation targeting, negligible numbers of these same antibody coated MSCs adhered to control surfaces coated with BSA under any shear stress. In literature, unmodified MSCs are not localized to the inflammation when injected intravenously [208]. In our *in vitro* system, the unmodified MSCs do not adhere in any measurable amount to the ICAM1-coated surface. In all, the *in vitro* shear data is supportive of a greater number of antibody-coated cell adhering to ICAM1-expressing regions than for unmodified cells. Additionally, the antibody coated cells are expected to specifically target areas of inflammation through a preferential adhesion to regions of ICAM1-expression.

Based on the higher *in vitro* retention of anti-ICAM1 coated MSCs through 0.1 mM biotinylation than 1 mM biotin coated cells, we selected this optimized coating condition for *in vivo* intravenous injection. Herein, we anticipated the antibody coated cells would

specifically target the ICAM1-rich endothelium in the inflamed, post-AMI heart tissue. To best mimic clinical implementation of MSC therapies post-AMI, we inject the MSCs into the retro-orbital vein of mice that survived for two hours following AMI by ligation of the left anterior descending coronary artery. In agreement with clinical injection via a catheter, the circulatory pathway for retro-orbital injection provides the heart a first opportunity for heart engraftment prior to encountering the lungs or spleen (Figure 6.8a). The mice were randomly assigned into three treatment groups (Figure 6.8b): buffer only (n=4; 100 μL 1x PBS), unmodified MSCs (n=5; 10^6 cells in 100 μL 1x PBS), and anti-ICAM1 coated MSCs (n=4; 10^6 cells in 100 μL 1x PBS). Following 24 h, the mice were sacrificed, and each heart, lung, and spleen was digested to isolate the cells residing in each organ. The quantities of injected MSC were identified based on GFP expression in flow cytometry. The number of MSCs retained in the heart had over 3-fold increase for the antibody coated cells when compared to the unmodified MSCs ($p < 0.05$, Figure 6.9a). This supports the hypothesis that the antibody coating encourages association of the coated MSC with the inflamed endothelium of the heart.

Interestingly, there was also a significant increase of anti-ICAM1 coated cells (n=3) being retained in the lungs and the spleen over unmodified cells (n=4; $p < 0.01$, Figure 6.9b and 6.9c). While MSC retention in the lung and spleen have been reported previously for unmodified MSCs [167, 209, 210], the increased retention with anti-ICAM1 coatings suggests the coating is also enhancing the MSC interactions at these sites. While significant inflammation is not expected at the lung and spleen following AMI, the basal level of ICAM1 expression on the endothelium may be driving the observed increase in off-target MSC retention. Additionally, the low shear stress in these capillary-abundant

organs may also attenuate MSC clearance and drive increased cell accumulation with minimal increases in adhesion [160].

As a result, we must conclude the antibody coating drives increased retention of MSCs in a nonspecific manner. Importantly, we still observe a significant modulation of the peri-infarct immune response with our anti-ICAM1 coated MSCs. $Ly6C^{hi}$ and Cd115 are the markers positive for inflammatory monocyte while $Ly6C^{hi}/Cd115^{-}$ represent neutrophils. The number of $Ly6C^{hi}$ monocytes in the heart was lower for the anti-ICAM1 MSCs group (n=3) than PBS alone (n=4; $P < 0.05$, Figure 6.10a) and uncoated cells. Similarly, neutrophils are a hallmark of the inflammation, and there were significantly fewer neutrophils in the antibody coated MSC group than only buffer and uncoated cell injection (n=4; $P < 0.05$, Figure 6.10b). While there appear to be fewer monocyte, macrophages or leukocytes present in the antibody coated MSC group, this difference was not conclusive ($P>0.05$, Figure 6.10c and 6.10d). In all, the antibody coated group offered a dramatic reduction of the inflammatory response post-MI.

6.5 Conclusions

Systemic IV administration is a more durable MSC delivery method for clinical therapy in a minimally invasive manner as compared to direct intramyocardial injection. Prior intravenous MSC delivery trials represent the modest cardiac improvement by MSC-mediated immunomodulation after AMI; however, the rapid clearance of injected cells by cardiac contraction and circulatory shear flow highly restrict MSC's therapeutic benefits in an infarct heart. To enhance the persistence of intravenously delivered MSCs in the inflamed heart, we demonstrated an ICAM1-targeted coating via biotin-streptavidin

bridging. The anti-ICAM1 coating significantly strengthened the cell resistance to physiological shears, supporting the feasibility of coated cells to strongly interact with post-inflammatory tissues. We support the increase in *in vivo* MSC homing to the inflamed heart compared to uncoated cells after cell delivery into circulatory shear blood. More importantly, the significant attenuation in immune cells activities by the delivery of anti-ICAM1 coated cells exhibited more effective immunosuppressive effects over non-ICAM1-targeted cell groups. In conclusion, this is a first proof-of-concept study to promote post-AMI immunosuppression by transporting ICAM1-adhesive MSCs to the targeted site of inflammation via *in vivo* intravenous injection.

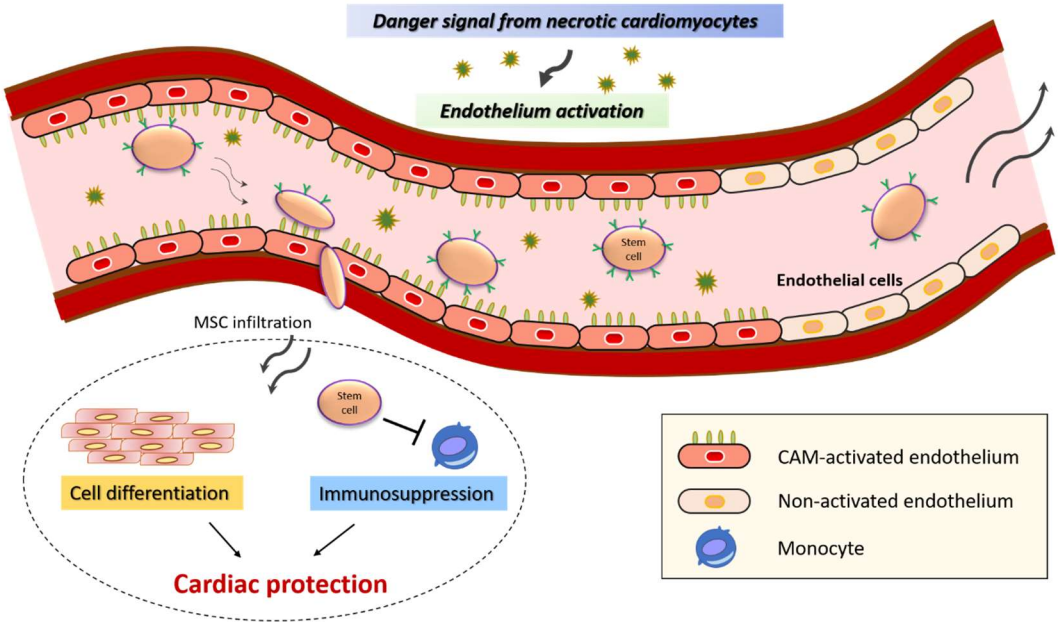

Figure 6-1. Systemic intravenous injection of therapeutic MSC to the site of inflammation.

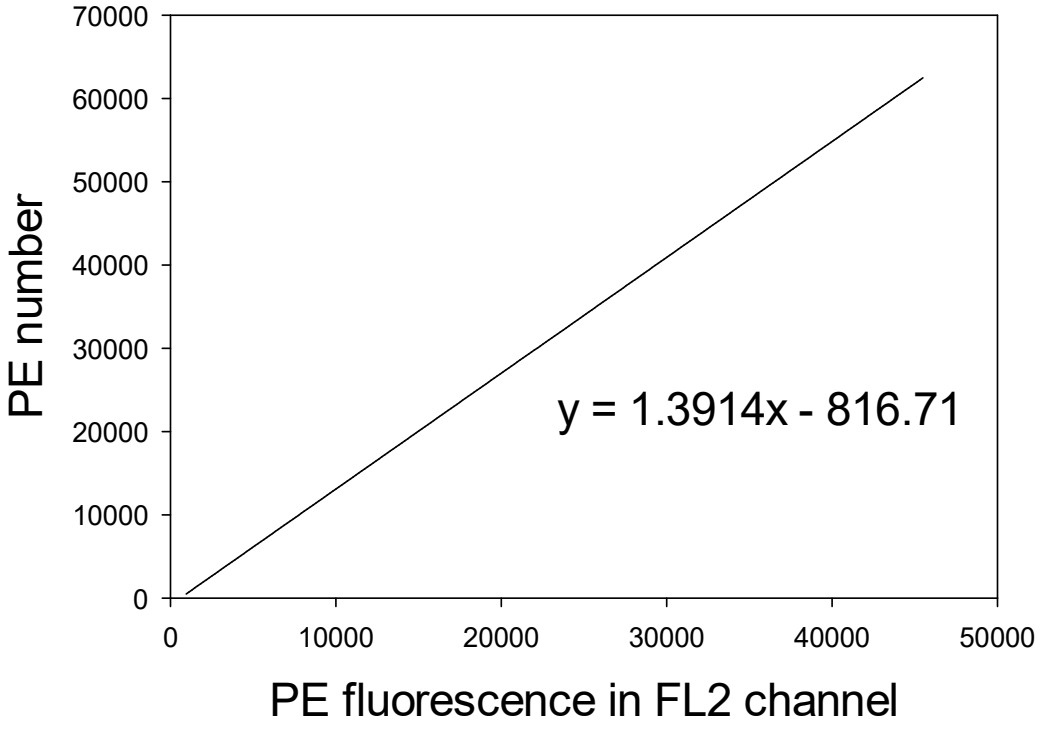

Figure 6-2. Standard calibration curve of PE quantitation bead.

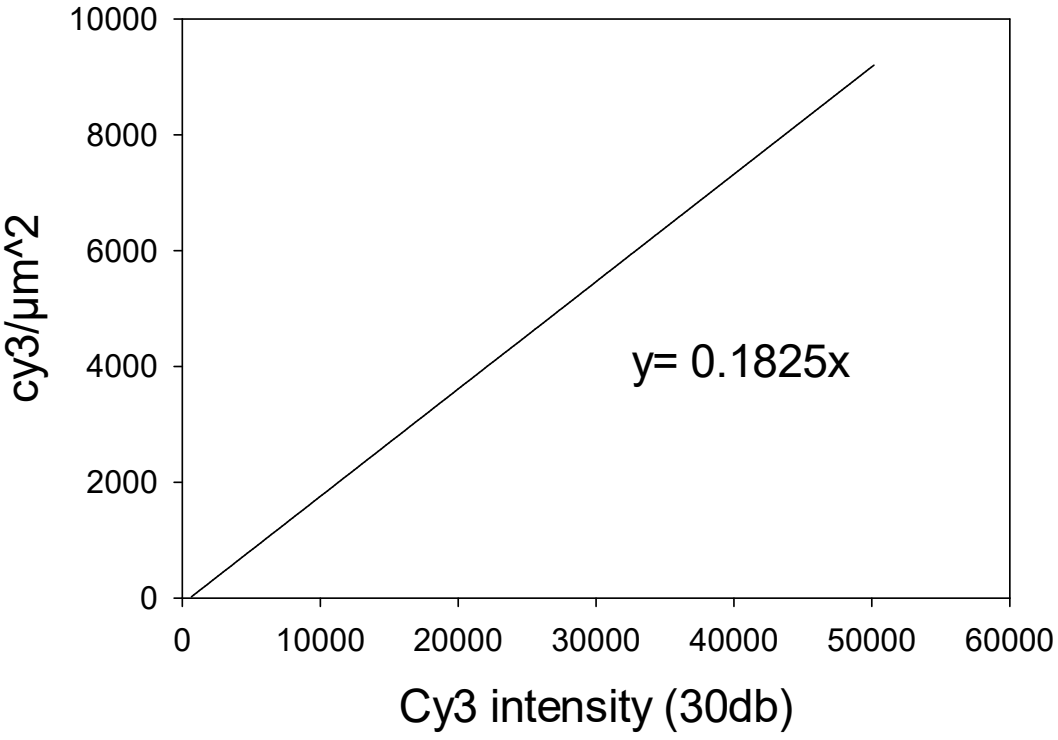

Figure 6-3. **Calibration curve of Cy3 fluorophore quantity.**

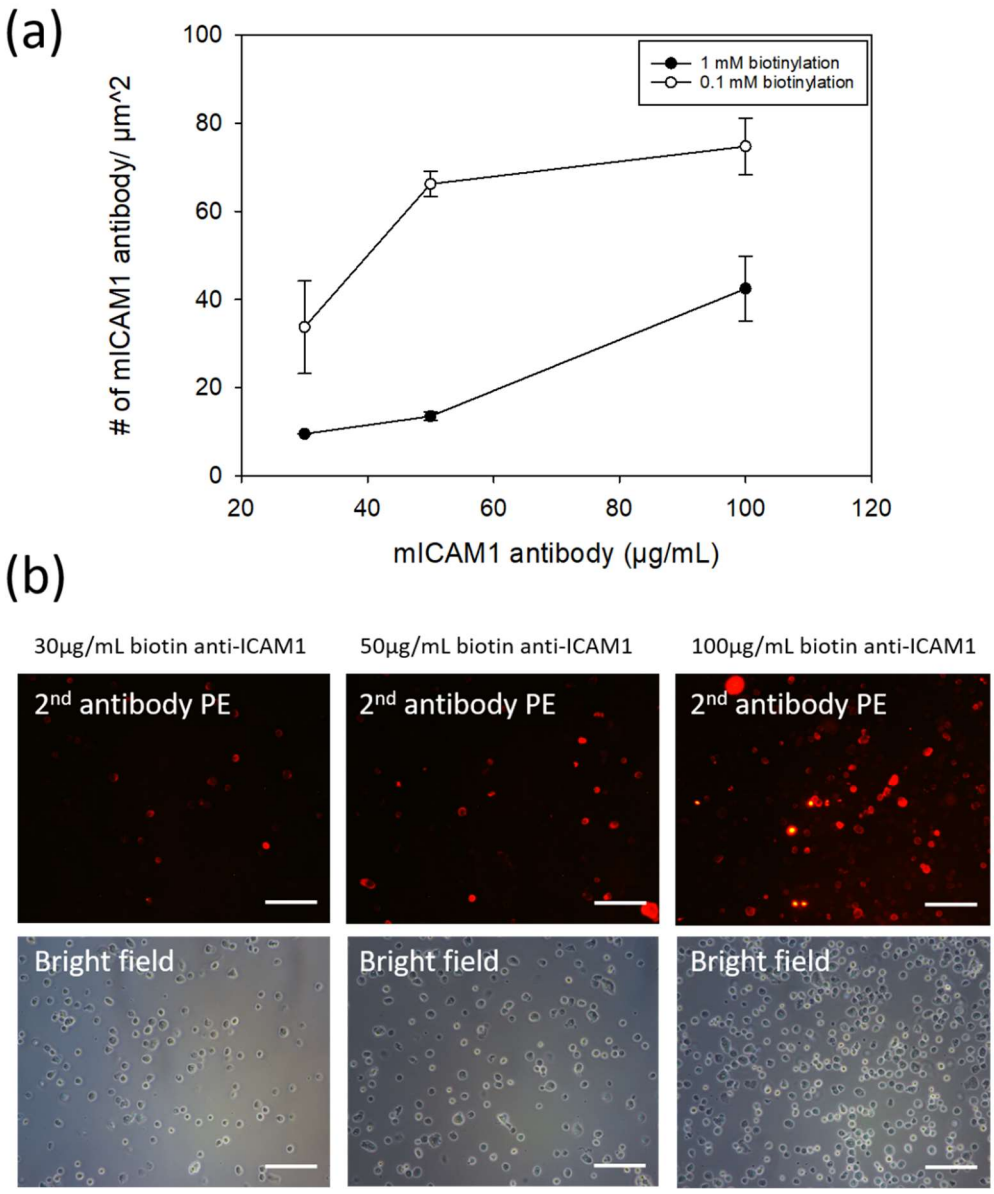

Figure 6-4. **Quantitation of incorporated antibody on MSCs.** (a) Quantitation of ICAM1 antibodies on the MSC surface with different antibody concentrations (30, 50 and 100 µg/mL) through secondary PE labeling. Cells were coated through 0.1 mM or 1mM NHS-ester biotinylation ($n \geq 3$). (b) Fluorescence image of antibody-coated cells through 1 mM biotinylation with different antibody concentration after secondary PE antibody staining. The scale bar is 100 µm.

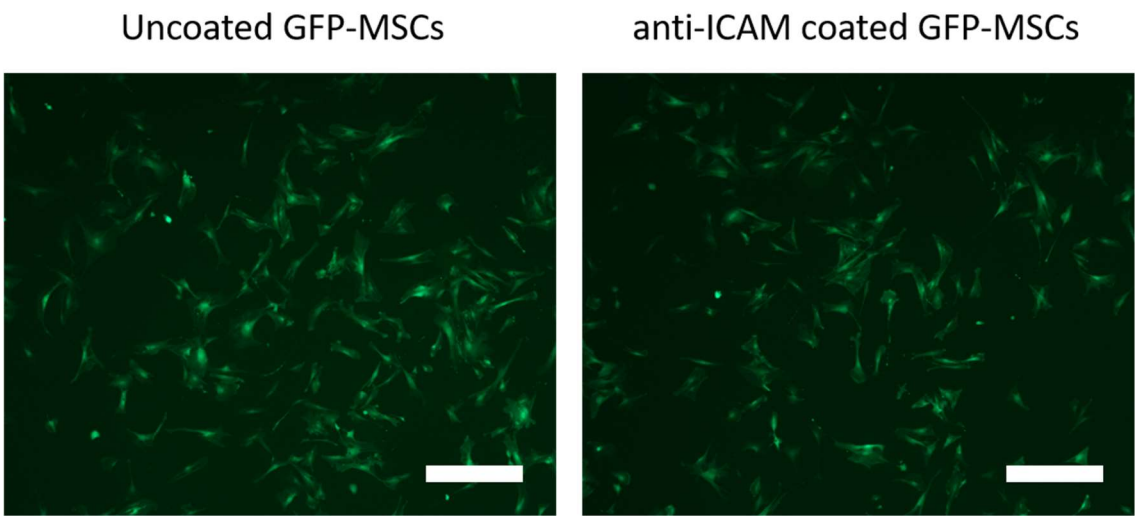

Figure 6-5. **Cell attachment after antibody coating.** The scar bar is 100μm.

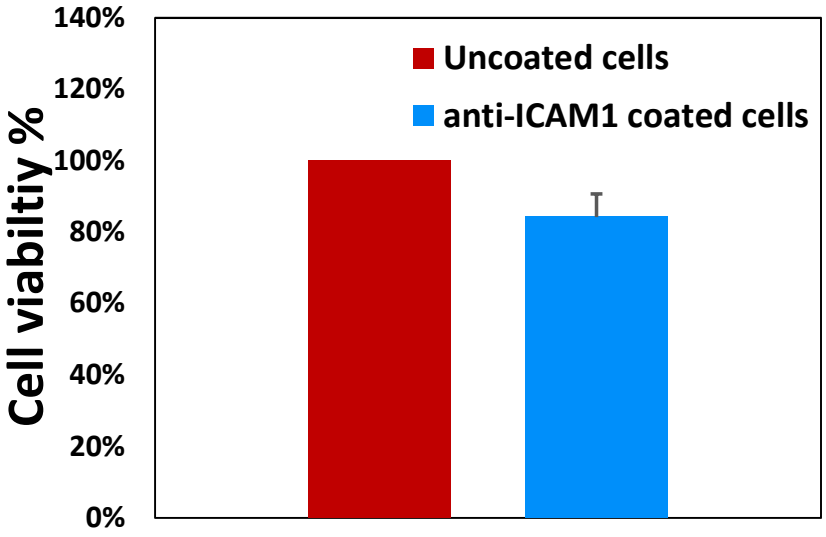

Figure 6-6. Cell viability MTT assay.

(a)

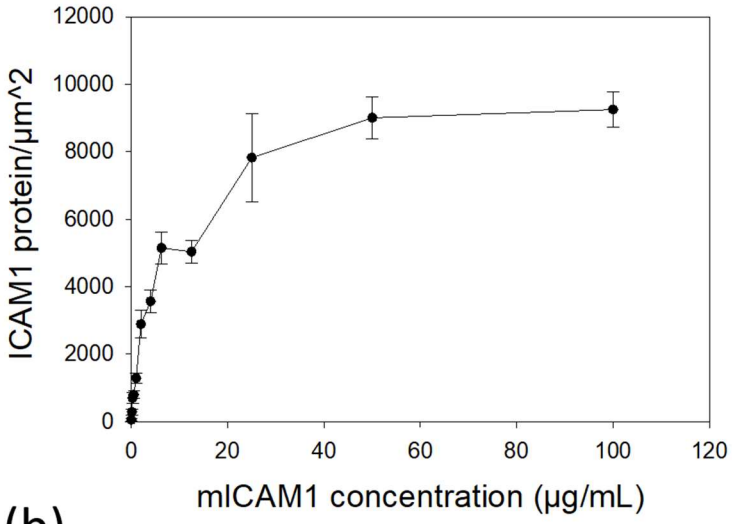
ICAM1 protein/μm^2
12000
10000
8000
6000
4000
2000
0
0
20
40
60
80
100
120
mICAM1 concentration (μg/mL)

(b)

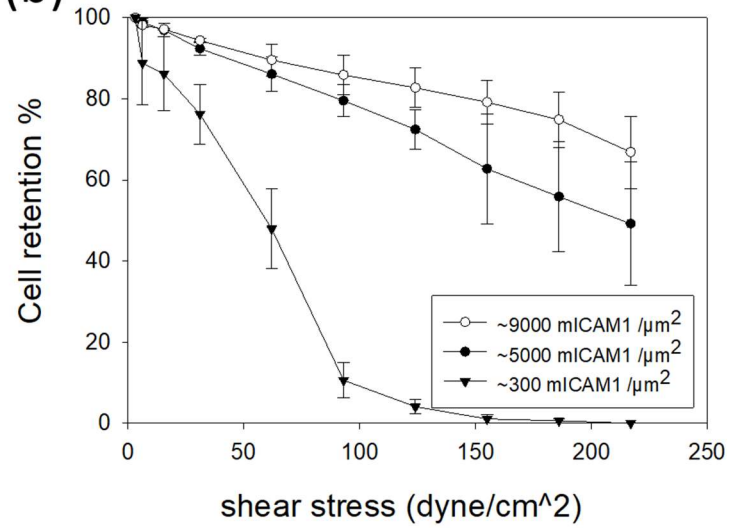
Cell retention %
100
80
60
40
20
0
0
50
100
150
200
250
shear stress (dyne/cm^2)
~9000 mICAM1 /μm2
~5000 mICAM1 /μm2
~300 mICAM1 /μm2

(c)

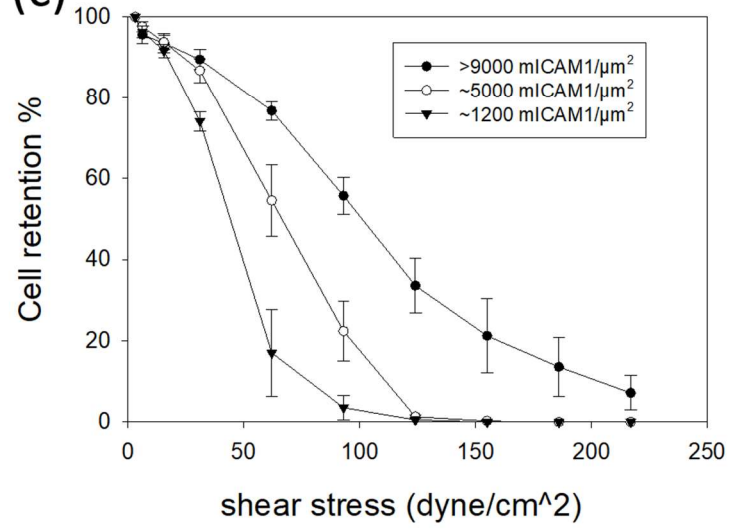
Cell retention %
100
80
60
40
20
0
0
50
100
150
200
250
shear stress (dyne/cm^2)
>9000 mICAM1/μm2
~5000 mICAM1/μm2
~1200 mICAM1/μm2

Figure 6-7. **Cell adhesion on mouse ICAM1-modifed glass and cell detachment under the presence of shear flow.** (a) Relationship of mouse ICAM1 protein density and protein concentration used for epoxide glass modification. (b) Cell retention and shear detachment of coated cells through 0.1 mM biotinylation under different mouse ICAM1 density ($n \geq 3$). (c) Cell retention and shear detachment of coated cells through 1 mM biotinylation under different mouse ICAM1 density ($n \geq 5$).

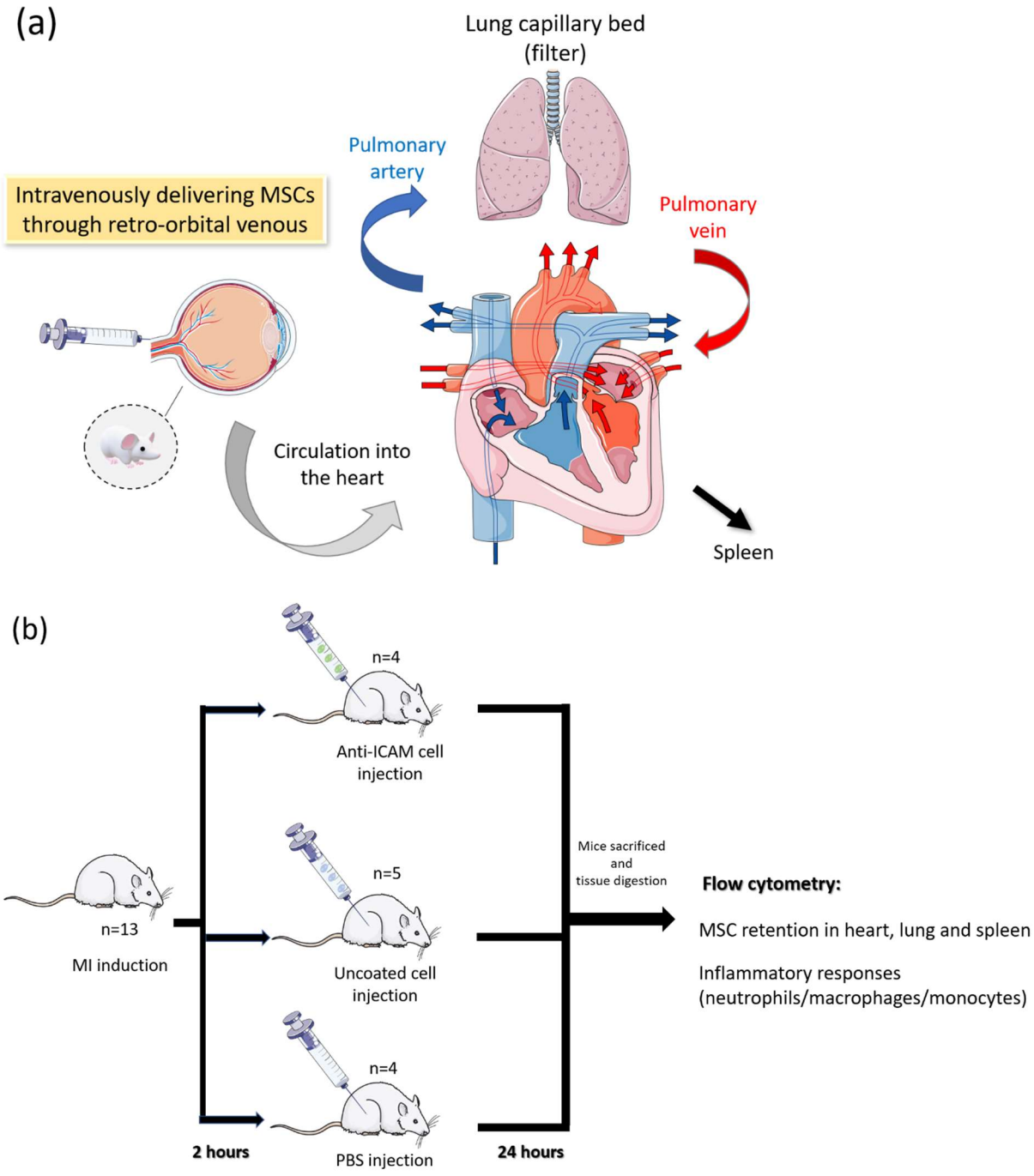

Figure 6-8. ***In vivo*** **Intravenous delivery of anti-ICAM1 coated MSCs in infarcted mouse model.** (a) The circulatory pathway of intravenously delivered MSCs through retro-orbital injection. (b) Timeline of MI induction, MSC injection and sample collection. The coated or uncoated cells were intravenously delivered into 2 hours after left anterior descending artery ligation. One day after injection, the cell samples in the heart, spleen and lung were collected for quantitative analysis through flow cytometry. The images were obtained from smart servier medical art (https://smart.servier.com/).

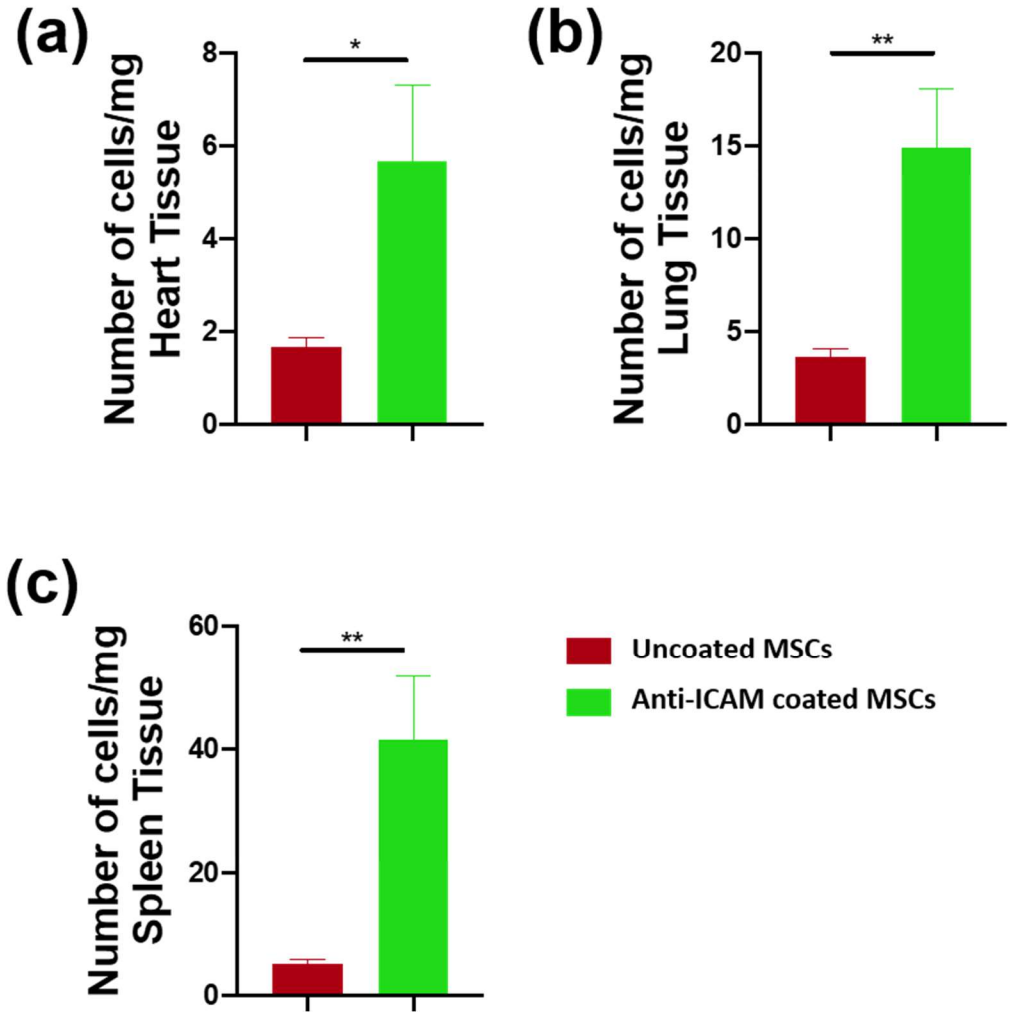

Figure 6-9. MSC accumulation in heart, spleen and lung. (a) Quantitative retention analysis of uncoated MSCs and anti-ICAM1-coated MSCs in the heart through flow cytometry. (b) Quantitative analysis of uncoated MSCs and anti-ICAM1-coated MSCs in the lung. (c) Quantitative analysis of uncoated MSCs and anti-ICAM1-coated MSCs in the spleen. Data points are presented as mean cell number, with error bars presenting standard error (n=4 for uncoated cells and n=3 for anti-ICAM1 coated MSCs).

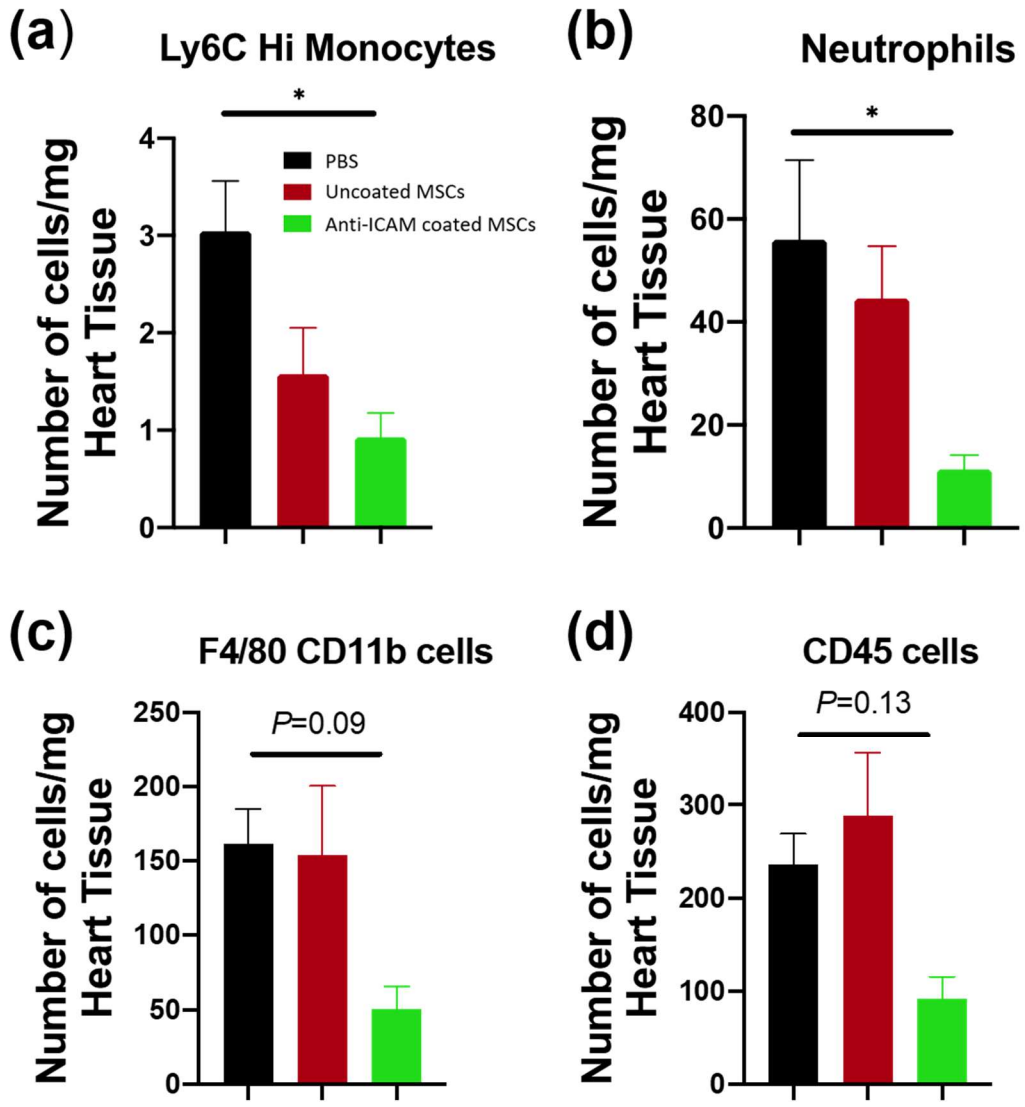

Figure 6-10. **Immunosuppressive effects in the heart.** Cell samples collected from the heart tissues after PBS, uncoated MSC or anti-ICAM1 coated MSC injection were quantified through flow cytometry by immunostaining with several antibodies, including anti-Ly6G/C, anti-CD45, anti-CD115, anti-CD11b and anti-F4/80. (a) Quantitative analysis of $Ly6C^{hi}$ monocytes in the heart. (b) Quantitative retention analysis of $Ly6C^{hi}/Cd115^{-}$ neutrophils. (c) Quantitative analysis of $Cd11b^{+}$ F4/80 cells in the heart. (d) Quantitative analysis of $Cd45^{+}$ cells in the heart. Data points are presented as mean cell number, with error bars presenting standard error (n=4 for uncoated cells and PBS injection, and n=3 for anti-ICAM1 coated MSCs).

CHAPTER 7. CONCLUSIONS AND FUTURE PERSPECTIVES

7.1 Conclusions

Cell surface coating provides non-intrinsic biological properties by incorporating functional biomaterials for transporter cells to specifically interact with their environment. Based on the diverse molecular structures and unique chemical property of a cell, we are allowed to specifically characterize cell surface lipids, proteins, and charged molecules through different modification strategies, including lipid intercalation, electrostatic deposition, ligand-receptor interaction, antigen-antibody affinity and covalent protein crosslinking. In this dissertation, we developed cell surface engineering techniques for cell mediated drug delivery or tissue targeting purposes primarily through covalent NHS-ester biotin modification.

Initial work in Chapter 3 proposed a method to generate nanoparticle-loaded polymeric patch on living cells through surface-mediated photolithographic polymerization. We photopolymerized a nanothin hydrogel pattern by incorporating photoinitiator on a biotinylated cell membrane. The fluorescence of fluorophore-encapsulated PEGDA hydrogel created on a photoinitiator-labeled microarray was used to estimate the film height of less than 100 nm on polymerized cells. The biotinylated microarray platform that mimicked the polymerization behavior on biotinylated cells assists us to precisely control the formation of a 10 μm stripe patch pattern by using a photomask with different irradiation parameters. We observed that the 5 min irradiating time was an optimized polymerization condition to create a hydrogel patch pattern with the

least pattern inaccuracy on living cells without affecting cell viability 2 days after polymerization.

Furthermore, in Chapter 5 and 6 we utilized an inflammation-targeted antibody coating on MSCs to promote local cell retention in a post-MI heart through intramyocardial or intravenous delivery route. We coated a layer of biotinylated antibody against human or mouse ICAM1 protein on a streptavidin-deposited biotinylated cell. Through direct cell injection into peri-infarct area immediately after the MI induction in mice, examination of retained cell number in the heart at day 3 from both IHC staining and flow cytometry indicated the four-time increased retention of anti-ICAM1 coated cells over uncoated ones showing the enhanced inflammation-sensing ability in the heart. The cells coated through 1mM biotinylation which exhibited ~7000 biotin/μm^2 and 23 anti-ICAM1/μm^2 indicated the available coating condition for cell retention enhancement. In addition, the anti-ICAM1 coated cells showed significantly increased adhesion force on both inflamed endothelium and ICAM1-modified surfaces in a presence of physiological shears (< 30 dyne/cm^2) as compared to untreated cells. In Chapter 7, the coated cells were intravenously delivered through retro-orbital venous in *in vivo* MI-induced mice model and were then circulated into flowing blood to reach the post-MI inflamed regions. In contrast to uncoated cells, we observed ~15-fold increase in coated MSC retention in the heart. The overall increase of coated MSC accumulation in heart, spleen and lung was also observed, as compared to uncoated cells or PBS injection, due to the high ICAM1 sensitivity of coated cells to target capillary network in these organs. More importantly, we also noticed the dramatically reduced inflammatory activities of multiple immune cells in the heart, including inflammatory monocytes, macrophages and neutrophils. This immunosuppression

outcome supports the improvement of cardiac therapeutic effects by the intravenous injection of inflammation-recognized MSCs. In conclusion, with our advances in integration of different material coatings, our strategy using cell surface covalent biotinylation enables the applications ranging from drug delivery to tissue engineering potentials.

7.2 Future perspectives

7.2.1 Designing a functional polymer coating for drug delivery

The traditional method to load drug into cell vehicle is through cellular uptake or internalization of nanocarriers. However, the dynamic intracellular degradation largely limits the drug stability during delivery. Herein, we have demonstrated cell surface engineering techniques to introduce a functionalized loading of exogenous biomaterial encapsulated in a cell-associated patch film. While our technique using photolithographic polymerization is only applicable in the adherent type of transport cells, such as stem cells, skeletal fibroblast or macrophage, the use of full surface coating on suspension cells, such as neutrophils or lymphocytes, is also a developing field for cell-based drug delivery. For future directions, the polymer coating on living cells can be designed with a desirable mechanical or biochemical property in a controllable drug release manner. To create a highly crosslinking polymeric payload with stable and durable drug encapsulation efficacy, the generation of cell surface polymerized scaffold can be altered by adjusting the reacting condition during polymerization, the quantity of reacting chains, the type of monomer crosslinker and the addition of functional conjugation on a polymer chain. Considering the rapid drug leakage through absorption or physical encapsulation, the particle chemistry of

encapsulated nanocarrier is an important factor to modulate the controlled release profile from the cell-coated polymer matrix. For the PEGDA hydrogel coating we generated on cells, the small mesh size (less than 10nm) allows complete encapsulation of nanoparticles between 10 and 100 nm in size, including liposomes or polystyrene nanoparticles [54]. With drug-loaded patch or polymer coating, we expect the development of a new generation of cell-mediated drug delivery that exploits the inherent cellular trafficking functions for local targeted therapy.

7.2.2 Selection of targeting ligand for tissue-targeted specificity

Our work demonstrated the significant improvement in cell retention and MSC-guided immunosuppression by intravenously injecting anti-ICAM1 coated MSCs. However, the cell entrapment in other organs could interfere the MSC therapeutic efficiency to rejuvenate local heart function. Hence, to enhance the cell transportation in the local heart, the selection of pathological targets that mainly express or accumulate in the infarcted myocardium will be the next exploring topic for ligand or antibody coated cells to precisely sense the post-MI injured destination. From our work, the key advantage of cell surface biotin modification is its possibility to incorporate various avidin or avidin/biotin-associated ligands to fit the applications for different tissue targeting. For instance, the membrane incorporation of antibody against tumor-specific receptor could assist the hitchhiking of cytotoxic T cells to attack the tumor-residing area. In the future, this coating method also provides a non-genetic methodology to apply tumor-recognized antibody on cytotoxic killer cells for tumor-eliminating applications.

APPENDIX 1. A549 cell viability and cytotoxicity assay treated with Sulfo-NHS-LC-biotin

The A549 cell line was cultured in RPMI-1640 medium containing 10% fetal bovine serum (FBS) and 1% streptomycin/penicillin at 37ºC incubator. Glass microscope slides (25mm x 75mm) were sterilized in a conical tube by ethanol overnight before cell culturing. After trypsinization with 5mL typsin for 5 minutes, A549 cells were cultured on the microscope slide with a cell density of 1.5 million cells per slide. After cell culture on the slides, A549 cells over 80% confluence on microscope slides were placed on ice for 20 min then washed with ice cold PBS three times and loaded into Whatman Chip-Clip. A 45mM Sulfo-NHS-LC-biotin (Thermo Scientific) was prepared in dimethyl sulfoxide no more than 5 min before incubation Then, cells were treated with 0.5mM, 1mM, 2mM, 4mM or 8mM of sulfo-NHS-LC-biotin solution diluted from stock solution in ice cold PBS for 20 min. After biotinylation, cells were rinsed with cold PBS twice and incubated with 0.1% calcein (Life Technologies) and 0.2% ethidium (Life Technologies) diluted in PBS+ 3%v/v FBS for 30 minutes. Images were observed with epi-fluorescence microscope (Nikon Eclipse T*i*-U) and analyzed by Image J software. Cell viability was calculated by the following equation: calcein positive cell number / [calcein labelled cell number + ethidium labelled cell number – calcein/ethidium double labelled cell number].

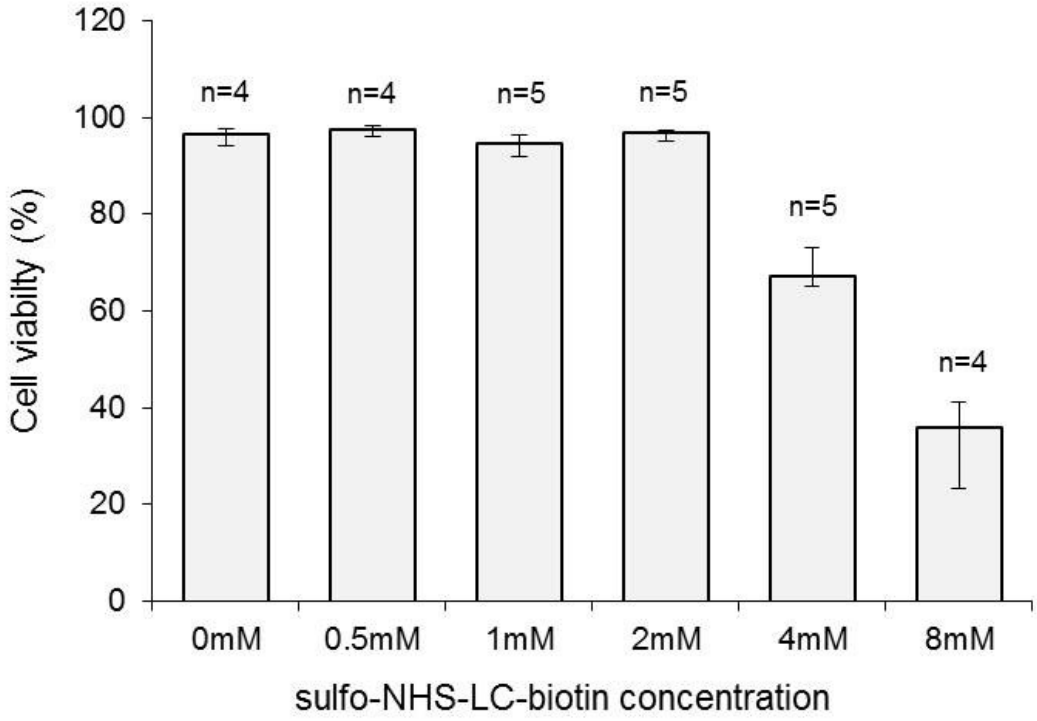

Figure A. 1: Calcein/ethidium analysis of sulfo-NHS-LC-biotin treated A549 viability. After treatment with 0mM, 0.5mM, 1mM, 2mM, 4mM and 8mM sulfo-NHS-LC-biotin, cells were stained by calcein for viability and ethidium for cell death.

APPENDIX 2. Microarray of polymerization-based amplification

Epoxy-functionalized slides were dipped in ethanol overnight before microarray printing for sterilization. Twelve serial dilutions of biotinylated bovine serum albumin (bBSA, 0.105, 0.262, 0.655, 1.638, 4.096, 10.24, 25.6, 64, 160, 400 and 1000 μg per mL) coupled with negative control group (0 μg/mLbBSA) were prepared in PBS 1X. The epoxy slides were printed by Affymetrix 417^{TM} Arrayer, with serial bBSA solutions pipetted into a 96 well plate. Each concentration of bBSA was duplicated into two spots on the slides. After drying overnight, the biotinylated epoxy-functionalized slides were loaded in Whatman Chip-Clip, incubated with 400 μl of 0.1% bovine serum albumin diluted in phosphate buffered saline (PBSA) in each Chip-Clip array well and covered with foil for 45 minutes. After each well rinsed with PBSA once, 400μl of SA-EITC (25 μg/mL) solution was added into array well in the absence of light for 30 minutes. After the conjugation of streptavidin and biotin has finished, each well was rinsed twice with 400 μl of PBSA with 5 minutes and once with deionized water. 350 μl of precursor monomer solution (259 μl PEGDA 575, 29 μl triethanolamine and 4.5 μl vinyl pyrollidinone dissolved in 895 μl deionized water) was pipetted into each well and placed in a clear plastic bag which has been purged with ultra-pure N_2 for 5 minutes. An LED lamp (Thorlabs M530L2-C1) with peak wavelength of 530 nm was adjusted to 1, 5, 10 or 15mW/cm^2 with a radiometer (International Light Technologies (model number ILT1400A). Polymerization commenced with the LED irradiation under continuous nitrogen flow for 20 minutes. After photopolymerization, the slides were rinsed with deionized water and dried overnight. The thickness of polymer film on each array spot was measured by Dektak 6M profilometer. The scanning parameters of surface profilometry

measurement were set with scan length of 4200 μm for 40 s, stylus force of 1 mg, and resolution of 0.350 μm per sample.

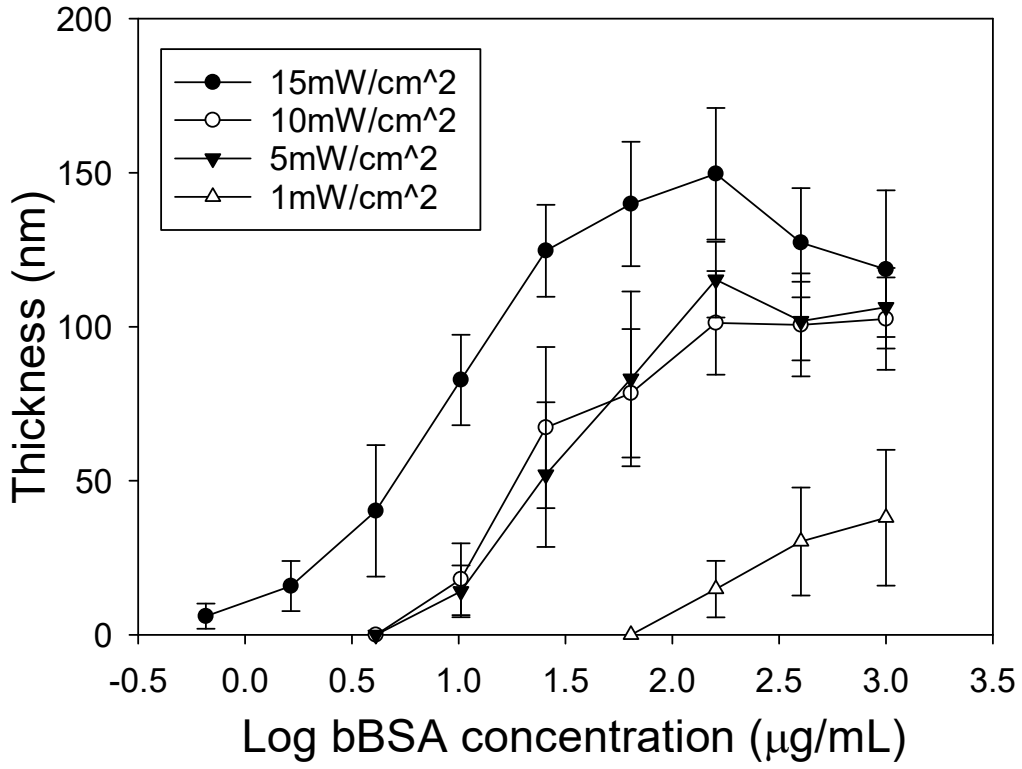

Figure A. 2. Relationship between bBSA concentration and the thickness of PEGDA hydrogel thickness under different light intensity.

APPENDIX 3. The setup of photolithographic patch polymerization

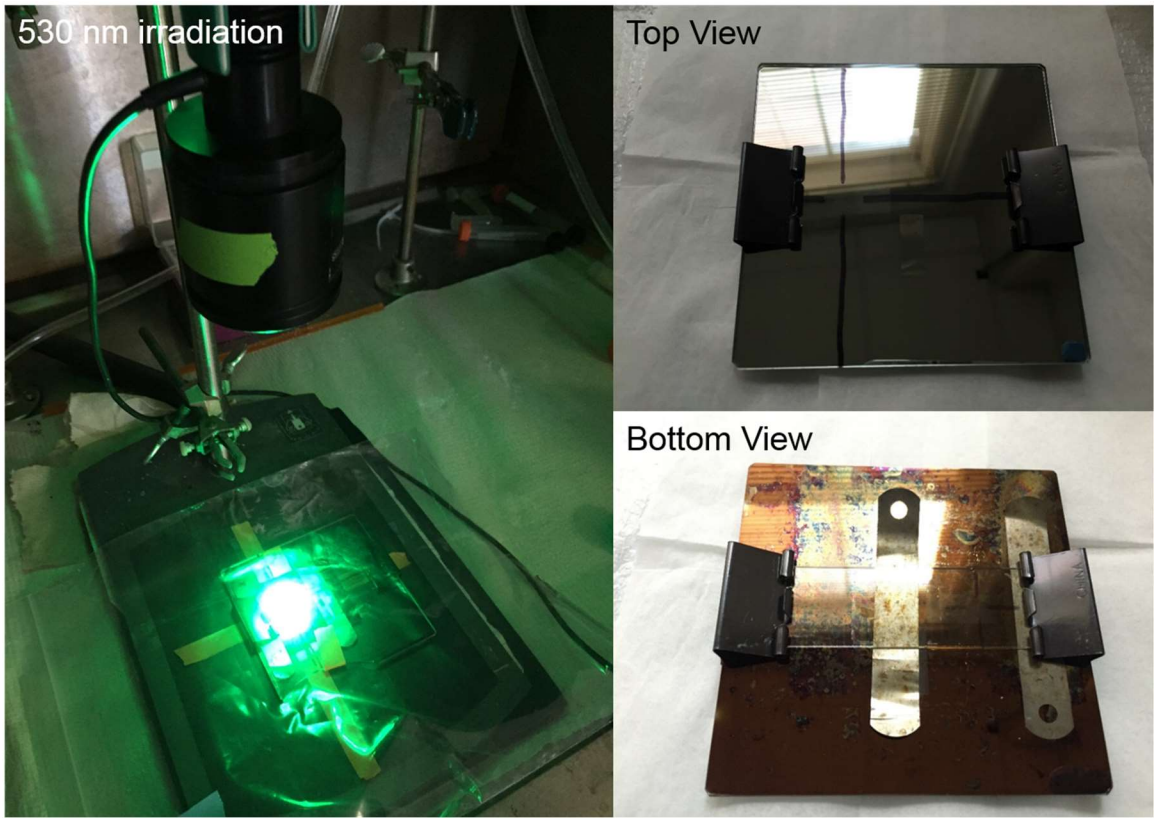

Figure A. 3. Photomask assembly for patch polymerization on a biotinylated microarray or slides of cultured cells. Reprinted from [182], Copyright 2017, with permission from American Chemical Society.

APPENDIX 4. Laminar flow chamber assay

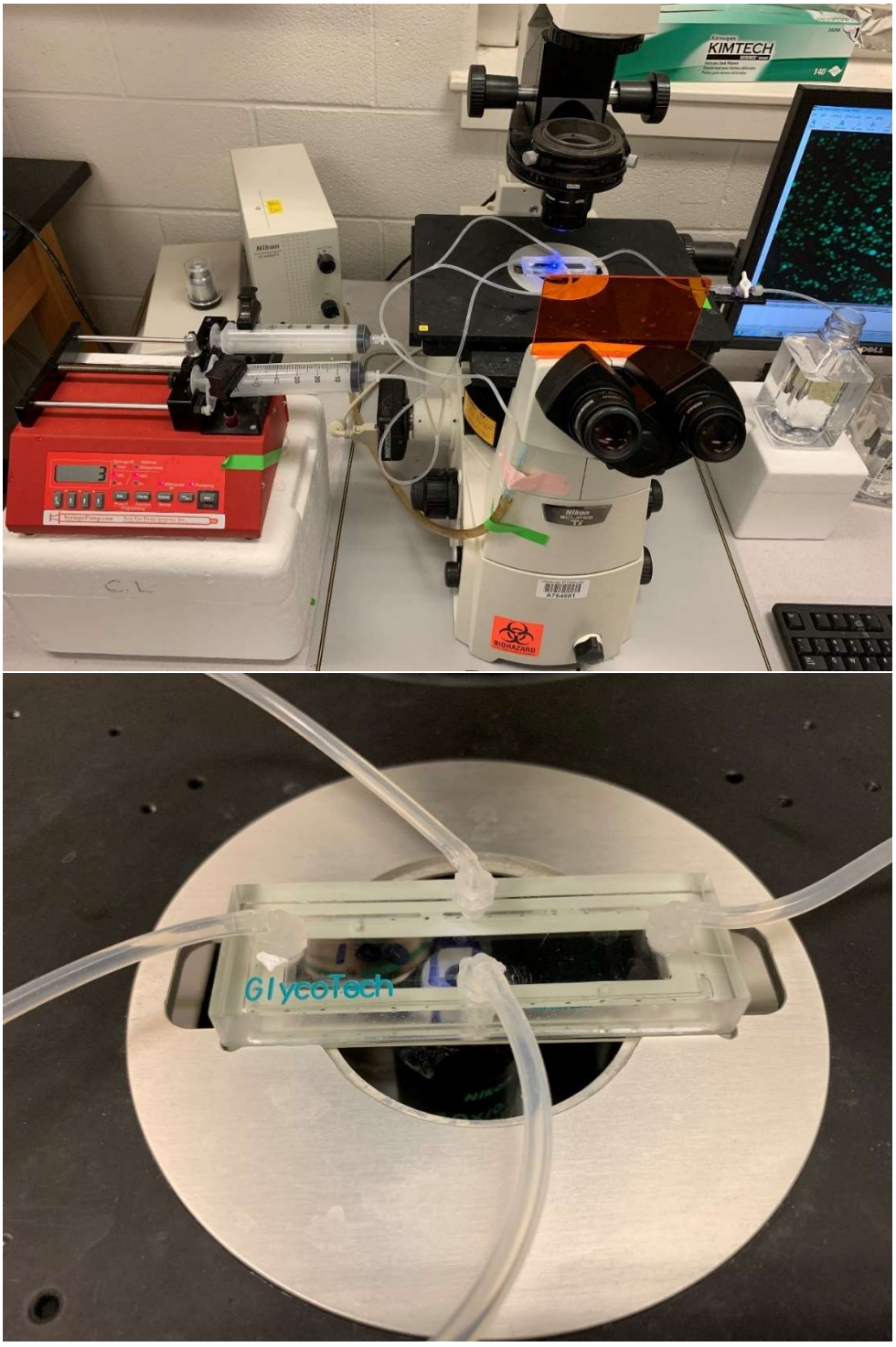

Figure A. 4. The setup of laminar flow chamber assay for cell detachment under shears.

REFERENCES

1. Zhang, C., et al., *Engineering CAR-T cells.* Biomarker research, 2017. **5**(1): p. 22.
2. Yong, S.-B., et al., *Recent challenges and advances in genetically-engineered cell therapy.* Journal of pharmaceutical investigation, 2018. **48**(2): p. 199-208.
3. Mansouri, S., et al., *Investigation of layer-by-layer assembly of polyelectrolytes on fully functional human red blood cells in suspension for attenuated immune response.* Biomacromolecules, 2011. **12**(3): p. 585-592.
4. Lee, J., et al., *Cytoprotective silica coating of individual mammalian cells through bioinspired silicification.* Angewandte Chemie International Edition, 2014. **53**(31): p. 8056-8059.
5. Veerabadran, N.G., et al., *Nanoencapsulation of stem cells within polyelectrolyte multilayer shells.* Macromolecular bioscience, 2007. **7**(7): p. 877-882.
6. Dzamukova, M.R., et al., *A direct technique for magnetic functionalization of living human cells.* Langmuir, 2011. **27**(23): p. 14386-14393.
7. Zhang, P., et al., *Top-Down fabrication of Polyelectrolyte-Thermoplastic hybrid microparticles for unidirectional drug delivery to single cells.* Advanced healthcare materials, 2013. **2**(4): p. 540-545.
8. Germain, M., et al., *Protection of mammalian cell used in biosensors by coating with a polyelectrolyte shell.* Biosensors and Bioelectronics, 2006. **21**(8): p. 1566-1573.
9. Wilson, J.T., et al., *Cell surface engineering with polyelectrolyte multilayer thin films.* Journal of the American Chemical Society, 2011. **133**(18): p. 7054-7064.
10. Ribeiro, R.D., et al., *Temporary single-cell coating for bioprocessing with a cationic polymer.* ACS applied materials & interfaces, 2017. **9**(15): p. 12967-12974.
11. Chung, H.A., et al., *Casual cell surface remodeling using biocompatible lipid-poly (ethylene glycol)(n): Development of stealth cells and monitoring of cell membrane behavior in serum-supplemented conditions.* Journal of Biomedical Materials Research Part A: An Official Journal of The Society for Biomaterials, The Japanese Society for Biomaterials, and The Australian Society for Biomaterials and the Korean Society for Biomaterials, 2004. **70**(2): p. 179-185.
12. Won, Y.-W., A.N. Patel, and D.A. Bull, *Cell surface engineering to enhance mesenchymal stem cell migration toward an SDF-1 gradient.* Biomaterials, 2014. **35**(21): p. 5627-5635.
13. Lim, K.S., et al., *Cell surface-engineering to embed targeting ligands or tracking agents on the cell membrane.* Biochemical and biophysical research communications, 2017. **482**(4): p. 1042-1047.
14. Jia, H.-R., et al., *Long-time plasma membrane imaging based on a two-step synergistic cell surface modification strategy.* Bioconjugate chemistry, 2016. **27**(3): p. 782-789.
15. Vabbilisetty, P., et al., *Chemical reactive anchoring lipids with different performance for cell surface re-engineering application.* ACS omega, 2018. **3**(2): p. 1589-1599.

16. Colsky, A.S. and J.S. Peacock, *Palmitate-derivatized antibodies can function as surrogate receptors for mediating specific cell-cell interactions.* Journal of immunological methods, 1989. **124**(2): p. 179-187.
17. Mao, S.-Y., *Biotinylation of antibodies*, in *Immunocytochemical Methods and Protocols*. 1994, Springer. p. 49-52.
18. Wisdom, G.B., *Conjugation of antibodies to horseradish peroxidase*, in *Immunochemical Protocols*. 2005, Springer. p. 127-130.
19. Tang, D., et al., *Multifunctional magnetic bead-based electrochemical immunoassay for the detection of aflatoxin B 1 in food.* Analyst, 2009. **134**(8): p. 1554-1560.
20. Gao, Z., et al., *Magnetic bead-based reverse colorimetric immunoassay strategy for sensing biomolecules.* Analytical chemistry, 2013. **85**(14): p. 6945-6952.
21. El-Sayed, I.H., X. Huang, and M.A. El-Sayed, *Selective laser photo-thermal therapy of epithelial carcinoma using anti-EGFR antibody conjugated gold nanoparticles.* Cancer letters, 2006. **239**(1): p. 129-135.
22. Sokolov, K., et al., *Real-time vital optical imaging of precancer using anti-epidermal growth factor receptor antibodies conjugated to gold nanoparticles.* Cancer research, 2003. **63**(9): p. 1999-2004.
23. Lilly, J.L. and B.J. Berron, *The role of surface receptor density in surface-initiated polymerizations for Cancer cell isolation.* Langmuir, 2016. **32**(22): p. 5681-5689.
24. Romero, G., et al., *Protective polymer coatings for high-throughput, high-purity cellular isolation.* ACS applied materials & interfaces, 2015. **7**(32): p. 17598-17602.
25. Lilly, J.L., et al., *Characterization of molecular transport in ultrathin hydrogel coatings for cellular immunoprotection.* Biomacromolecules, 2015. **16**(2): p. 541-549.
26. Sakai, S., et al., *Cell-selective encapsulation in hydrogel sheaths via biospecific identification and biochemical cross-linking.* Biomaterials, 2015. **53**: p. 494-501.
27. HOSHINO, N., R. NAKAJIMA, and I. YAMAZAKI, *The effect of polymerization of horseradish peroxidase on the peroxidase activity in the presence of excess H2O2: a background for a homogeneous enzyme immunoassay.* The Journal of Biochemistry, 1987. **102**(4): p. 785-791.
28. Kohri, M., *Development of HRP-mediated enzymatic polymerization under heterogeneous conditions for the preparation of functional particles.* Polymer journal, 2014. **46**(7): p. 373.
29. Nitta, T., et al., *Induction of cytotoxicity in human T cells coated with anti-glioma× anti-CD3 bispecific antibody against human glioma cells.* Journal of neurosurgery, 1990. **72**(3): p. 476-481.
30. Kuo, S.-R., L. Wong, and J.-S. Liu, *Engineering a CD123xCD3 bispecific scFv immunofusion for the treatment of leukemia and elimination of leukemia stem cells.* Protein Engineering, Design & Selection, 2012. **25**(10): p. 561-570.
31. Kaneko, T., et al., *Cytotoxicity of cytokine-induced killer cells coated with bispecific antibody against acute myeloid leukemia cells.* Leukemia & lymphoma, 1994. **14**(3-4): p. 219-229.

32. Morshed, S.A., R. Latif, and T.F. Davies, *Characterization of thyrotropin receptor antibody-induced signaling cascades.* Endocrinology, 2008. **150**(1): p. 519-529.
33. Li, K., et al., *Modulation of Notch signaling by antibodies specific for the extracellular negative regulatory region of NOTCH3.* Journal of Biological Chemistry, 2008. **283**(12): p. 8046-8054.
34. Yan, S.R. and G. Berton, *Antibody-induced engagement of β2 integrins in human neutrophils causes a rapid redistribution of cytoskeletal proteins, Src-family tyrosine kinases, and p72syk that precedes de novo actin polymerization.* Journal of leukocyte biology, 1998. **64**(3): p. 401-408.
35. Misra, S., et al., *Interactions between hyaluronan and its receptors (CD44, RHAMM) regulate the activities of inflammation and cancer.* Frontiers in immunology, 2015. **6**: p. 201.
36. Almalik, A., et al., *Hyaluronic acid (HA) presentation as a tool to modulate and control the receptor-mediated uptake of HA-coated nanoparticles.* Biomaterials, 2013. **34**(21): p. 5369-5380.
37. Swiston, A.J., et al., *Surface functionalization of living cells with multilayer patches.* Nano letters, 2008. **8**(12): p. 4446-4453.
38. Doshi, N., et al., *Cell-Based Drug Delivery Devices Using Phagocytosis-Resistant Backpacks.* Advanced Materials, 2011. **23**(12).
39. Swiston, A.J., et al., *Freely suspended cellular "backpacks" lead to cell aggregate self-assembly.* Biomacromolecules, 2010. **11**(7): p. 1826-1832.
40. Gilbert, J.B., et al., *Orientation-Specific Attachment of Polymeric Microtubes on Cell Surfaces.* Advanced Materials, 2013. **25**(41): p. 5948-5952.
41. Blackall, D.P., et al., *Polyethylene glycol–coated red blood cells fail to bind glycophorin A–specific antibodies and are impervious to invasion by the Plasmodium falciparum malaria parasite.* Blood, 2001. **97**(2): p. 551-556.
42. Hsiao, S.C., et al., *Direct cell surface modification with DNA for the capture of primary cells and the investigation of myotube formation on defined patterns.* Langmuir, 2009. **25**(12): p. 6985-6991.
43. Zhao, W., et al., *Cell-surface sensors for real-time probing of cellular environments.* Nature nanotechnology, 2011. **6**(8): p. 524.
44. Sarkar, D., et al., *Chemical engineering of mesenchymal stem cells to induce a cell rolling response.* Bioconjugate chemistry, 2008. **19**(11): p. 2105-2109.
45. Sarkar, D., et al., *Engineered cell homing.* Blood, 2011. **118**(25): p. e184-e191.
46. Cheng, H., et al., *Nanoparticulate cellular patches for cell-mediated tumoritropic delivery.* ACS nano, 2010. **4**(2): p. 625-631.
47. Gottipati, A., et al., *Gelatin Based Polymer Cell Coating Improves Bone Marrow-Derived Cell Retention in the Heart after Myocardial Infarction.* Stem Cell Reviews and Reports, 2019: p. 1-11.
48. Kim, J.Y., et al., *Cytocompatible Polymer Grafting from Individual Living Cells by Atom-Transfer Radical Polymerization.* Angewandte Chemie International Edition, 2016. **55**(49): p. 15306-15309.
49. Luo, N., et al., *Surface-initiated photopolymerization of poly (ethylene glycol) methyl ether methacrylate on a diethyldithiocarbamate-mediated polymer substrate.* Macromolecules, 2002. **35**(7): p. 2487-2493.

50. Kızılel, S., V.H. Pérez-Luna, and F. Teymour, *Photopolymerization of poly (ethylene glycol) diacrylate on eosin-functionalized surfaces.* Langmuir, 2004. **20**(20): p. 8652-8658.
51. Hansen, R.R., et al., *Quantitative evaluation of oligonucleotide surface concentrations using polymerization-based amplification.* Analytical and bioanalytical chemistry, 2008. **392**(1-2): p. 167.
52. Avens, H.J. and C.N. Bowman, *Development of fluorescent polymerization-based signal amplification for sensitive and non-enzymatic biodetection in antibody microarrays.* Acta biomaterialia, 2010. **6**(1): p. 83-89.
53. Avens, H.J., T.J. Randle, and C.N. Bowman, *Polymerization behavior and polymer properties of eosin-mediated surface modification reactions.* Polymer, 2008. **49**(22): p. 4762-4768.
54. Avens, H.J., et al., *Fluorescent polymeric nanocomposite films generated by surface-mediated photoinitiation of polymerization.* Journal of Nanoparticle Research, 2011. **13**(1): p. 331-346.
55. Lilly, J.L., et al., *Interfacial polymerization for colorimetric labeling of protein expression in cells.* PloS one, 2014. **9**(12): p. e115630.
56. Lilly, J.L., et al., *Comparison of eosin and fluorescein conjugates for the photoinitiation of cell-compatible polymer coatings.* PloS one, 2018. **13**(1): p. e0190880.
57. Davis, K.A., et al., *Coatings on mammalian cells: interfacing cells with their environment.* Journal of biological engineering, 2019. **13**(1): p. 5.
58. Anselmo, A.C. and S. Mitragotri, *Cell-mediated delivery of nanoparticles: taking advantage of circulatory cells to target nanoparticles.* Journal of controlled release, 2014. **190**: p. 531-541.
59. Fliervoet, L.A. and E. Mastrobattista, *Drug delivery with living cells.* Advanced drug delivery reviews, 2016. **106**: p. 63-72.
60. Jeanbart, L. and M.A. Swartz, *Engineering opportunities in cancer immunotherapy.* Proceedings of the National Academy of Sciences, 2015. **112**(47): p. 14467-14472.
61. Dong, X., D. Chu, and Z. Wang, *Leukocyte-mediated delivery of nanotherapeutics in inflammatory and tumor sites.* Theranostics, 2017. **7**(3): p. 751.
62. Lutterotti, A., et al., *Antigen-specific tolerance by autologous myelin peptide–coupled cells: a phase 1 trial in multiple sclerosis.* Science translational medicine, 2013. **5**(188): p. 188ra75-188ra75.
63. Ramirez, C.N., C. Antczak, and H. Djaballah, *Cell viability assessment: toward content-rich platforms.* Expert opinion on drug discovery, 2010. **5**(3): p. 223-233.
64. Kontos, S., et al., *Engineering antigens for in situ erythrocyte binding induces T-cell deletion.* Proceedings of the National Academy of Sciences, 2013. **110**(1): p. E60-E68.
65. Anselmo, A.C., et al., *Monocyte-mediated delivery of polymeric backpacks to inflamed tissues: a generalized strategy to deliver drugs to treat inflammation.* Journal of Controlled Release, 2015. **199**: p. 29-36.

66. Spaeth, E., et al., *Inflammation and tumor microenvironments: defining the migratory itinerary of mesenchymal stem cells.* Gene therapy, 2008. **15**(10): p. 730.
67. Rosenberg, S.A., et al., *Use of tumor-infiltrating lymphocytes and interleukin-2 in the immunotherapy of patients with metastatic melanoma.* New England Journal of Medicine, 1988. **319**(25): p. 1676-1680.
68. Yu, P. and Y.-X. Fu, *Tumor-infiltrating T lymphocytes: friends or foes?* Laboratory investigation, 2006. **86**(3): p. 231.
69. Su, Y., et al., *Design strategies and applications of circulating cell-mediated drug delivery systems.* ACS biomaterials science & engineering, 2015. **1**(4): p. 201-217.
70. Kawakami, Y., et al., *Identification of a human melanoma antigen recognized by tumor-infiltrating lymphocytes associated with in vivo tumor rejection.* Proceedings of the National Academy of Sciences, 1994. **91**(14): p. 6458-6462.
71. Buckanovich, R.J., et al., *Endothelin B receptor mediates the endothelial barrier to T cell homing to tumors and disables immune therapy.* Nature medicine, 2008. **14**(1): p. 28.
72. Stephan, M.T., et al., *Therapeutic cell engineering with surface-conjugated synthetic nanoparticles.* Nature medicine, 2010. **16**(9): p. 1035.
73. Stephan, M.T., et al., *Synapse-directed delivery of immunomodulators using T-cell-conjugated nanoparticles.* Biomaterials, 2012. **33**(23): p. 5776-5787.
74. Choi, J., et al., *Use of macrophages to deliver therapeutic and imaging contrast agents to tumors.* Biomaterials, 2012. **33**(16): p. 4195-4203.
75. Cao, P., et al., *Intraperitoneal administration of neural stem cell–nanoparticle conjugates targets chemotherapy to ovarian tumors.* Bioconjugate chemistry, 2017. **28**(6): p. 1767-1776.
76. Manish, G. and S. Vimukta, *Targeted drug delivery system: a review.* Res J Chem Sci, 2011. **1**(2): p. 135-138.
77. Bae, Y.H. and K. Park, *Targeted drug delivery to tumors: myths, reality and possibility.* Journal of Controlled Release, 2011. **153**(3): p. 198.
78. Li, L., et al., *Silica nanorattle–doxorubicin-anchored mesenchymal stem cells for tumor-tropic therapy.* ACS nano, 2011. **5**(9): p. 7462-7470.
79. Ruoslahti, E., *Peptides as targeting elements and tissue penetration devices for nanoparticles.* Advanced materials, 2012. **24**(28): p. 3747-3756.
80. Singh, R. and J.W. Lillard, *Nanoparticle-based targeted drug delivery.* Experimental and molecular pathology, 2009. **86**(3): p. 215-223.
81. Zhang, Y., et al., *Drug-Eluting Conformal Coatings on Individual Cells.* Cellular and Molecular Bioengineering: p. 1-16.
82. Cruise, G.M., et al., *A sensitivity study of the key parameters in the interfacial photopolymerization of poly (ethylene glycol) diacrylate upon porcine islets.* Biotechnology and bioengineering, 1998. **57**(6): p. 655-665.
83. Leung, C.T. and J.S. Brugge, *Tumor self-seeding: bidirectional flow of tumor cells.* Cell, 2009. **139**(7): p. 1226-1228.
84. Comen, E., L. Norton, and J. Massague, *Clinical implications of cancer self-seeding.* Nature reviews. Clinical oncology, 2011. **8**(6): p. 369.

85. Goel, A., et al., *Exploring targeted pulmonary delivery for treatment of lung cancer.* International journal of pharmaceutical investigation, 2013. **3**(1): p. 8.
86. Lin, W., et al., *In vitro toxicity of silica nanoparticles in human lung cancer cells.* Toxicology and applied pharmacology, 2006. **217**(3): p. 252-259.
87. Harris, J.M., *Poly (ethylene glycol) chemistry: biotechnical and biomedical applications*. 2013: Springer Science & Business Media.
88. Lin, S., et al., *Influence of physical properties of biomaterials on cellular behavior.* Pharmaceutical research, 2011. **28**(6): p. 1422-1430.
89. Jordan, J.E. and S. Sarvotham, *Gradual reperfusion reduces infarct size and endothelial injury but augments neutrophil accumulation.* The Annals of thoracic surgery, 1997. **64**(4): p. 1099-1107.
90. Jackson, K.A., et al., *Regeneration of ischemic cardiac muscle and vascular endothelium by adult stem cells.* The Journal of clinical investigation, 2001. **107**(11): p. 1395-1402.
91. Herreros, J., et al., *Autologous intramyocardial injection of cultured skeletal muscle-derived stem cells in patients with non-acute myocardial infarction.* European heart journal, 2003. **24**(22): p. 2012-2020.
92. Oshima, H., et al., *Differential myocardial infarct repair with muscle stem cells compared to myoblasts.* Molecular Therapy, 2005. **12**(6): p. 1130-1141.
93. Orlic, D., et al., *Bone marrow cells regenerate infarcted myocardium.* Nature, 2001. **410**(6829): p. 701.
94. Orlic, D., et al., *Mobilized bone marrow cells repair the infarcted heart, improving function and survival.* Proceedings of the National Academy of Sciences, 2001. **98**(18): p. 10344-10349.
95. Beltrami, A.P., et al., *Adult cardiac stem cells are multipotent and support myocardial regeneration.* Cell, 2003. **114**(6): p. 763-776.
96. Amado, L.C., et al., *Cardiac repair with intramyocardial injection of allogeneic mesenchymal stem cells after myocardial infarction.* Proceedings of the National Academy of Sciences, 2005. **102**(32): p. 11474-11479.
97. Krause, U., et al., *Intravenous delivery of autologous mesenchymal stem cells limits infarct size and improves left ventricular function in the infarcted porcine heart.* Stem cells and development, 2007. **16**(1): p. 31-38.
98. Mias, C., et al., *Mesenchymal stem cells promote matrix metalloproteinase secretion by cardiac fibroblasts and reduce cardiac ventricular fibrosis after myocardial infarction.* Stem cells, 2009. **27**(11): p. 2734-2743.
99. Swirski, F.K. and M. Nahrendorf, *Macrophage-stem cell crosstalk after myocardial infarction*. 2013, Journal of the American College of Cardiology.
100. Ben-Mordechai, T., et al., *Macrophage subpopulations are essential for infarct repair with and without stem cell therapy.* Journal of the American College of Cardiology, 2013. **62**(20): p. 1890-1901.
101. Ghannam, S., et al., *Immunosuppression by mesenchymal stem cells: mechanisms and clinical applications.* Stem cell research & therapy, 2010. **1**(1): p. 2.
102. Polchert, D., et al., *IFN-γ activation of mesenchymal stem cells for treatment and prevention of graft versus host disease.* European journal of immunology, 2008. **38**(6): p. 1745-1755.

103. Ren, G., et al., *Mesenchymal stem cell-mediated immunosuppression occurs via concerted action of chemokines and nitric oxide.* Cell stem cell, 2008. **2**(2): p. 141-150.
104. Sato, K., et al., *Nitric oxide plays a critical role in suppression of T-cell proliferation by mesenchymal stem cells.* Blood, 2007. **109**(1): p. 228-234.
105. Duffy, M.M., et al., *Mesenchymal stem cell effects on T-cell effector pathways.* Stem cell research & therapy, 2011. **2**(4): p. 34.
106. Wise, A.F., et al., *Human mesenchymal stem cells alter macrophage phenotype and promote regeneration via homing to the kidney following ischemia-reperfusion injury.* American Journal of Physiology-Renal Physiology, 2014. **306**(10): p. F1222-F1235.
107. Selmani, Z., et al., *Human leukocyte antigen-G5 secretion by human mesenchymal stem cells is required to suppress T lymphocyte and natural killer function and to induce CD4+ CD25highFOXP3+ regulatory T cells.* Stem cells, 2008. **26**(1): p. 212-222.
108. Aggarwal, S. and M.F. Pittenger, *Human mesenchymal stem cells modulate allogeneic immune cell responses.* Blood, 2005. **105**(4): p. 1815-1822.
109. Xu, G., et al., *The role of IL-6 in inhibition of lymphocyte apoptosis by mesenchymal stem cells.* Biochemical and biophysical research communications, 2007. **361**(3): p. 745-750.
110. Gentek, R. and G. Hoeffel, *The innate immune response in myocardial infarction, repair, and regeneration*, in *The Immunology of Cardiovascular Homeostasis and Pathology*. 2017, Springer. p. 251-272.
111. Ji, S.T., et al., *Promising therapeutic strategies for mesenchymal stem cell-based cardiovascular regeneration: from cell priming to tissue engineering.* Stem cells international, 2017. **2017**.
112. Oswald, J., et al., *Mesenchymal stem cells can be differentiated into endothelial cells in vitro.* Stem cells, 2004. **22**(3): p. 377-384.
113. Tang, J., et al., *Mesenchymal stem cells participate in angiogenesis and improve heart function in rat model of myocardial ischemia with reperfusion.* European Journal of Cardio-Thoracic Surgery, 2006. **30**(2): p. 353-361.
114. Rodrigues, M., L.G. Griffith, and A. Wells, *Growth factor regulation of proliferation and survival of multipotential stromal cells.* Stem cell research & therapy, 2010. **1**(4): p. 32.
115. Wang, C.-H., et al., *The critical role of ECM proteins within the human MSC niche in endothelial differentiation.* Biomaterials, 2013. **34**(17): p. 4223-4234.
116. Guo, X., et al., *Cardiomyocyte differentiation of mesenchymal stem cells from bone marrow: new regulators and its implications.* Stem cell research & therapy, 2018. **9**(1): p. 44.
117. Qian, Q., et al., *5-Azacytidine induces cardiac differentiation of human umbilical cord-derived mesenchymal stem cells by activating extracellular regulated kinase.* Stem cells and development, 2011. **21**(1): p. 67-75.
118. Makino, S., et al., *Cardiomyocytes can be generated from marrow stromal cells in vitro.* The Journal of clinical investigation, 1999. **103**(5): p. 697-705.

119. Hashi, C.K., et al., *Antithrombogenic property of bone marrow mesenchymal stem cells in nanofibrous vascular grafts.* Proceedings of the National Academy of Sciences, 2007. **104**(29): p. 11915-11920.
120. Agis, H., et al., *Activated platelets increase fibrinolysis of mesenchymal progenitor cells.* Journal of Orthopaedic Research, 2009. **27**(7): p. 972-980.
121. Neuss, S., et al., *Secretion of fibrinolytic enzymes facilitates human mesenchymal stem cell invasion into fibrin clots.* Cells Tissues Organs, 2010. **191**(1): p. 36-46.
122. Frangogiannis, N.G., *Targeting the inflammatory response in healing myocardial infarcts.* Current medicinal chemistry, 2006. **13**(16): p. 1877-1893.
123. Muller, W.A., *Leukocyte–endothelial-cell interactions in leukocyte transmigration and the inflammatory response.* Trends in immunology, 2003. **24**(6): p. 326-333.
124. Granger, D.N. and E. Senchenkova. *Inflammation and the Microcirculation*. in *Colloquium series on integrated systems physiology: from molecule to function*. 2010. Morgan & Claypool Life Sciences.
125. Dunne, J.L., et al., *Control of leukocyte rolling velocity in TNF-α–induced inflammation by LFA-1 and Mac-1.* Blood, 2002. **99**(1): p. 336-341.
126. Sundd, P., et al., *Biomechanics of leukocyte rolling.* Biorheology, 2011. **48**(1): p. 1-35.
127. Muro, S. and V. Muzykantov, *Targeting of antioxidant and anti-thrombotic drugs to endothelial cell adhesion molecules.* Current pharmaceutical design, 2005. **11**(18): p. 2383-2401.
128. Koval, M., et al., *Size of IgG-opsonized particles determines macrophage response during internalization.* Experimental cell research, 1998. **242**(1): p. 265-273.
129. Garnacho, C., et al., *Delivery of acid sphingomyelinase in normal and niemann-pick disease mice using intercellular adhesion molecule-1-targeted polymer nanocarriers.* Journal of Pharmacology and Experimental Therapeutics, 2008. **325**(2): p. 400-408.
130. Muro, S., E.H. Schuchman, and V.R. Muzykantov, *Lysosomal enzyme delivery by ICAM-1-targeted nanocarriers bypassing glycosylation-and clathrin-dependent endocytosis.* Molecular Therapy, 2006. **13**(1): p. 135-141.
131. Muro, S., et al., *Slow intracellular trafficking of catalase nanoparticles targeted to ICAM-1 protects endothelial cells from oxidative stress.* American Journal of Physiology-Cell Physiology, 2003. **285**(5): p. C1339-C1347.
132. Calderon, A.J., et al., *Flow dynamics, binding and detachment of spherical carriers targeted to ICAM-1 on endothelial cells.* Biorheology, 2009. **46**(4): p. 323-341.
133. Sarkar, D., et al., *Engineered mesenchymal stem cells with self-assembled vesicles for systemic cell targeting.* Biomaterials, 2010. **31**(19): p. 5266-5274.
134. Jeong, J.H., et al., *Leukocyte-mimicking stem cell delivery via in situ coating of cells with a bioactive hyperbranched polyglycerol.* Journal of the American Chemical Society, 2013. **135**(24): p. 8770-8773.
135. Ko, I.K., T.J. Kean, and J.E. Dennis, *Targeting mesenchymal stem cells to activated endothelial cells.* Biomaterials, 2009. **30**(22): p. 3702-3710.

136. Ko, I.K., et al., *Targeting improves MSC treatment of inflammatory bowel disease.* Molecular Therapy, 2010. **18**(7): p. 1365-1372.
137. Vandergriff, A.C., et al., *Magnetic targeting of cardiosphere-derived stem cells with ferumoxytol nanoparticles for treating rats with myocardial infarction.* Biomaterials, 2014. **35**(30): p. 8528-8539.
138. Santoso, M.R. and P.C. Yang, *Magnetic nanoparticles for targeting and imaging of stem cells in myocardial infarction.* Stem cells international, 2016. **2016**.
139. Takahashi, M., *Role of the SDF-1/CXCR4 system in myocardial infarction.* Circulation Journal, 2010. **74**(3): p. 418-423.
140. Penn, M.S., *Importance of the SDF-1: CXCR4 axis in myocardial repair*. 2009, Am Heart Assoc.
141. Seguin, J., et al., *Myosin: a highly sensitive indicator of myocardial necrosis after cardiac operations.* The Journal of thoracic and cardiovascular surgery, 1989. **98**(3): p. 397-401.
142. Yamada, T., et al., *Myosin light chain I grade: a simple marker for the severity and prognosis of patients with acute myocardial infarction.* American heart journal, 1998. **135**(2): p. 329-334.
143. Sawicki, G., H. Leon, and J. Sawicka, *Degradation of myosin light chain in isolated rat hearts subjected to ischemia-reperfusion injury.* A New Intracellular Target for Matrix Metalloproteinase. **2**(112): p. 544-552.
144. Lee, R.J., et al., *Antibody targeting of stem cells to infarcted myocardium.* Stem cells, 2007. **25**(3): p. 712-717.
145. Zhao, T.C., et al., *Targeting human CD34+ hematopoietic stem cells with anti-CD45× anti-myosin light-chain bispecific antibody preserves cardiac function in myocardial infarction.* Journal of applied physiology, 2008. **104**(6): p. 1793-1800.
146. Zachar, L., D. Bačenková, and J. Rosocha, *Activation, homing, and role of the mesenchymal stem cells in the inflammatory environment.* Journal of inflammation research, 2016. **9**: p. 231.
147. Vestweber, D., *How leukocytes cross the vascular endothelium.* Nature Reviews Immunology, 2015. **15**(11): p. 692.
148. Mbongue, J., et al., *The role of indoleamine 2, 3-dioxygenase in immune suppression and autoimmunity.* Vaccines, 2015. **3**(3): p. 703-729.
149. Ren, G., et al., *Species variation in the mechanisms of mesenchymal stem cell-mediated immunosuppression.* Stem cells, 2009. **27**(8): p. 1954-1962.
150. Waterman, R.S., et al., *A new mesenchymal stem cell (MSC) paradigm: polarization into a pro-inflammatory MSC1 or an Immunosuppressive MSC2 phenotype.* PloS one, 2010. **5**(4): p. e10088.
151. Kim, J. and P. Hematti, *Mesenchymal stem cell–educated macrophages: A novel type of alternatively activated macrophages.* Experimental hematology, 2009. **37**(12): p. 1445-1453.
152. François, M., et al., *Human MSC suppression correlates with cytokine induction of indoleamine 2, 3-dioxygenase and bystander M2 macrophage differentiation.* Molecular Therapy, 2012. **20**(1): p. 187-195.
153. Melief, S.M., et al., *Multipotent stromal cells induce human regulatory T cells through a novel pathway involving skewing of monocytes toward anti-inflammatory macrophages.* Stem Cells, 2013. **31**(9): p. 1980-1991.

154. Wu, Y., et al., *Mesenchymal stem cells enhance wound healing through differentiation and angiogenesis.* Stem cells, 2007. **25**(10): p. 2648-2659.
155. Roura, S., et al., *Human umbilical cord blood-derived mesenchymal stem cells promote vascular growth in vivo.* PloS one, 2012. **7**(11): p. e49447.
156. Kadivar, M., et al., *In vitro cardiomyogenic potential of human umbilical vein-derived mesenchymal stem cells.* Biochemical and biophysical research communications, 2006. **340**(2): p. 639-647.
157. Nishiyama, N., et al., *The significant cardiomyogenic potential of human umbilical cord blood-derived mesenchymal stem cells in vitro.* Stem cells, 2007. **25**(8): p. 2017-2024.
158. Sheng, C.C., L. Zhou, and J. Hao, *Current stem cell delivery methods for myocardial repair.* BioMed research international, 2013. **2013**.
159. Steinhoff, G., et al., *Stem cells and heart disease-Brake or accelerator?* Advanced drug delivery reviews, 2017. **120**: p. 2-24.
160. Kurtz, A., *Mesenchymal stem cell delivery routes and fate.* International journal of stem cells, 2008. **1**(1): p. 1.
161. Barbash, I.M., et al., *Systemic delivery of bone marrow–derived mesenchymal stem cells to the infarcted myocardium: feasibility, cell migration, and body distribution.* Circulation, 2003. **108**(7): p. 863-868.
162. Kraitchman, D.L., et al., *Dynamic imaging of allogeneic mesenchymal stem cells trafficking to myocardial infarction.* Circulation, 2005. **112**(10): p. 1451.
163. Freyman, T., et al., *A quantitative, randomized study evaluating three methods of mesenchymal stem cell delivery following myocardial infarction.* European heart journal, 2006. **27**(9): p. 1114-1122.
164. Dow, J., et al., *Washout of transplanted cells from the heart: a potential new hurdle for cell transplantation therapy.* Cardiovascular research, 2005. **67**(2): p. 301-307.
165. Terrovitis, J., et al., *Noninvasive quantification and optimization of acute cell retention by in vivo positron emission tomography after intramyocardial cardiac-derived stem cell delivery.* Journal of the American College of Cardiology, 2009. **54**(17): p. 1619-1626.
166. Quevedo, H.C., et al., *Allogeneic mesenchymal stem cells restore cardiac function in chronic ischemic cardiomyopathy via trilineage differentiating capacity.* Proceedings of the National Academy of Sciences, 2009. **106**(33): p. 14022-14027.
167. Müller-Ehmsen, J., et al., *Effective engraftment but poor mid-term persistence of mononuclear and mesenchymal bone marrow cells in acute and chronic rat myocardial infarction.* Journal of molecular and cellular cardiology, 2006. **41**(5): p. 876-884.
168. Mongrain, R. and J. Rodés-Cabau, *Role of shear stress in atherosclerosis and restenosis after coronary stent implantation.* Revista espanola de cardiologia, 2006. **59**(01): p. 1-4.
169. Toma, C., et al., *Human mesenchymal stem cells differentiate to a cardiomyocyte phenotype in the adult murine heart.* Circulation, 2002. **105**(1): p. 93-98.

170. Grieve, S.M., et al., *Microvascular obstruction by intracoronary delivery of mesenchymal stem cells and quantification of resulting myocardial infarction by cardiac magnetic resonance.* Circulation: Heart Failure, 2010. **3**(3): p. e5-e6.
171. Lipowsky, H.H., et al., *Mesenchymal stem cell deformability and implications for microvascular sequestration.* Annals of biomedical engineering, 2018. **46**(4): p. 640-654.
172. Al-Darraji, A., et al., *Azithromycin therapy reduces cardiac inflammation and mitigates adverse cardiac remodeling after myocardial infarction: Potential therapeutic targets in ischemic heart disease.* PloS one, 2018. **13**(7): p. e0200474.
173. Martinez, F.O. and S. Gordon, *The M1 and M2 paradigm of macrophage activation: time for reassessment.* F1000prime reports, 2014. **6**.
174. Zhuang, X., et al., *Fluorescence quenching: A tool for single-molecule protein-folding study.* Proceedings of the National Academy of Sciences, 2000. **97**(26): p. 14241-14244.
175. Ballerstadt, R. and J. Schultz, *Competitive-binding assay method based on fluorescence quenching of ligands held in close proximity by a multivalent receptor.* Analytica Chimica Acta, 1997. **345**(1-3): p. 203-212.
176. Van der Loos, C.M., P.K. Das, and H. Houthoff, *An immunoenzyme triple-staining method using both polyclonal and monoclonal antibodies from the same species. Application of combined direct, indirect, and avidin-biotin complex (ABC) technique.* Journal of Histochemistry & Cytochemistry, 1987. **35**(11): p. 1199-1204.
177. Dancil, K.-P.S., D.P. Greiner, and M.J. Sailor, *A porous silicon optical biosensor: detection of reversible binding of IgG to a protein A-modified surface.* Journal of the American Chemical Society, 1999. **121**(34): p. 7925-7930.
178. Zijlstra, P., P.M. Paulo, and M. Orrit, *Optical detection of single non-absorbing molecules using the surface plasmon resonance of a gold nanorod.* Nature nanotechnology, 2012. **7**(6): p. 379.
179. Cunningham, K.S. and A.I. Gotlieb, *The role of shear stress in the pathogenesis of atherosclerosis.* Laboratory investigation, 2005. **85**(1): p. 9.
180. Jeong, S.-K., J.-Y. Lee, and R.S. Rosenson, *Association between ischemic stroke and vascular shear stress in the carotid artery.* Journal of Clinical Neurology, 2014. **10**(2): p. 133-139.
181. Papaioannou, T.G. and C. Stefanadis, *Vascular wall shear stress: basic principles and methods.* Hellenic J Cardiol, 2005. **46**(1): p. 9-15.
182. Wu, P.-J., et al., *Hydrogel patches on live cells through surface-mediated polymerization.* Langmuir, 2017. **33**(27): p. 6778-6784.
183. Baragi, V.M., et al., *Transplantation of adenovirally transduced allogeneic chondrocytes into articular cartilage defects in vivo.* Osteoarthritis and Cartilage, 1997. **5**(4): p. 275-282.
184. Malhi, H. and S. Gupta, *Hepatocyte transplantation: new horizons and challenges.* Journal of hepato-biliary-pancreatic surgery, 2001. **8**(1): p. 40-50.
185. Hofmann, M., et al., *Monitoring of bone marrow cell homing into the infarcted human myocardium.* Circulation, 2005. **111**(17): p. 2198-2202.

186. Brenner, W., et al., *111In-labeled CD34+ hematopoietic progenitor cells in a rat myocardial infarction model.* Journal of Nuclear Medicine, 2004. **45**(3): p. 512-518.
187. Thygesen, K., et al., *Third universal definition of myocardial infarction.* Circulation, 2012. **126**(16): p. 2020-2035.
188. Prabhu, S.D. and N.G. Frangogiannis, *The biological basis for cardiac repair after myocardial infarction: from inflammation to fibrosis.* Circulation research, 2016. **119**(1): p. 91-112.
189. Shi, Y., et al., *Mesenchymal stem cells: a new strategy for immunosuppression and tissue repair.* Cell research, 2010. **20**(5): p. 510.
190. Shi, Y., et al., *How mesenchymal stem cells interact with tissue immune responses.* Trends in immunology, 2012. **33**(3): p. 136-143.
191. Espagnolle, N., et al., *CD54-mediated interaction with pro-inflammatory macrophages increases the immunosuppressive function of human mesenchymal stromal cells.* Stem cell reports, 2017. **8**(4): p. 961-976.
192. Van den Akker, F., S. De Jager, and J. Sluijter, *Mesenchymal stem cell therapy for cardiac inflammation: immunomodulatory properties and the influence of toll-like receptors.* Mediators of inflammation, 2013. **2013**.
193. Du, Y., et al., *Immuno-inflammatory regulation effect of mesenchymal stem cell transplantation in a rat model of myocardial infarction.* Cytotherapy, 2008. **10**(5): p. 469-478.
194. Imanishi, Y., et al., *Allogenic mesenchymal stem cell transplantation has a therapeutic effect in acute myocardial infarction in rats.* Journal of molecular and cellular cardiology, 2008. **44**(4): p. 662-671.
195. Cao, Y., et al., *Human adipose tissue-derived stem cells differentiate into endothelial cells in vitro and improve postnatal neovascularization in vivo.* Biochemical and biophysical research communications, 2005. **332**(2): p. 370-379.
196. Alviano, F., et al., *Term amniotic membrane is a high throughput source for multipotent mesenchymal stem cells with the ability to differentiate into endothelial cells in vitro.* BMC developmental biology, 2007. **7**(1): p. 11.
197. Sasaki, M., et al., *Mesenchymal stem cells are recruited into wounded skin and contribute to wound repair by transdifferentiation into multiple skin cell type.* the Journal of immunology, 2008. **180**(4): p. 2581-2587.
198. Silva, G.V., et al., *Mesenchymal stem cells differentiate into an endothelial phenotype, enhance vascular density, and improve heart function in a canine chronic ischemia model.* Circulation, 2005. **111**(2): p. 150-156.
199. Kawada, H., et al., *Nonhematopoietic mesenchymal stem cells can be mobilized and differentiate into cardiomyocytes after myocardial infarction.* Blood, 2004. **104**(12): p. 3581-3587.
200. Xu, W., et al., *Mesenchymal stern cells from adult human bone marrow differentiate into a Cardiomyocyte phenotype in vitro.* Experimental biology and medicine, 2004. **229**(7): p. 623-631.
201. Fukuda, K., *Development of regenerative cardiomyocytes from mesenchymal stem cells for cardiovascular tissue engineering.* Artificial organs, 2001. **25**(3): p. 187-193.

202. Mathieu, E., et al., *Intramyocardial delivery of mesenchymal stem cell-seeded hydrogel preserves cardiac function and attenuates ventricular remodeling after myocardial infarction.* PloS one, 2012. **7**(12): p. e51991.
203. Hu, X., et al., *Optimal temporal delivery of bone marrow mesenchymal stem cells in rats with myocardial infarction.* European Journal of Cardio-Thoracic Surgery, 2007. **31**(3): p. 438-443.
204. Nagaya, N., et al., *Intravenous administration of mesenchymal stem cells improves cardiac function in rats with acute myocardial infarction through angiogenesis and myogenesis.* American Journal of Physiology-Heart and circulatory physiology, 2004. **287**(6): p. H2670-H2676.
205. Left, S.A.-I.E.I., *Intravenously Delivered Mesenchymal Stem Cells.* Circ Res, 2017. **120**: p. 1598-1613.
206. Hare, J.M., et al., *A randomized, double-blind, placebo-controlled, dose-escalation study of intravenous adult human mesenchymal stem cells (prochymal) after acute myocardial infarction.* Journal of the American College of Cardiology, 2009. **54**(24): p. 2277-2286.
207. Cahall, C.F., et al., *A quantitative perspective on surface marker selection for the isolation of functional tumor cells.* Breast cancer: basic and clinical research, 2015. **9**: p. BCBCR. S25461.
208. Castelo-Branco, M.T., et al., *Intraperitoneal but not intravenous cryopreserved mesenchymal stromal cells home to the inflamed colon and ameliorate experimental colitis.* PloS one, 2012. **7**(3): p. e33360.
209. Meyer, K., et al., *ICAM-1 upregulation in distant tissues after hepatic ischemia/reperfusion: a clue to the mechanism of multiple organ failure.* Journal of pediatric surgery, 1998. **33**(2): p. 350-353.
210. Assis, A.C.M., et al., *Time-dependent migration of systemically delivered bone marrow mesenchymal stem cells to the infarcted heart.* Cell transplantation, 2010. **19**(2): p. 219-230.

EDUCATION

National Chung Cheng University (NCCU), (Chiayi, Taiwan) 09/2010-07/2012
Degree: M.S. in Chemical Engineering;
Thesis: Reconstruction of Signaling Transduction Pathway in HeLa Cells via Protein-protein-interaction and Bioinformatical Database and Pathway Analysis of Qualitative Model

Feng Chia University (FCU), (Taichung, Taiwan) 09/2006-06/2010
Degree: B.S. in Chemical Engineering;

PUBLICATIONS

1. Davis, K. A.*; **Wu, P.-J**.*; Cahall, C. F.; Li, C.; Gottipati, A.; Berron, B. J., Coatings on mammalian cells: interfacing cells with their environment. ***Journal of biological engineering*** 2019, 13 (1), 5.

(*equal contribution)

2. **Wu, P.-J.**; Lilly, J. L.; Arreaza, R.; Berron, B. J., Hydrogel patches on live cells through surface-mediated polymerization. ***Langmuir*** 2017, 33 (27), 6778-6784.
3. Lin, C.-W.; Wei, K.-C.; Liao, S.-s.; Huang, C.-Y.; Sun, C.-L.; **Wu, P.-J.**; Lu, Y.-J.; Yang, H.-W.; Ma, C.-C. M., A reusable magnetic graphene oxide-modified biosensor for vascular endothelial growth factor detection in cancer diagnosis. ***Biosensors and Bioelectronics*** 2015, 67, 431-437.
4. **Wu, P.-J.**; Wu, W.-H.; Chen, T.-C.; Lin, K.-T.; Lai, J.-M.; Huang, C.-Y. F.; Wang, F.-S., Reconstruction and analysis of a signal transduction network using HeLa cell protein–protein interaction data. ***Journal of the Taiwan Institute of Chemical Engineers*** 2014, 45 (6), 2835-2842.
5. **Wu, P.-J**., "Reconstruction of signaling transduction pathway in HeLa cells via protein-protein interaction and bioinformatical database and pathway analysis of qualitative model." ***Master's Thesis*** 2012

HONORS & AWARDS

08/2015 ***Outstanding Thesis Award,*** *Taiwan Institute of Chemical Engineers*
06/2012 ***Excellent Poster Award***, 17th Conference of Biochemical Engineering Society of Taiwan, (Kaohsiung, Taiwan)
09/2007-01/2009 ***Advancement and Diligence Scholarship (3x)***, FCU
09/2007-01/2009 ***Sung Shan Tzu-Yu Temple Scholarship (2x)***, (Taiwan)